Theses and Dissertations1. Thesis and Dissertation Collection, all items

1974

Reduction of out-of-plane distortion in fillet welded high strength aluminum.

Henry, Robert W.

Massachusetts Institute of Technology

http://hdl.handle.net/10945/17204

REDUCTION OF OUT-OF-PLANE DISTORTION
IN FILLET WELDED HIGH STRENGTH ALUMINUM

Robert W. Henry

REDUCTION OF OUT-OF-PLANE DISTORTION

IN FILLET WELDED HIGH STRENGTH ALUMINUM

BY

Robert W. Henry

B.S., U.S. Coast Guard Academy (1969)

SUBMITTED IN PARTIAL FULFILLMENT OF THE REQUIREMENTS

FOR THE DEGREES OF MASTER OF SCIENCE IN OCEAN

ENGINEERING AND MASTERS OF SCIENCE IN MECHANICAL

ENGINEERING

at the

Massachusetts Institute of Technology

May, 1974

REDUCTION OF OUT-OF-PLANE DISTORTION
IN FILLET WELDED HIGH STRENGTH ALUMINUM

by

Robert W. Henry

Submitted to the Department of Ocean Engineering
in May, 1974, in partial fulfillment of the
requirements for the degree of Master of Science
in Ocean Engineering and Masters of Science
in Mechanical Engineering.

ABSTRACT

Out-of-plane distortion caused by angular changes
at fillet welds in aluminum structural panels was examined
from two viewpoints.

In the first phase of this work a series of experiments
was conducted to examine elastic-plastic prestraining of
test specimens to be fillet welded as a means of reducing
out-of-plane distortion. Data gathered from these tests
was correlated with previous experiments in the use of
aluminum. A guide in the use of elastic-plastic prestrain-
ing for 3/8" and 1/2" was developed.

In phase two of this work a two-dimensional program was
adapted to the structural aluminum panels used in phase one
and tested for accuracy. The program, based on pure

stress, was found to be inaccurate in predicting the behav-
iors of the fillet welded aluminum panels.

Thesis Supervisor: Dr. Koichi Masubuchi
Title: Professor of Naval Architecture

TABLES OF CONTENTS

LIST OF TABLES

LIST OF FIGURES

1.0 - AN INTRODUCTION TO WELDING
HIGH STRENGTH ALUMINUM ALLOYS

1.1 - Welding High Strength Aluminum Alloys

The ever increasing use of high strength aluminum in the fabrication of structures has in recent years accelerated due to a greater understanding, through research, of its potentials. Aluminum alloys, based on one of the Earth's most abundant minerals, have value primarily derived from several characteristics:

    a. a high strength to weight ratio,

    b. an excellent corrosion resistance,

    c. good strength and toughness at a wide range of temperatures (most notable at low temperatures), and

    d. the ability to form high strength weldable alloys. [1]

Since it is well known that the properties required in an aluminum alloy weldment depend on the service condition of the structure, one must be very careful in predicting the expected loads, environmental constraints, life expectancy and reliability. Basically any welded high strength aluminum structure should have high strength coupled with good weldability. In many applications the material must have good resistance to corrosion and be free from stress-corrosion cracking (as in marine use). In specific applications notch toughness, good ductility and

adequate fatigue properties are also important.

We have learned, though, that any one aluminum alloy can-
not possess all these properties. High strength is usually
bought at the price of poor weldability. High strength alloys
are also often susceptible to corrosion attack. Any structure
requiring high strength must be analysed and trade-offs must
be evaluated to meet the required needs. To date the welding
of high strength aluminum alloys offers one of the biggest
problems in structural fabrication.

Aluminum and its alloys can be jointed by most of the
forty welding processes defined by the American Welding
Society. [2] Obviously the process selection will depend primar-
ily on the application as well as from considerations of
strength requirement, configuration, quality, desired finish,
number and thickness (or gage) of metal.

The welding methods which are most frequently used to join
high strength aluminum alloys are discussed below. They include
Gas Tungsten Arc (GTA), Gas Metal Arc (GMA), Electron Beam
and Plasma Arc.

GTA Welding

The GTA process uses a high intensity heat source and has
fluxless welding capability. An arc is struck between the
nonconsumable tungsten electrode and the work piece (usually
less than 1/8 inch gage). A helium or helium-argon mixture
is used for the shielding gas to protect the arc and the

molten weld. This process is performed using either direct
current straight polarity for good weld penetration and faster
welding speed because the heat is concentrated at the work,
or direct current reverse polarity for good arc-cleaning
action. Traditionally, the method of GTA welding of alum-
inum has been with AC input power.

GMA Welding

This process uses a consumable wire electrode that
coalesces with the base metal in a molten pool protected
by an inert gas shield. The process uses direct current
reverse polarity to take advantage of the cathodic cleaning
action and high current densities for high disposition rate
and fast welding speeds needed for welding heavier gages
of aluminum. [3]

Electron Beam Welding

This process is fairly new but has the advantage of a
high strength weld, good joint efficiency, a narrow weld,
and small heat affected zone. The welding is accomplished
by bombarding the base piece with a dense stream of high-
velocity electrons. No filler metal is required but the
process must take place in an air evacuated chamber.

Plasma Arc Welding

The process is basically a modification of the GTA

process. In Plasma Arc the arc is tightly constricted by means of a high velocity sheath of gas flowing around the arc making possible a higher concentration of energy (heat) at the weld site for greater weld penetration and weld speed.

Although GTA and GMA are the most widely used welding techniques for high strength aluminum, electron beam and plasma arc offer advantages that can give them future significance. Laser beam techniques also have a promising future but at present lasers are used more for plate alignment before fabrication than for joining.

1.2 - Problems Associated with Welding High Strength Aluminum Alloys

Although the knowledge of welding high strength aluminum has been rapidly expanding there are many problems associated with it that still plague the industry. Briefly discussed below are cracking, porosity, stress corrosion, incomplete fusion, and distortion.

Cracking

Cracking in aluminum alloy weldments can be classified by cracking above the solidus and cracking below the solidus. Cracking above the solidus line occurs in weld metal when sodidification has reached the point of continuity between adjacent crystals so that cooling and contraction produce

tensile stresses. This form of hot cracking can be minimized by the proper selection of weld filler metal.

On the other hand, cracking below the solidus line is the result of intermetallic compounds precipitating out during the cooling process causing a decrease in grain boundary strength when the alloys are depleted at the outer cystal boundaries. This form of cracking is dependent on composition, microstructure, and the degree of restraint imposed on the cooling weld.

Porosity

In general, porosity in weldments is formed by the entrapment of evolved gases in the solidifying weld metal through the mechanism of nucleation and growth. The weld defects due to porosity become more and more important as higher strength alloys are developed. Experimental results indicate that the ultimate tensile strength of a transverse weld specimen decreases with increasing porosity. Porosity has also been found to decrease a metal's ductility and fatigue life. Investigators feel that hydrogen or water contaminants are the major cause of weld porosity.

Stress Corrosion

This problem, not unique to welding high strength aluminum alloys, is a complex interaction of corrosive attack

-15-

and sustained stress which results in cracking. The inter-
action is initiated if the material is susceptible to selective
corrosion along a continuous path where irregularities are
present such as a grain boundary (i. e., weld path). If the
particular piece is in tension, stress corrosion cracking
can occur. The problem is doubly complicated when you examine
the numerous ways that simple selective corrosion can occur. [4]

Incomplete Fusion

Incomplete fusion arises mainly from the strong affinity
of aluminum for oxygen. This oxide tends to persist as a
film that interferes with the wetting action necessary for
weld fusion and causes a failure of fused weld metal to coalesce
with the adjacent base metal or with the previously deposited
weld metal.

Residual Stress and Shrinkage Distortion

One of the most serious problems facing the fabrication
engineer is the residual stress and distortion induced during
the welding of an aluminum structure. There are, in general,
three reasons for this problem that make control of weld
distortion in aluminum more critical than with steel--

a. Aluminum, having a higher heat conductivity will
    have the welding heat conducted in wider areas.
    Expansion and contraction of aluminum is much more

pronounced than in steel.

b. Aluminum has a greater coefficient of thermal expansion
    than steel.

c. Aluminum alloys have lower yield strengths producing
    larger plastic zones near the weld than steel.

See Table 1.2.1 for a comparative study of steel and aluminum. [3]

During welding complex strains in the weld metal and
annexed base metal region are induced during the non-uniform
heating and cooling phase. Their respective stresses combine
and react to produce internal forces that can cause bending,
rotation and buckling. Collectively they are known as welding
shrinkage distortion. The induced stresses are usually
accompanied by plastic upsetting and even material yield in
some instances. Residual stresses and the resulting distorions
due to welding are effected in varying degrees by base plate
and weld metal material properties, specimen length, plate
thickness, welding process and welding sequence.

The distortions found in fabricated structures are caused
by three fundamental dimensional changes that are known to
occur during the welding process; transverse shrinkage occur-
ing perpendicular to the weld line, longitudianl shrinkage
which occurs parallel to the weld line and out-of-plane
angular distortion where rotation occurs around the weld line.
These fundamental distortions are shown in Figure 1.2.1.
Distortions which can occur in practical weldments are far
more complex as can be seen in Figure 1.2.2.

TABLE 1.2.1

COMPARISON OF SOME PHYSICAL PROPERTIES

BETWEEN STEEL AND ALUMINUM

	STEEL	ALUMINUM
Density lb/in^3	0.284	0.097
E, 10^6 psi	30	10.2
ys, 10^3 psi	35 — 150	30 — 50
Strength to weight ys/ X 10^3 in	123 — 530	300 — 500
Thermal Conductivity , BTU/h/ft^2/ft/^{o}F	26.2	130
Coefficient Linear Thermal Expansion , 10^{-6} / ^{o}F	3.8	13
Electrical Resistivity 10^{-6} /in	9.7	2.7
Melting point, ^{o}F	2800	1220
Melting point of oxide ^{o}F (FeO , Al_2O_3)	2400	3700
Fatigue, 10^3 psi	½ of uts — 30	10 — 20
Poisson Ratio	.29	.33
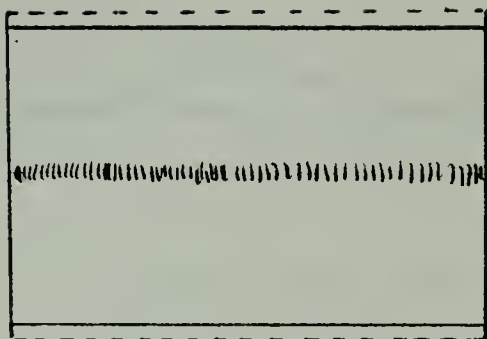
TRANSEVERSE SHRINKAGE
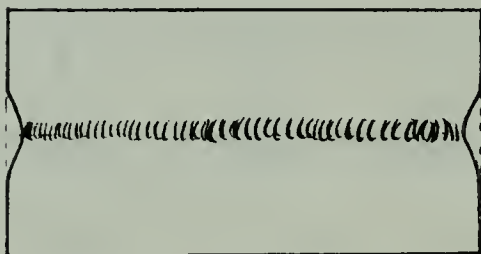
LONGITUDINAL SHRINKAGE

ANGULAR -ROTATION

FIGURE 1.2.1 FUNDAMENTAL WELDING DISTORTIONS[6]

BUCKLING DISTORTION
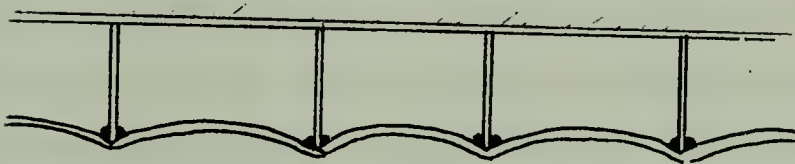
ANGULAR CORRIGATION FAILURE
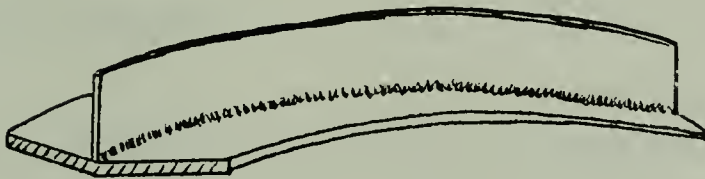
COMBINATION OF LONGITUDINAL

AND ANGULAR DISTORTION

FIGURE 1.2.2

COMPLEX WELDING DISTORTIONS IN PRACTICAL WELDMENTS [6]

Longitudinal and transverse distortions can be designed out of structures and accounted for before fabrication by making allowances for proper shrinkage. Angular changes, particularily in the area of the fillet weld, are more difficult to make allowances for and usually have to be corrected by some type of post welding operation or by a welding operation which includes procedures for distortion reduction.

1.3 - Methods Used to Reduce Welding Distortion

Methods used presently to reduce weld distortion include proper selection of the specimen, welding process, welding sequence, forced cooling, stress-relief annealing, peening, flame straightening, vibratory stress-relief, electromagnetic hammer and external constrains. [7] Each method is briefly discussed below.

Specimen Selection

Many investigations have been conducted in both steel and aluminum into the effects of various factors on the magnitude and distribution of residual stresses in welds as a function of specimen variables (i.e., length, width, thickness, base-plate, and weld metal properties). Each parameter can directly influence the distribution of residual stresses in a test piece. It is beyond the scope of this work to describe each variable in detail but since we are concerned with angular

out-of-plane distortion we can review several basic obser-
vations..

The length and width of a material determine the general
magnitudes of its residual stresses. As length or width are
increased the residual stress will increase to a point and
then remain constant. In general, longitudinal residual stresses
must be zero at both ends of the weld and high tensile stresses
exist in the central regions of the weld. Transverse residual
stresses are tensile in central areas and compressive in the
areas near the plate ends with the maximum stress occuring
at the plate ends. [3] Figure 1.3.1 has been included to
demonstrate this effect in a non-dimensional form.

Angular distortion as a function of thickness with
assumed infinite length and width measurements describes a
curve that in general takes the form of Figure 1.3.2. Low
angular distortion for small thicknesses is attributed mainly
to the fact that the heat input conducts almost uniformly
out away from the weld with little variation in the thickness
direction. Low angular distortion for thick plates results
from a large stiffness coefficient for the thicker plates
enabling them to resist bending moments induced by residual
stresses. [8]

Welding Process

Welding processes now used in fabrication of high strength
aluminum alloy structures in general produce similar residual

-22-
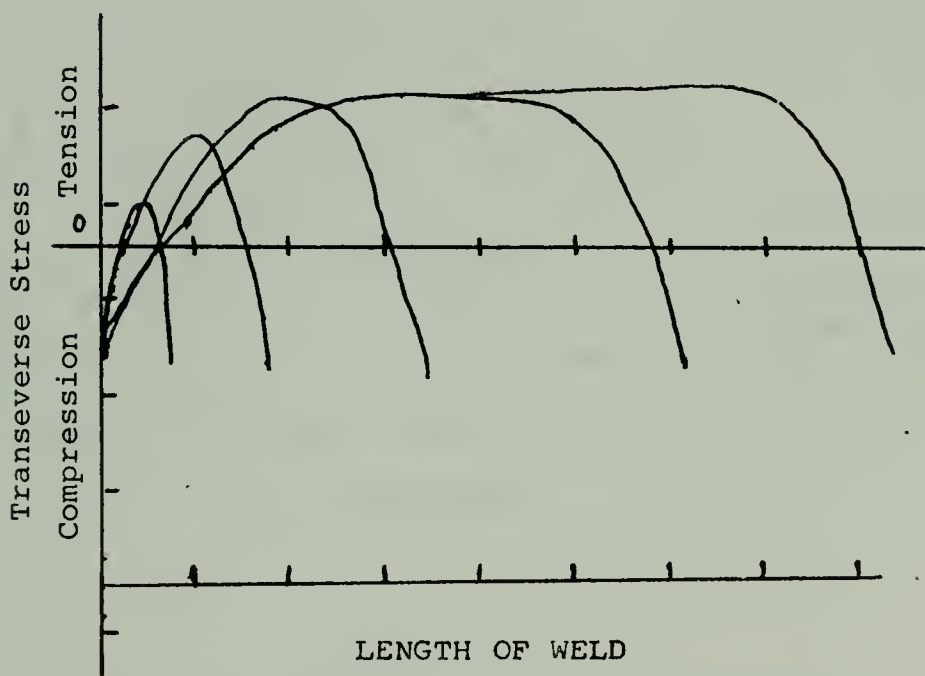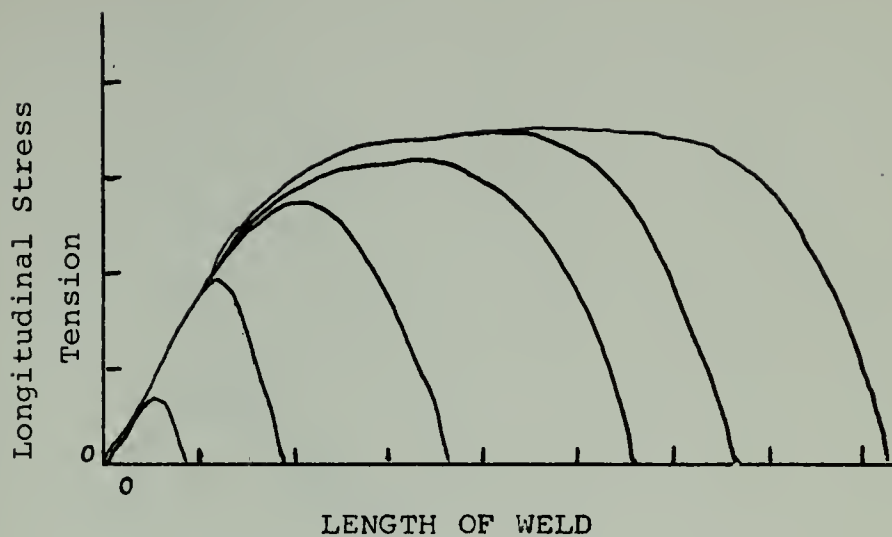
FIGURE 1.3.1

RESIDUAL STRESSES VS. LENGTH*WIDTH VARIABLES (GENERAL)[3]
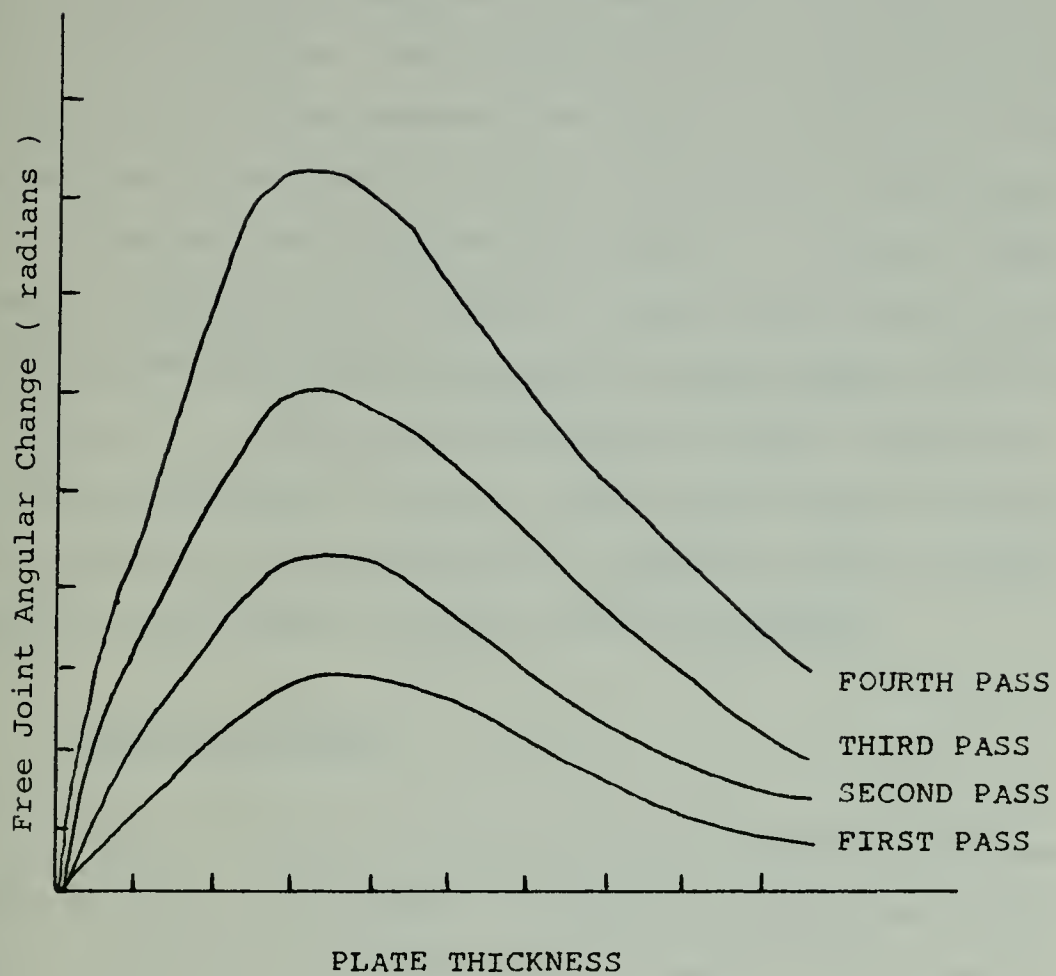
FIGURE 1.3.2

ANGULAR DISTORTION VERSUS THICKNESS (GENERAL)[8]

stresses. They include shielded metal arc, submerged arc,
GMA and GTA welding. We can, though, be general and observe
that residual stress is an indirect function of welding heat
input and as we use processes that have high heat inputs we
can expect greater residual distortions, not to mention reduced
ultimate strengths. The Marshall Space Flight Center inves-
tigators found that reduced heat input and narrow weld-metal
areas gave higher weld strengths and smaller distortions. [9]

Satisfactory electron-beam welds in aluminum alloys
require significantly lower heat inputs than either GMA or
GTA, but because the electron-beam process must be done in
a vacuum it is presently restricted to small components.
Japan is presently testing a large electron-beam installa-
tion used in the fabrication of aluminum spheres approxi-
mately eighty feet in diameter for LNG tankers.

Welding Sequence

Kihara [10] observed that as far as residual stresses
were concerned, the effect of welding sequence had only a
minor influence on longitudinal stresses. On the other
hand, transverse residual stresses were largely affected
by welding sequence. Welding sequence can be fundamentally
related to three standpoints -

    a. classification by the relation between welding
        direction as a whole and the welding direction
        of each block,

b. classification by welding direction,

   c. classification by multi-pass method.

   Many investigators have studied the three parameters
above in various combinations. Figure 1.3.3 shows only a
few of the welding sequence methods. It was observed that
differences in welding sequence caused significant difference
in transverse distortion. Block welding sequences were gen-
erally found to cause less shrinkage than the multi-layer
sequence approach. Symmetrical welding sequences were found
to generate less non-uniformity than multi-pass methods. [10]

Forced Cooling

   Previously we discussed residual distortion as a function
of heat input. Since maximum temperature and time at temperature
are known to be significant in measuring effective weld heat
input we can speculate that by controlling the weld heat
temperature and time at temperature we can, in effect, control
such factors as ultimate tensile strength, yield strength,
elongation and distortion.

   This can be achieved in one way by the absorbtion of
heat from the base plate by forced cooling with cryogenic
liquids such as CO_2 or liquid nitrogen. As can be seen from
Tables 1.3.1 and 1.3.2 all forms of altering the thermal
patterns were effective to some degree in reducing warpage
and distortion, the most effective being a combination of
cooling and follow-up auxillary heating. This method has
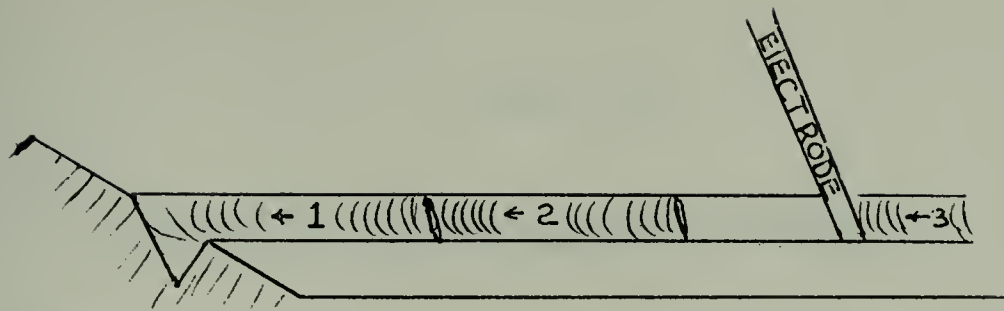
A. BACKSTEP SEQUENCE
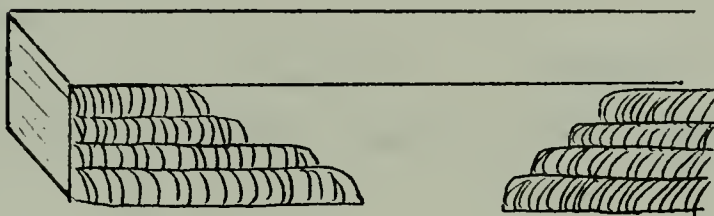
B. BLOCK SEQUENCE

C. BUILD-UP SEQUENCE
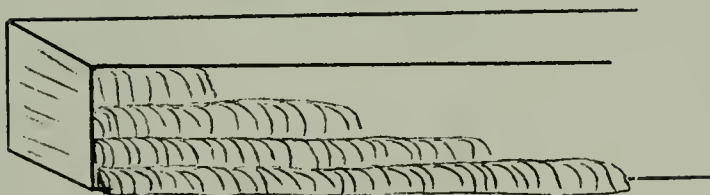
D. CASCADE SEQUENCE

FIGURE 1.3.3

DIFFERENT WELDING SEQUENCES

TABLE 1.3.1

EFFECT OF THERMAL PATTERNS ON WARPAGE [3]

Principle Factors Producing Thermal Pattern	Warpage in Degrees					
	Maximum		Minimum		Typical	
	Bow	Peak	Bow	Peak	Bow	Peak
Unchilled	− .08	+ 1.6	0	0	− 0.4	+ 1.2
Chilled only-front side	− 1.2	+ 3.5	0	0	− 0.8	+ 1.2
Chilled only-back side	− 0.8	+ 0.6	0	0	− 0.8	+ 0.6
Chilled and auxilliary heat	+ 0.3	− 0.3	0	0	+ 0.2	0

TABLE 1.3.2

EFFECT OF THERMAL PATTERNS ON RESIDUAL STRESSES [3]

Principle Thermal Pattern Factors	Residual Stress (PSI)					
	Maximum		Minimum		Typical	
	Long.	Trans.	Long.	Trans.	Long.	Trans.
Unchilled	+22.5 K	−12.3 K	+17.6 K	− 3.0 K	+21.0 K	− 7.0 K
Chilled only-front side	+22.5 K	− 8.0 K	+12.2 K	− 1.6 K	+12.0 K	− 7.5 K
Chilled only-back side	+20.3 K	− 7.8 K	+11.9 K	− 4.0 K	+15.0 K	− 5.0 K
Chilled, auxilliary heat	+ 9.2 K	−12.6 K	+ 1.1 K	+ .8 K	+ 3.0 K	− 2.0 K

been found to reduce residual stresses by as much as 95%.
It can be noted that forced altering of the thermal patterns
of a weld by cryogenic cooling also increased the material's
tensile yield strength by about 15% and reduced porosity
(to a lesser extent). [3]

Stress - Relief Annealing

Just as cold work induced stresses are relieved by
annealing, residual stresses due to welding can be relieved
in the same manner. By proper annealing the microscopic
grain number, size and growth rate are controlled to reduce
induced stresses. In the same manner as cryogenic cooling,
proper tempering of a weld's thermal cycle can be used to
reduce distortion.

For both forced cooling and stress - relief, annealing
optimum thermal patterns suitable for specific weldments
can be developed by a combination of theoretical and empirical
methods or through newly developed computer-aided programming
techniques.

Flame Straightening

This method used in reducing distortion is universally
accomplished with the use of an oxyacetylene flame for
essentially the application of heat to a localized area of
metal to cause dimensional changes. The three basic factors

influencing flame straightening techniques as discussed by
R. Holt [11] are the following:

a. the thermal expansion of the material with an increase
in temperature;

b. the variation of the yield strength of the material
with increasing temperature; and,

c. the behavior of the modulus of elasticity at elevated
temperatures.

In practice, three types of flame straightening tech-
niques are used, usually, in combination with water quenching--

a. line heating parallel to the weld line,

b. line heating on the back side of the weld line,

c. spot heating.

The analysis of flame straightening techniques is not
a simple one because of the many variables involved such as
boundary conditions, dimensions, temperatures used and
their location, quenching methods, and initial degree of
distortion. We can comment on several observations though:

a. water quenching of flame heated material achieves
a greater removal of distortion than air cooling;

b. spot heating is less effective than line heating;

c. high temperature flame straightening has detrimental
effects on the material properties of the base
metal.

For closer control of heat input to the work piece several authors have suggested using induction heating or plasma arc torches. [12]

Vibratory Stress Relief

This method of distortion removal is simple in concept and involves little in the way of expensive equipment. During cooling the test piece is forced to vibrate at its resonant frequency for a length of time dependent on the weight of the work piece. During this time, the low frequency vibrations (0 to 100 c. p. s.) induce a realignment of the lattice structure reducing the residual stress level. [13, 14]

Electromagnetic Hammer

This system relies on a magnetic field induced in the base plate to increase the plate's kinetic energy during metal forming. A rapid and predictable acceleration of the deformation is allowed and distortion reduction results. This method was satisfactorily tested on the Saturn rocket system and is being evaluated for marine use at Avondale Shipyard, Inc. in New Orleans, Louisiana.

External Constraints

In most practical work of fabricating welded structures

external constraints are normally used to reduce distortion.
By the selection of appropriate strong-backs, jigs, clamps
and rollers, investigators [5, 6, 7, 10, 12, 15] have found
that induced distortions can be reduced.

1.4 - Reduction of Out-of-plane Distortion in Fillet Welded High Strength Aluminum By Elastic-plastic Prestraining

The initial thrust of this thesis is the reduction of
out-of-plane distortion in a one pass double fillet welded
"tee" of high strength aluminum by elastic-plastic prestraining.
There is little recorded evidence that much analysis of
out-of-plane distortion was done before 1950. In the last
thirty-five years a great effort has been spent to reduce
out-of-plane distortion in steel by various methods including
elastic-plastic prestraining. [16] Today many steel fabrications
are constructed using external constraints of one form or
another. However, as in most problems associated with the
use of aluminum, experimentation in out-of-plane distortion
has been slow. Chapter 2 of this work is devoted to expanding
our knowledge of aluminum fabrication.

1.5 - Computer Aided Analysis in the Prediction of Out-of-plane Weld Distortion in High Strength Aluminum

With the advent of the computer man has been able to

adopt computer-aided techniques in solving problems that

formerly involved extensive experimentation combined with

complex theoretical and analytical follow-up work. Simple

one-dimensional computer programs have given way to n-dimen-

sional, finite element programs that can solve problems

previously far too complex to tackle. With a suitable computer

program, an investigator can reduce the number of actual

experiments he must perform to a minimum, and rely on computer

simulations to provide the main bulk of information. It is

the author's intention in the second half of the work to tie

together several functioning computer programs now at M. I. T.

into a reliable package that can accurately simulate the out-

of-plane deformation that occurs in fillet welded high strength

aluminum. If successful, this program shall accurately

simulate the exact welding procedures used in an actual test

model of a single pass, double fillet welded "tee". The

investigation shall be restrained to one- and two-dimensional

programs.

2.0 - ELASTIC-PLASTIC PRESTRAINING OF HIGH-STRENGTH ALUMINUM ALLOY DURING FILLET WELDING TO REDUCE OUT-OF-PLANE DISTORTION

2.1 - General

The objective of this chapter is to develop a technique of elastic-plastic prestraining of flat plate aluminum alloy to reduce out-of-plane distortion from fillet welding. Through literary research it was determined that the significant variables are degree of prestraining (i.e., amount of induced curvature), plate thickness, plate span and length, welding process (including parameters), and number of passes. By using a uniform plate span and length, and relying on gas metal arc welding with the parameters specified by the material being welded, the number of variables are reduced to the degree of prestraining, plate thickness, and number of passes.

Once these parameters have been exercised and functional relationships developed, the results will be corrlated into a form suitable for incorporation into standard fabrication methods (a shipyard, for instance). This technique has already been done for steel. [16]

2.2 - Preparation of the Experiment

Constraining jig

Figure 2.2.1 shows schematically the method of
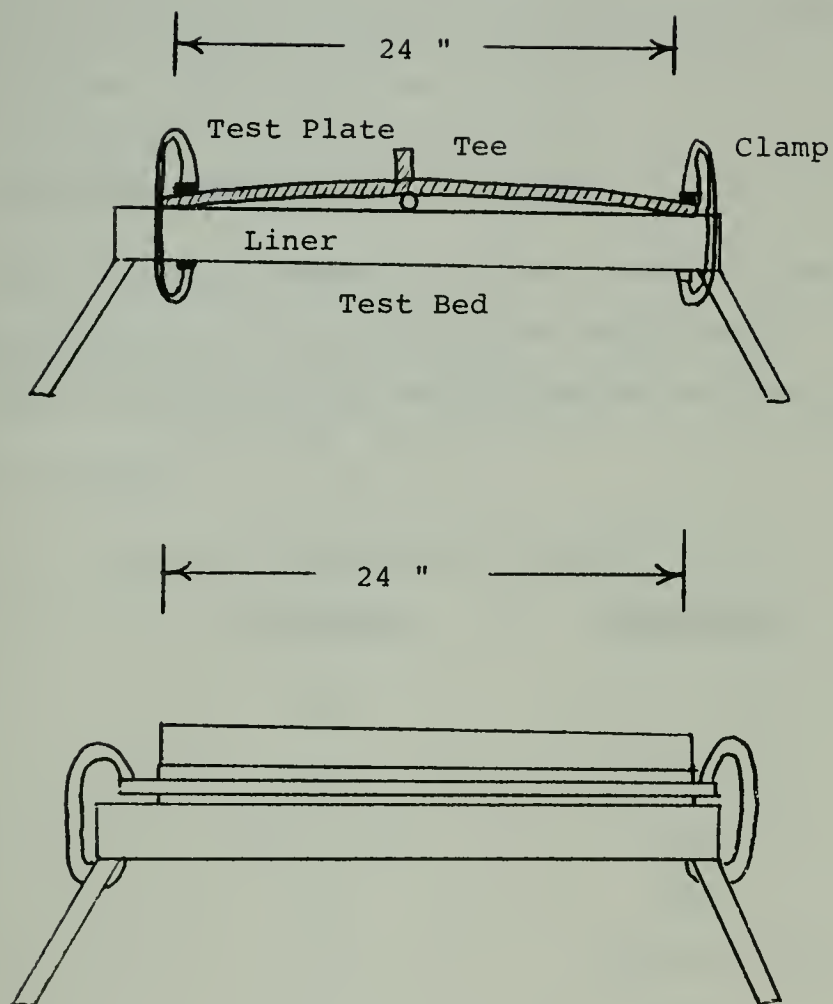
FIGURE 2.2.1 SCHEMATIC PICTORIAL OF TEST SETUP

prestraining used in this exercise. Note that the clamps only hold the bottom plate tips to the table and do not force them to be tangent. The round bar is placed under the plate along the the longitudinal centerline (also the weld line) to induce reverse curvature counteracting the out-of-plane distortion from welding.

Material and Material Properties

5456 aluminum-magnesium alloy plate was donated by ALCOA and used for this particular experiment.

The characteristics and properties of the material are as follows: [17], [18], [19], [20]

1. Chemical composition (typical)

Elements	Percentage
Mg	4.7 - 5.5
Mn	.50 - 1.0
Si + Fe	.40
Zn	.25
Cr	.05 - .20
Ti	.20
Al	Remainder

2. Physical properties (room temperature)

density	.096 lbm/in^3
specific heat	.23 BTU/lbm $^{\circ}$F
liquidus temperature	1060 $^{\circ}$F - 1180 $^{\circ}$F

thermal conductivity　　.185 X 10^{-2} BTU/in sec °F

thermal diffusivity　　8.35 X 10^{-2} in^2/sec

3.　Mechanical properties (room temperature)

modulus of elasticity　　　　　　10.2 X 10^6 psi

modulus of rigidity　　　　　　3.75 X 10^6 psi

min. tensile strength　　　　　42　X 10^3 psi

min. yield strength　　　　　37　X 10^3 psi

Poissons ratio　　　　　　　　　　.33

The filler metal applicable for this type of welding
was 5556 and has the following chemical composition:

Element	Percentage
Mg	4.7 - 5.5
Mn	.50 - 1.0
Si + Fe	.40
Zn	.25
Cr	.05 - .20
Cu	.10
Al	.94

Test Specimen

All test specimens were 24" by 24". Table 2.2.1
details the specimen parameters by plate model number.
Thicknesses of .250", .375", and .50" were used because
they had the greatest susceptibility to welding distortion. [8]

-38-

TABLE 2.2.1

TEST SPECIMEN DISCRIPTION AND WELD CONDITIONS

MODEL #	THICKNESS INCHES	TEE INCHES	LINER INCHES	# OF PASSES	VOLTS DCRP	AMPS	SPEED IN/MIN
1	.250	6	.440	1	22.5	215	14.5
2	.250	6	.375	1	22.5	210	11
3	.250	6	.254	1	22.5	180	12
4	.375	6	.95	3	21.5	230	19
5	.375	6	.185	3	21.5	230	17
6	.375	6	.245	3	21.5	230	19
7	.375	3	.000	3	22	240	17
8	.375	3	.254	3	22	240	13
9	.375	3	.125	3	22	240	12
10	.50	6	.95	3	22	240	17
11	.50	6	.185	3	22	240	16
12	.50	6	.254	3	22	240	18
13	.50	3	.000	3	22.5	250	13
14	.50	3	.125	3	22.5	250	13
15	.50	3	.254	3	22.5	250	13

The different liner sizes were selected from a study outline in Appendix B, in the hope that they would bracket the "ideal" liner diameter for minimum angular distortion.

Welding Equipment

1. Power Supply - Westinghouse Type R. S. Silicon Rectifier, Constant Voltage Power.

2. Wire Feeder - Airco Wire Feeder Model AHF-L(117 v/3A).

3. Welding Process - Gas Metal Arc, DCRP, using He Semi- Automatic, hand-held gun.

2.3 - Conduct of the Experiment

Welding Conditions

Initial weld conditions are specified for each model in Table 2.2.1. Welding parameters at first were set to conform to ALCOA specifications for their material and were subsequently varied where necessary to produce a clean, smooth and spatter free weld. Arc travel speed became a function of plate thickness and plate preparation.

Experimental Test Procedure

The model to be welded was first prestrained as shown in Figure 2.2.1. The flange tee was tacked into position along the longitudinal centerline. One fillet was then welded from right to left (because of the wire feed charac-

teristics of the gun). While the plate was still hot
(approximately 30 seconds), the second fillet was welded
right to left. Still clamped, the plate was allowed to cool
to room temperature (approximately 80° F). The plate was
then unclamped, and moved to the measurement table. Inside
calipers and a micrometer were used to obtain the amount
of out-of-plane deflection at the plate ends. The plate
was then taken back to the welding platform, reclamped
with the same roller underneath, and the next pass welded.
This process was repeated for each plate depending on the
specified number of passes.

2.4 - Results

The recorded deflection readings were divided by the
span length to give deflection in radians. Reduced data
is found in Table 2.4.1. Figures 2.4.1 and 2.4.2 plot
angular distortion versus liner height for 3/8" and 1/2"
plates. Figure 2.4.3 and Figure 2.4.4 plot liner height
versus plate thickness, for base plates with 3" and 6"
tees, respectively.

2.5 - Analysis of Experimental Results

Referencing Appendix A, an analysis was conducted on
angular distortion under various constraints. [8] Assuming
small deflections, elastic strain and a two dimensional
model of reasonable accuracy, the appendix ties together

TABLE 2.4.1

REDUCED DATA OF ANGULAR DISTORTION

Plate Number	Distortion in Radians ($\times 10^{-2}$)		
	Pass 1	Pass 2	Pass 3
1	—	—	—
2	—	—	—
3	—	—	—
4	+ .442	+ .973	+ 1.56
5	- .11	+ .32	+ .91
6	- .837	- .078	+ .33
7	+ .62	+ 1.39	+ 1.43
8	- 1.3	- .85	- .18
9	- .334	- .192	- .268
10	+ 1.0	+ 1.8	+ 2.04
11	+ .35	+ 1.23	+ 1.315
12	+ .07	+ .71	+ .81
13	+ 1.22	+ 2.322	+ 2.55
14	+ .278	+ 1.0	+ 1.26
15	- .3185	- .119	+ .186

FIGURE 2.4.] CURVES OF ANGULAR DISTORTION VERSUS LINER HEIGHT FOR .375" PLATE, 5456 Al.ALLOY

LINER HEIGHT IN INCHES

ANGULAR DISTORTION IN RADIANS (10^{-3})

	3"Tee	6"Tee
PASS 1	●	O
PASS 2	■	□
PASS 3	▲	◁
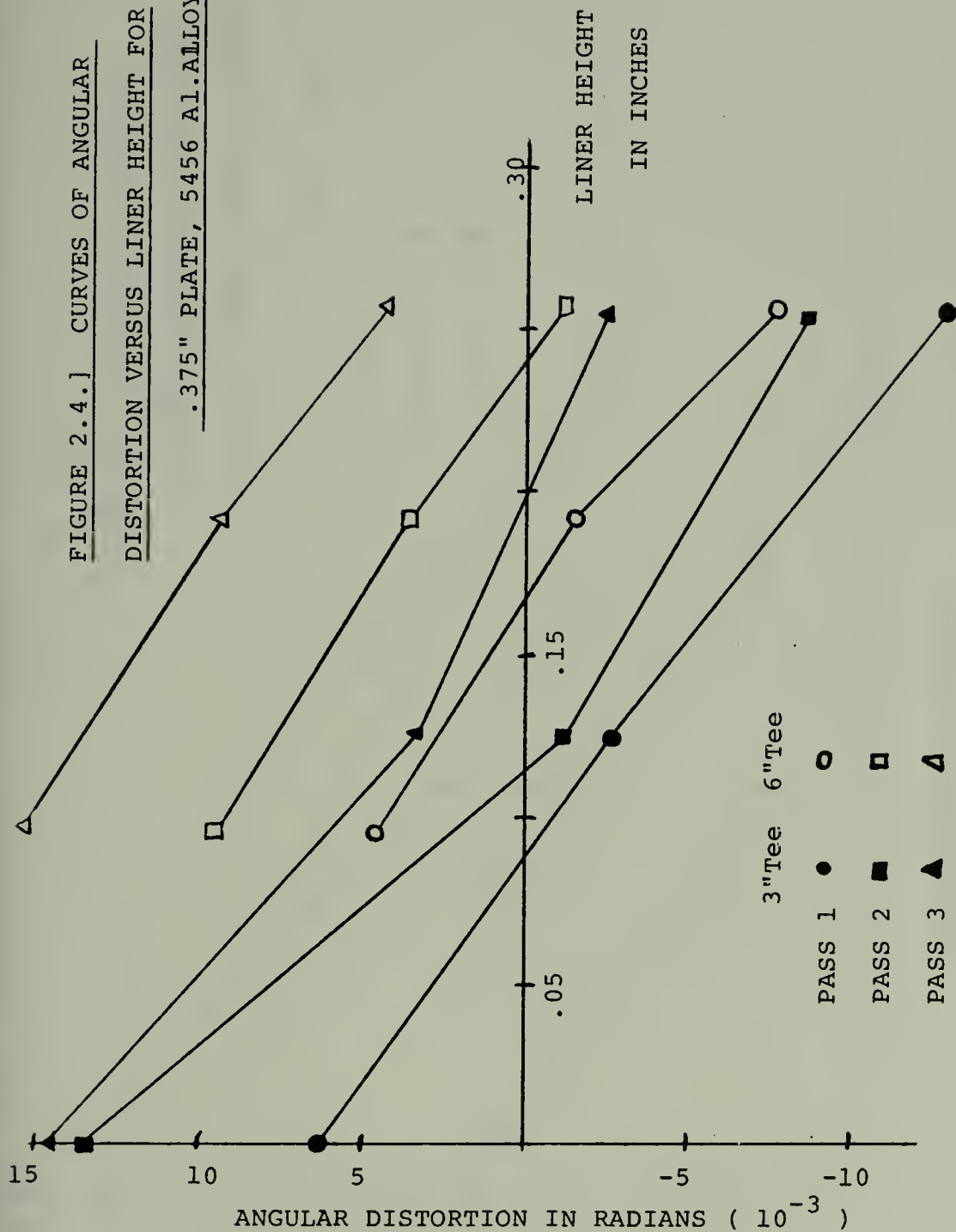
FIGURE 2.4.2 CURVES OF ANGULAR

DISTORTION VERSUS LINER HEIGHT

FOR .50 " PLATE, 5456 Al. ALLOY

-44-
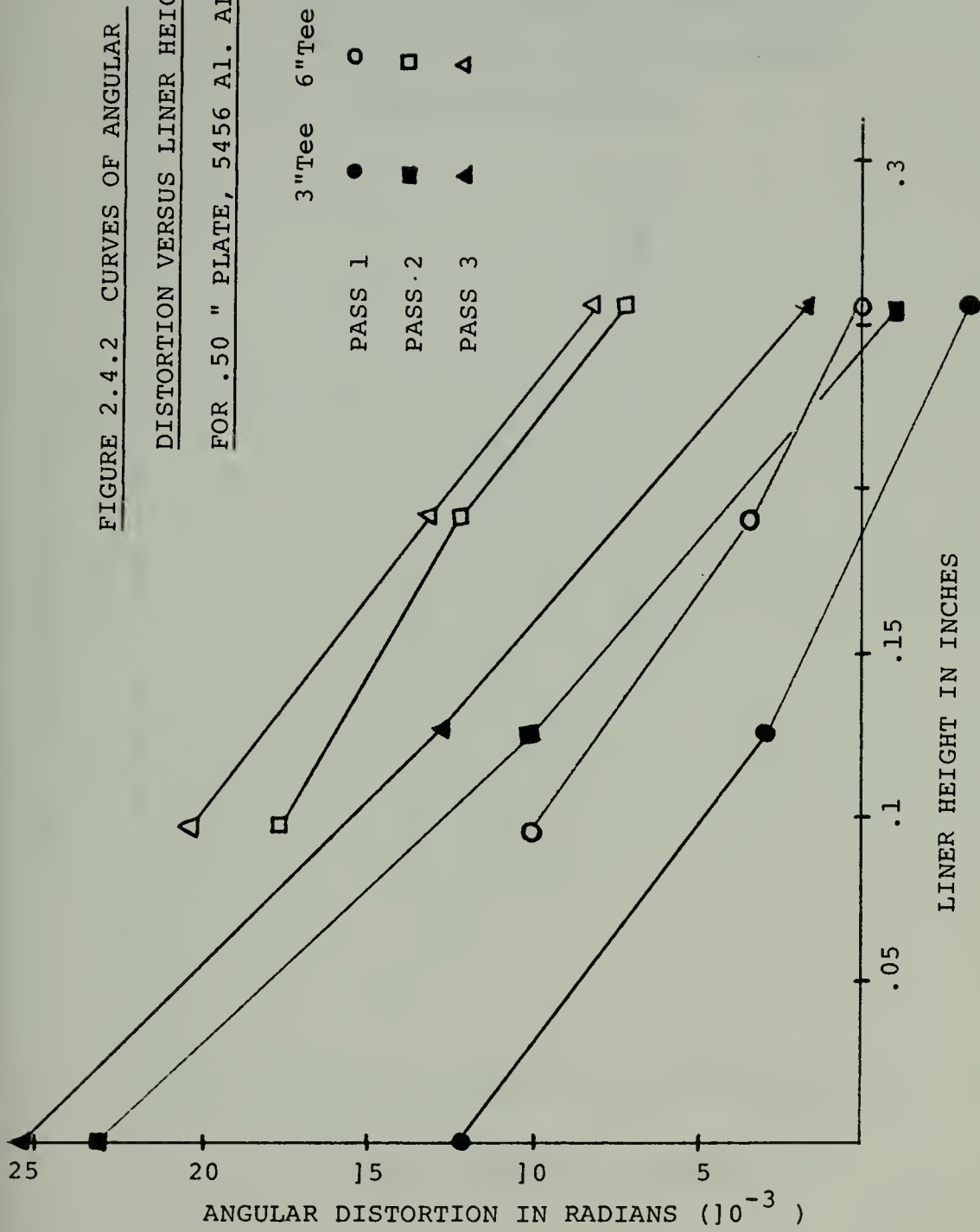
FIGURE 2.4.3 CURVES OF IDEAL LINER
HEIGHT VERSUS PLATE THICKNESS FOR A
TEE HEIGHT OF 3", 5456 Al. ALLOY
PLATE SIZE 24"x24"
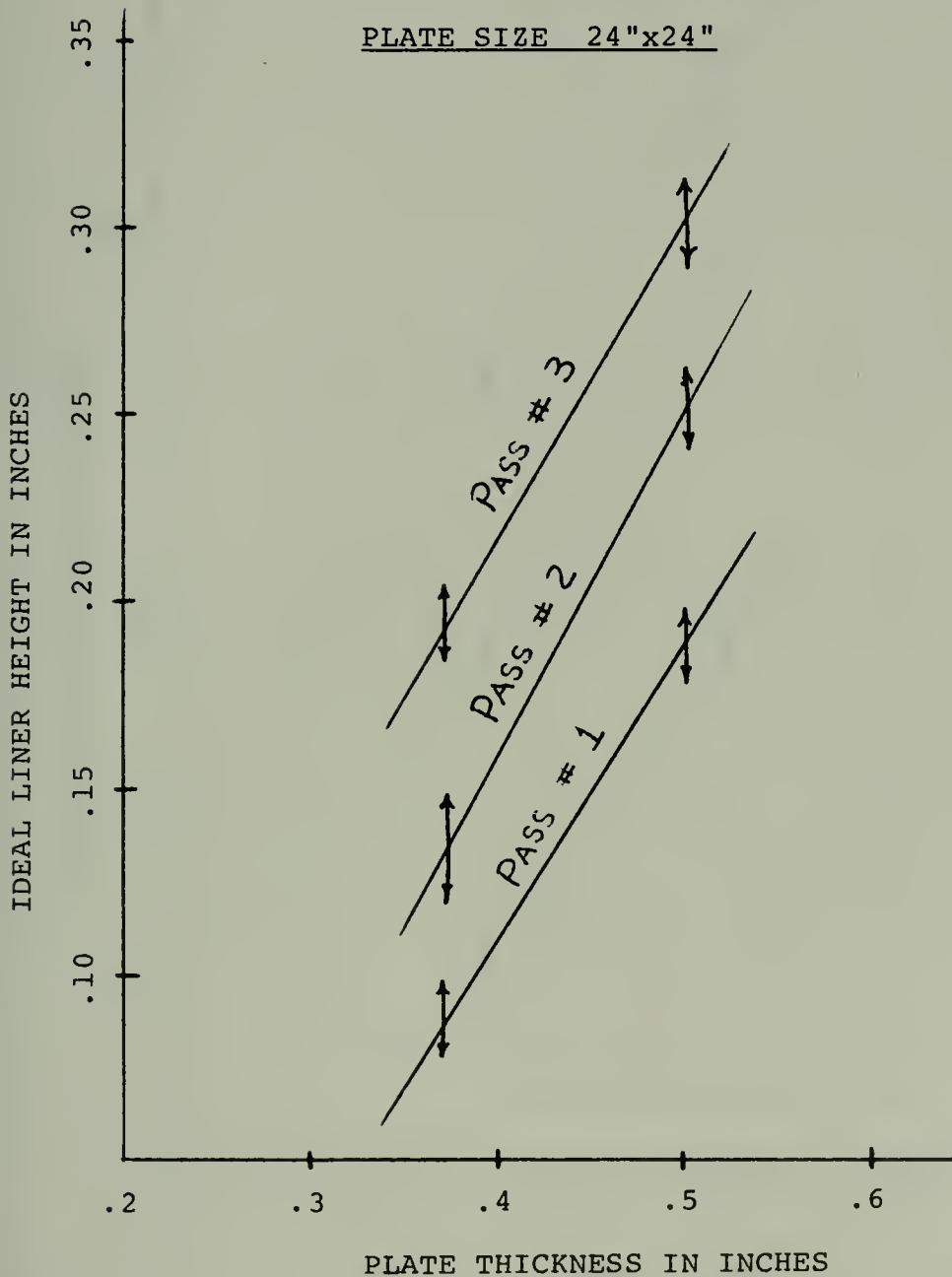
FIGURE 2.4.4   CURVES OF IDEAL LINER HEIGHT VERSUS PLATE THICKNESS FOR A TEE HEIGHT OF 6", 5456 Al. ALLOY, PLATE SIZE 24"x24"
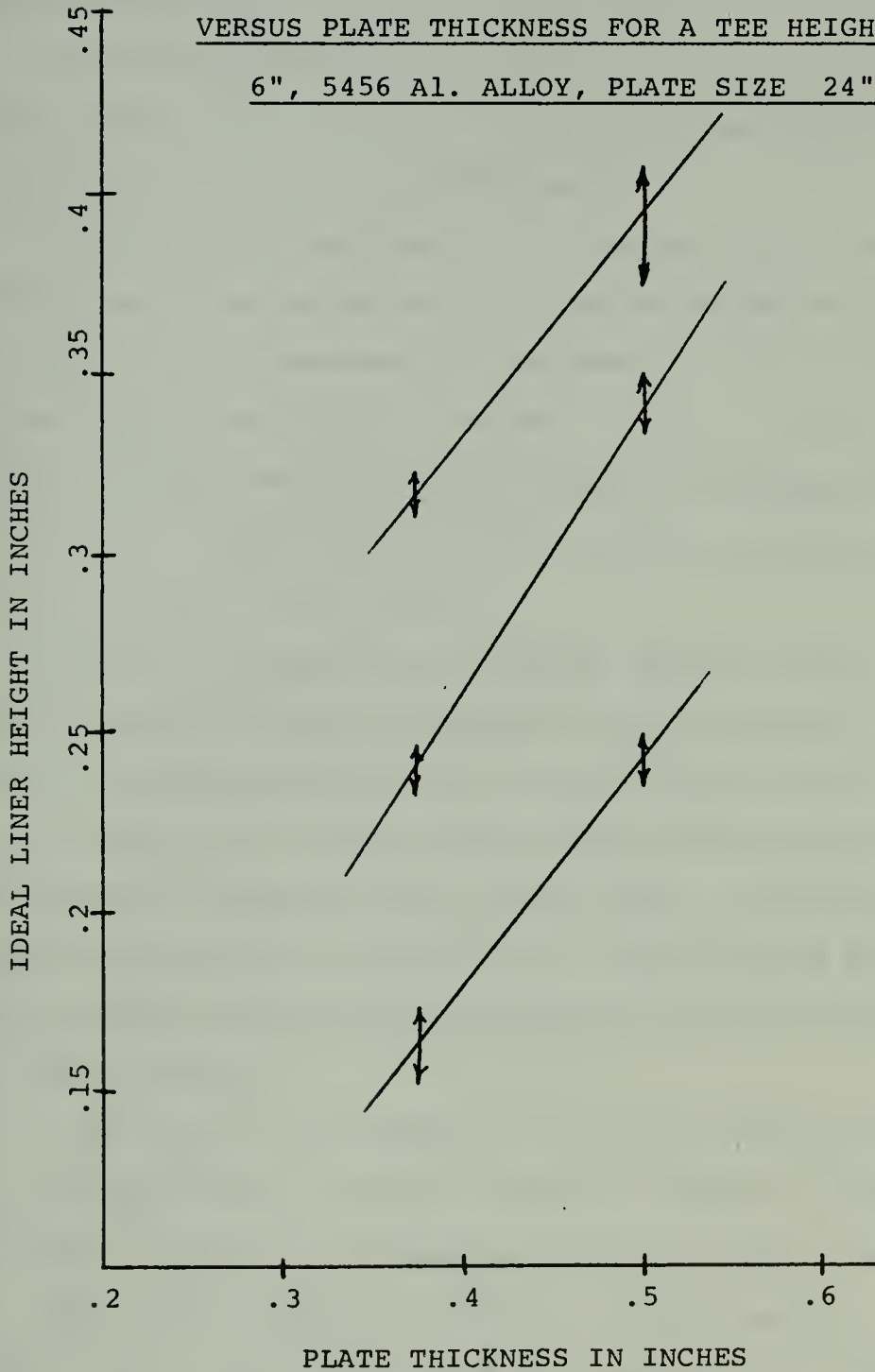
much of the work done on angular distortion in aluminum. Figure A.3 provides a reasonable analytic extension of the experimental data plotted on Figure 2.4.3.

Examining another tract in the interpretation of experimental results, the analysis now develops an industrial guideline for prestraining aluminum.

With reference to Appendix B, the assumption has been offered that by matching surface strains along the intended weld line, through prebending the shape to be fillet welded, angular distortion can be minimized. What is really being done is to match interior strain patterns because, for the simple shapes considered, strain is usually uniform and linear (for small deflections).

Appendix B supplies displacement versus strain for several aluminum plate thicknesses and weld spans. These figures are super-imposed on the data results from Figure 2.4.3 (3" tees), which plots plate thickness versus required deflection for minimum angular distortion. The combination of these two figures is Figure 2.5.1, Upper Plate Maximum Surface Strain Versus Plate Thickness, for 3" tees and 1, 2, and 3 passes.

To make use of this curve, enter with the plate thickness and required number of passes (given in material specifications), and find the required surface strain along the weld line. As an example, consider a job order for a 10 foot plate, 1/2" thick, of 5456 aluminum alloy with 3" tees located every foot.

FIGURE 2.5.1 MAX. UPPER STRAIN (TENSION) VERSUS PLATE THICKNESS FOR 3" TEES WITH 1,2, AND 3 PASSES
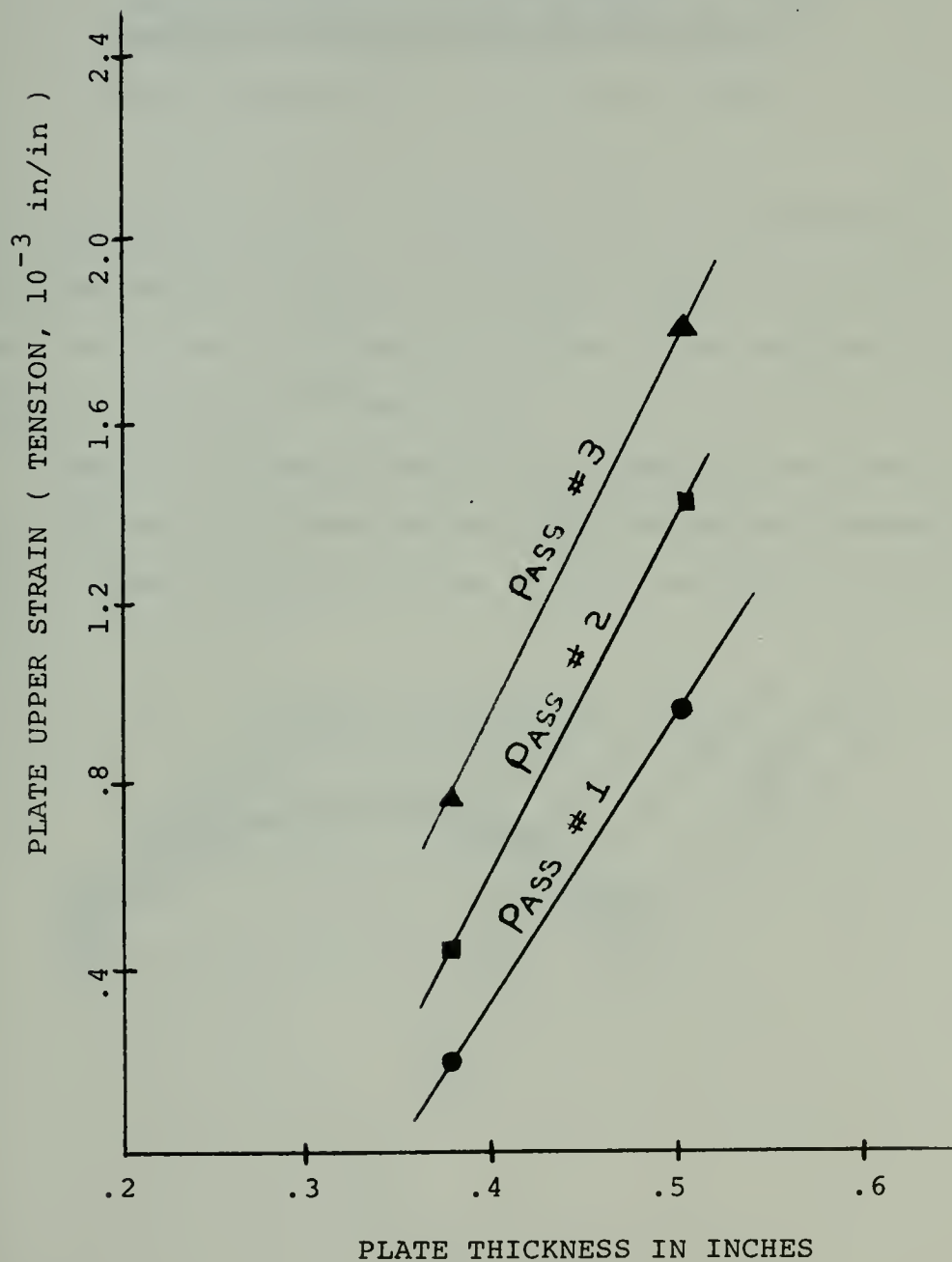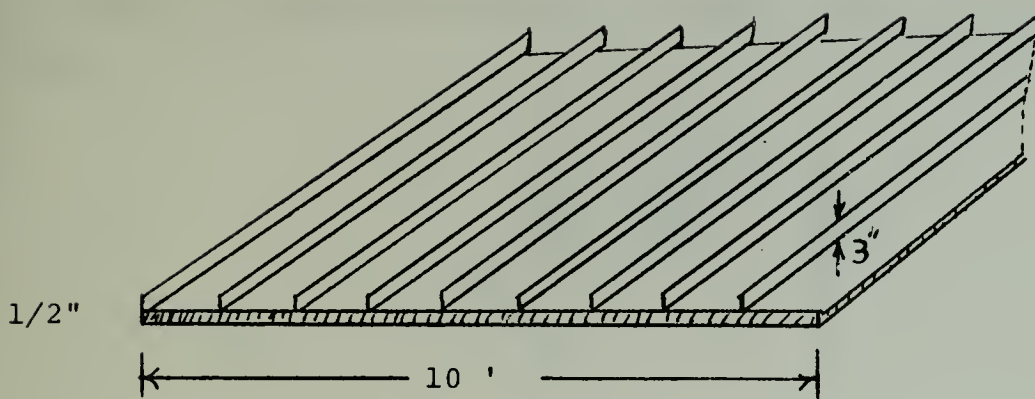
Specifications call for the plate to be GMA welded with
three passes per fillet. Entering Figure 2.5.1 at "t"
equal to .5" and 3 passes per fillet, the required surface
strain is 1.82×10^{-3} in./ in.

   Common industrial practice in handling the same distor-
tion problem with steel is to clamp the plate, before welding,
onto a curved platform in the form of an arc of a circle.
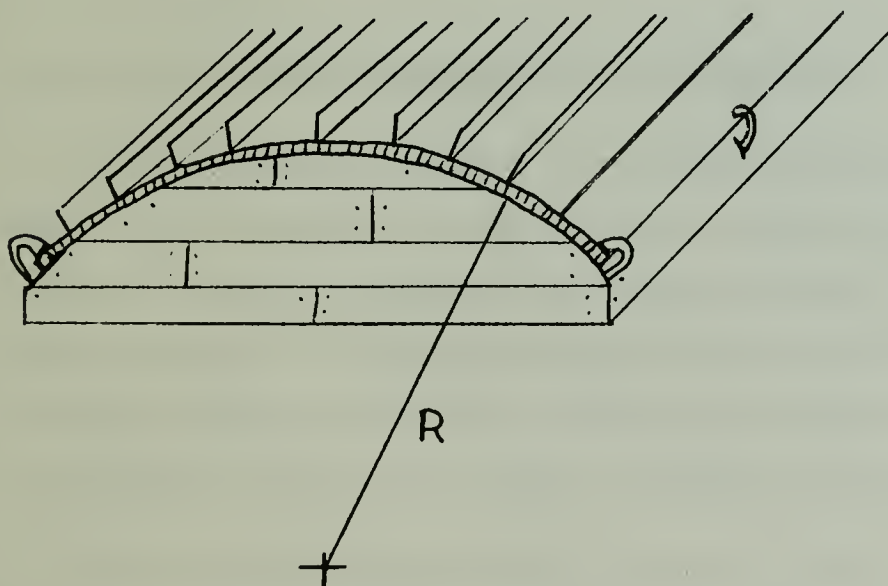
From Timoshenko [21] and Kumose [16], the formula for arc radius is found knowing plate thickness and surface strain.

$$R = t/2\varepsilon$$
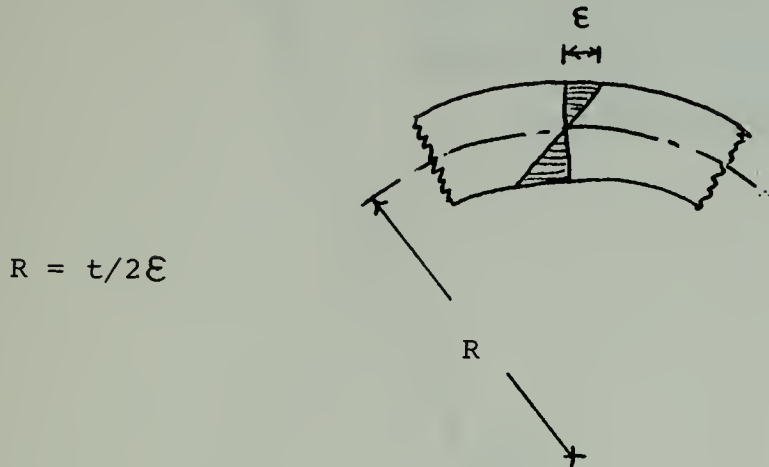
Figure 2.5.2, Plate Thickness Versus Arc Radius, takes the above equation for arc radius and applies it to Figure 2.5.1, Plate Thickness Versus Surface Strain.

In the specific example discussed above, using Figure 2.5.2, the manufacturer would be required to use an arc radius of 23 feet.

2.6 - Experimental Observations and Comments

A. The significant variance in welding speed (see Table 2.2.1) was due, in part, to the varying types of surface finish found on each different plate. The welding speed was found to be dependent on how fast the oxide coating could be broken down in front of the welding gun as it was moved down the weld line.

B. For consistency each "tee" was of the same thick-

FIGURE 2.5.2 ARC RADIUS VERSUS
PLATE THICKNESS FOR 3" TEES WITH
1,2, AND 3 PASSES
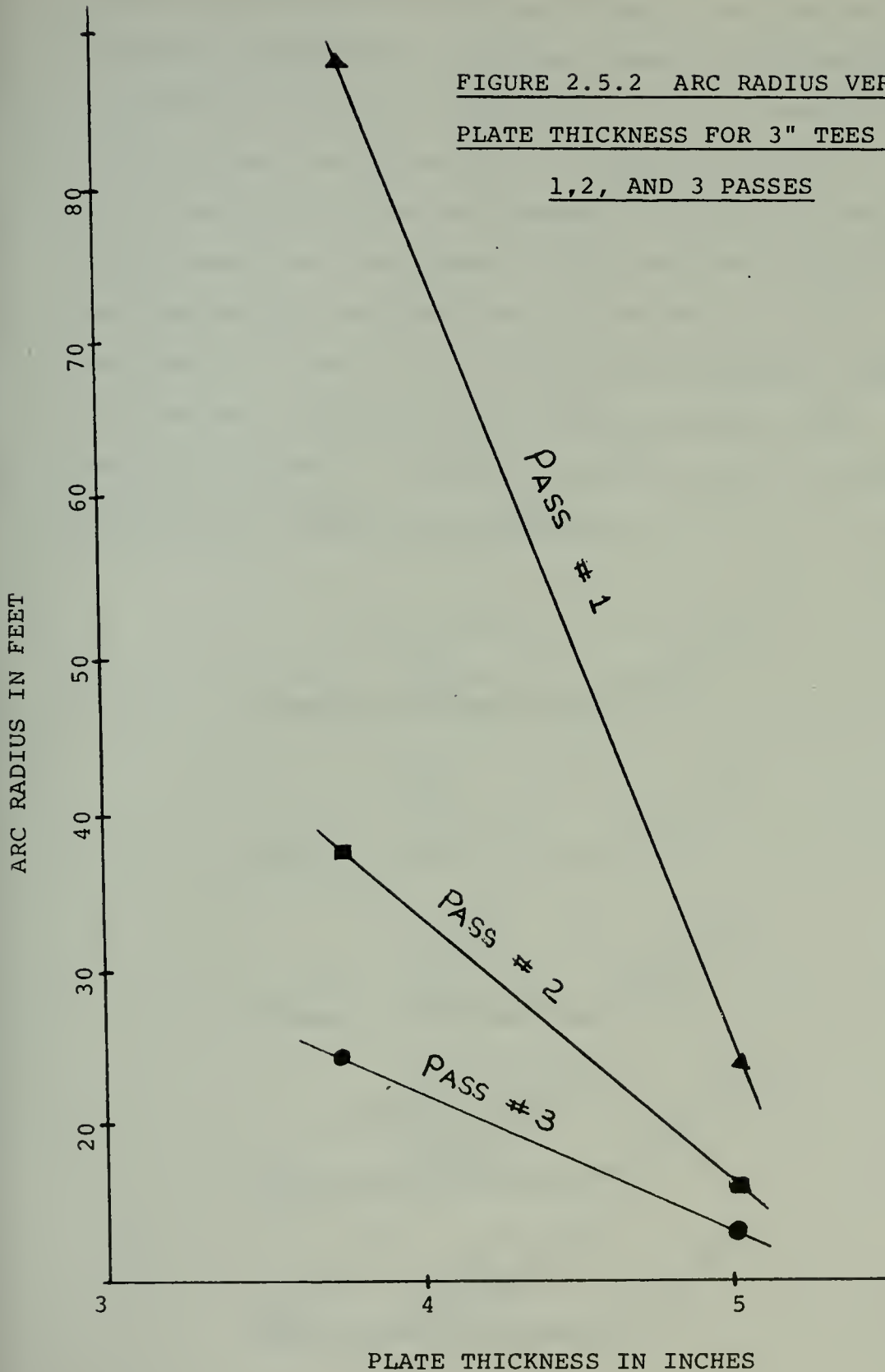
ness as the base plate flange since it was assumed
that the dimensions of the "tee" were not influencing
the amount of angular distortion. This assumption
was in error, as can be seen by comparing Figures
2.4.3 and 2.4.4. Further research should be conducted
with respect to the types of "tee" used and their effect
on longitudinal and rotational distortion. It is
believed that each of the combinations sketched below
will produce significantly different results when
similarly welded. Note all base plates have the same
lengths and widths and thicknesses.
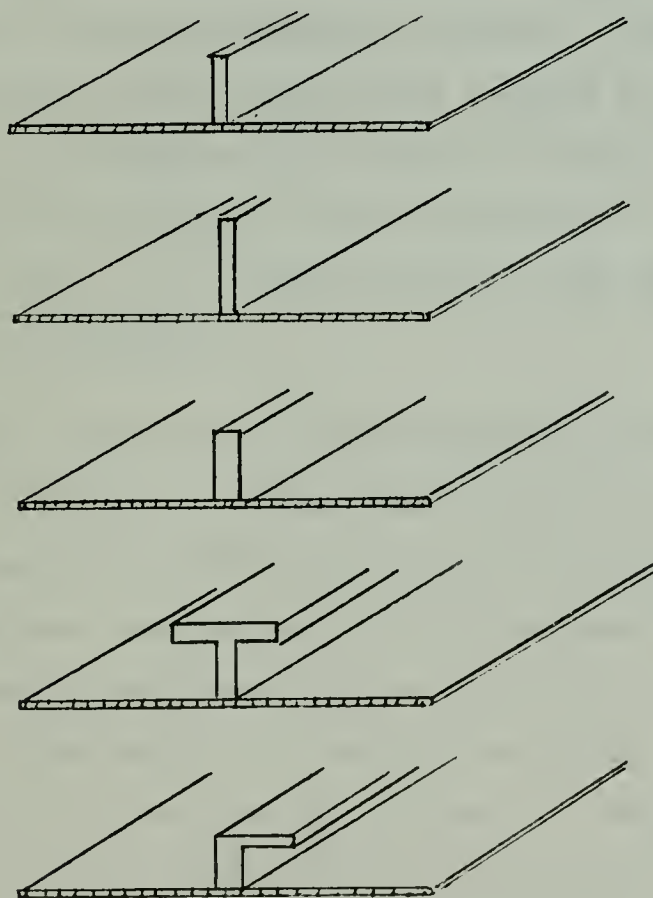
C. The interest in this experiment was only in out-of-plane angular distortion (rotation). Therefore, simple, straight, full passes were made with little concern for minimizing the other types of distortion. The assumption was made that, for small distortions, angular out-of-plane distortion was uncoupled from transverse and longitudinal distortion. Also assumed was that, at any transverse cut (away from end boundary effects), the two-dimensional picture of angular distortion would be similar.

However, experimental results showed that there was a variance up to 25% in angular distortion across the plate in the longitudinal direction, indicating a coupling with other distortions because of our welding procedure. To minimize this effect, future experimentors should use welding sequence techniques discussed in Chapter 1 while still maintaining the same heat input to the plate specimen.

D. Reliable data for this experiment was not obtained from the ¼" plates. Distortions, in both the angular and longitudinal directions, coupled with plate buckling to produce complex curvatures that were unsuitable for measurement and beyond the scope of this work to analyze. Plate buckling from butt welds has been analyzed, and is reviewed in reference 7 (Figure 27, page 27). No such graph exists at present for fillet welding.

2.7 - Conclusions and Recommendations

In conclusion, it has been found that prestraining aluminum alloy plate is an effective method of reducing out-of-plane angular distortion. The method can easily be incorporated into current plate welding processes with only small corrections to the numerical tape programs now used in plate assembly lines.

It is believed that this method of constraining is the most restrictive, allowing only a minimum of distortion during welding. Elastic prestraining can be compared to plastic preforming as a mechanical means of distortion reduction. In plastic prebending, the plate is bent over a die and then welded unconstrained. The inherent problem with this method is that the plate is allowed the full "free" angular distortion during welding. A small percentage error would be almost unnoticeable in the elastic prestraining method, but would become most obvious in plastic prebending because of the large angular change.

It should be understood that the results obtained in this chapter are useful only if similar welding conditions are used. The results, although representative, would not apply if another welding technique was substituted. The author realizes, that in modern plate fabrication subassembly lines, welding processes are far more efficient than the methods used in this experiment.

In recommending additional efforts to solidify what

is known about elastic prestraining, it should be pointed
out that this work is the first known effort in this par-
ticular area of distortion reduction. Reviewing Figure
A.3, it can be pointed out that the lines beyond .50" and
before .375" are merely approximate extrapolations. There
is no evidence to support their accuracy. The author
recommends that additional research be conducted to evaluate,
as a minimum, 1/4", 5/8", and 3/4" aluminum alloys.

Efforts should also be pointed at determining and
quantifying the coupling influences on out-of-plane angular
distortion.

Physical research is only one answer to the problem
of lack of data. In Chapters 3 and 4, an attempt is made
to simulate the fillet welding process by computer application.
It is not hard to envision future investigators conducting
only a few "representative" welding experiments and using
the computer, through simulation, to fill in the rest of
the necessary information.

3.0 - EXPERIMENTAL OBSERVATION OF OUT-OF-PLANE
DISTORTION IN FILLET WELDED ALUMINUM

3.1 - General

The objective of the next two chapters is to draw from
man's previous experience in computer technology and, in
particular, the predictability of heat input, temperature
distributions, strain and distortion, and mold the several
programs into one that can reliably simulate the actual
effects of welding. In this chapter a description of the
experiment performed and resulting observations will be
given. Chapter 4 will be the computer simulated follow-up
of this experiment.

3.2 - Preparation of the Experiment

Supporting jig

Figure 3.2.1 shows schematically the welding jig used
to support the test plate. Special care was taken to insure
that the distortions recorded were only those produced from
thermal strains. The jig was clamped to a rigid steel bed
that had both the ability to rotate and tilt.

Material and material properties

The material used in this experiment was aluminum-magnesium
structural alloy 5052-H32, strain hardened, and non-heat-

-57-

ROTATING BED

TEST PLATE

TO INSTRUMENTS

TEST PLATE

CLAMPS

TO INSTRUMENTS
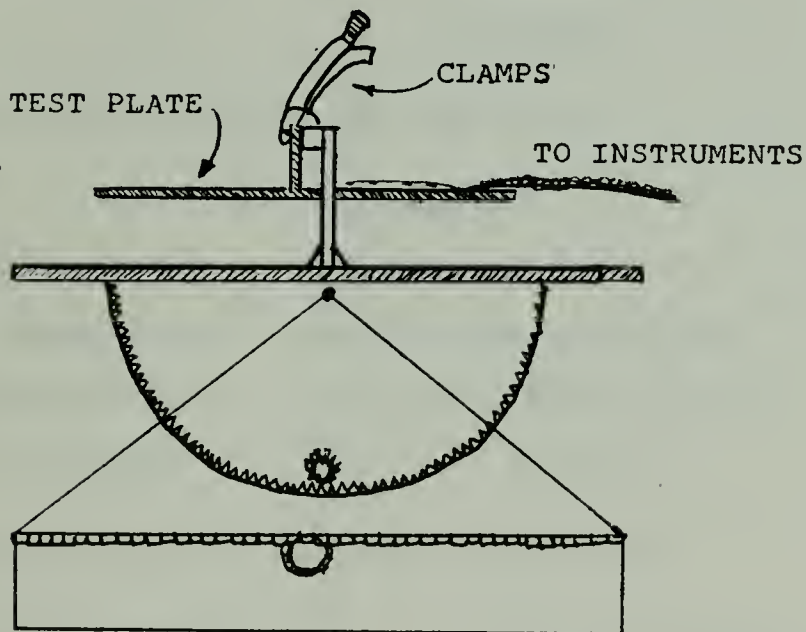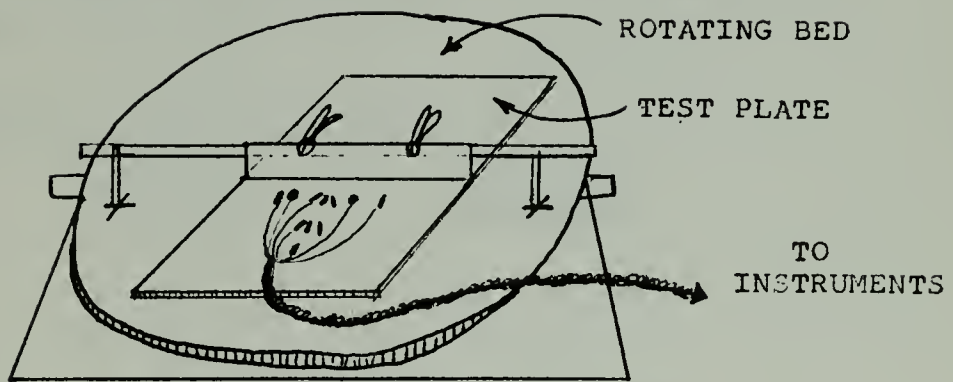
FIGURE 3.2.1

PICTORIAL SCHEMATIC OF THE TESTING SETUP

-57-

treatable. This material was selected because of its large
use in marine and general structural fabrications.

The characteristics and properties of the material
are as follows: [17, 18, 19, 20]

1. Chemical composition (typical)

Elements	Percentage
Mg	2.2 - 2.8
Mn	.10
Cr	0.15 - 0.35
Cu	.10
Zn	.10
Si + Fe	.45
Al	Remainder

2. Physical properties (room temperature)

density   .097 lbm/in^3

specific heat   .23 BTU/lbm ^{O}F

liquidus temperature   1120 ^{O}F (approximately)

thermal conductivity   .185 X 10^{-2} BTU/in sec ^{O}F

thermal diffusivity   8.2 X 10^{-2} in^2/sec

3. Mechanical properties (room temperature)

modulus of elasticity   10.2 X 10^6 PSI

modulus of rigidity   3.8 X 10^6 PSI

min. tensile strength   33 X 10^3 PSI

min. yield strength   28 X 10^3 PSI

poissons ratio   .334

-58-

Filler metal selection was based on ease of welding
and material on hand. Filler wire 4043 was used and had
the following chemical composition:

Element	Percentage
Mn	.05
Zn	.10
Mg	.05
Cu	.30
Si	4.5 - 6.0
Fe	.8
Ti	.2
Al	Remainder

Test Specimen

A 0.50 inch thick plate was used in this study because
of its ease of handling and two-dimensional characteristics.
With the welding conditions imposed, it would not approach
critical bending or buckling. Figure 3.2.2 shows a plate
layout with dimensions and locations of test gages.

Sensors and Instrumentation

1. Strain gages.

   Two types of gages were used in this investigation,
the SR-4 single foil element gage and the SR-4 rosette
(45 degree). Properties are listed below. [22]

FIGURE 3.2.2 TEST PLATE LAYOUT

SIDE A

SIDE B

5052-H32 Al. Alloy

1/2 in. gage plate

▮ - Single Strain Gage

\|/ - Rosette Strain Gage

● - Thermocouple

12"

18"

½"

2½"

1¼"

6"

4"

1½"
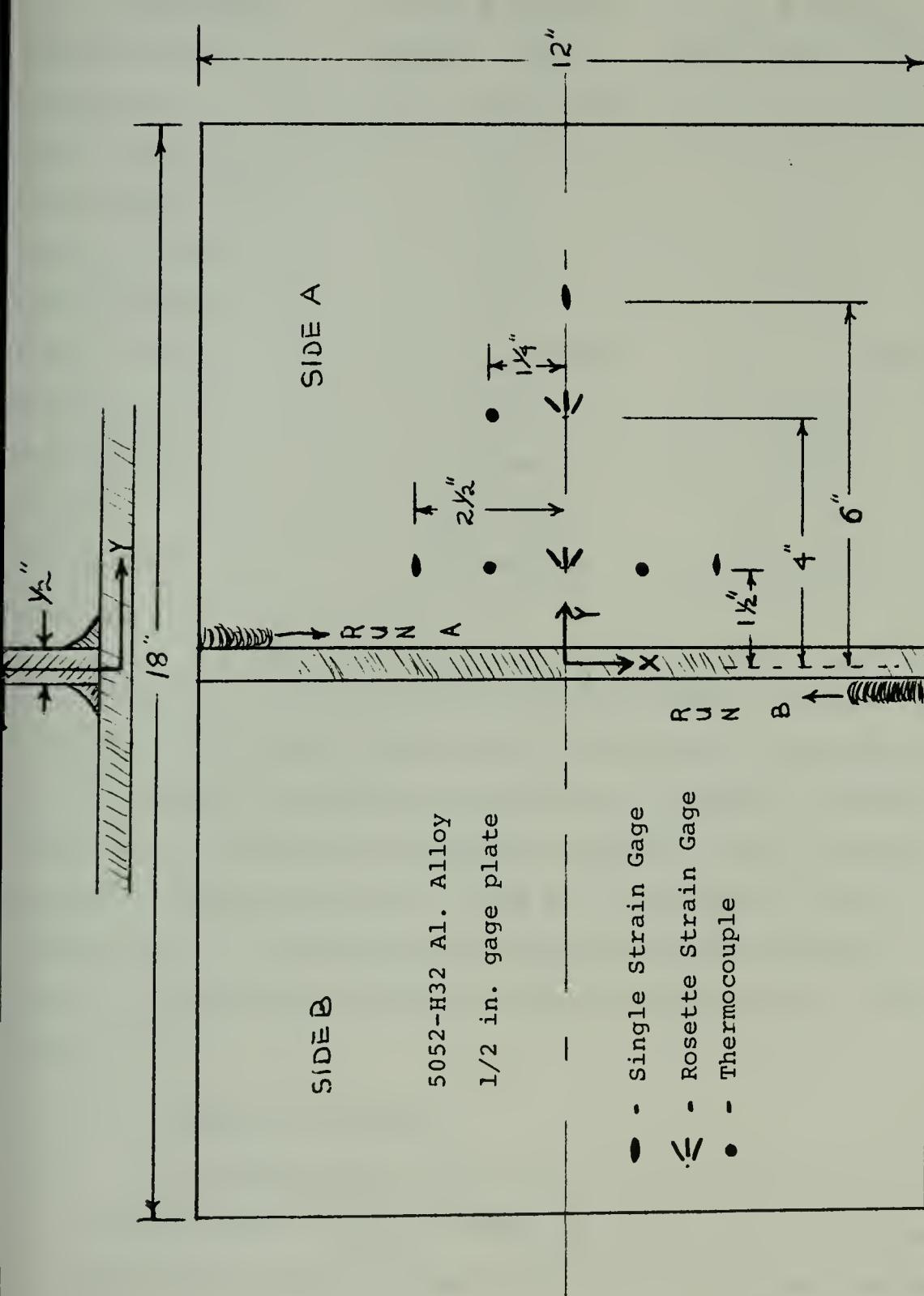
GAGE

Property	SR - 4 Single	SR - 4 Rosette
Designation	FAE-25-12S13	FAER-18RB-12S13-ET
Manufacture	BLH Electronics	BLH Electronics
Grid length (in.)	0.25	3 / 16
Grid width (in.)	0.13	0.90
Overall length (in.)	0.35	0.280
Overall width (in.)	0.13	0.54
Thermal Range	$- 50$ to $+ 400^{\circ}F$	$- 50$ to $+ 400^{\circ}F$
Resistance	120 Ω	120 Ω
Gage Factor	2.08	2.03
Cement	EPY - 550	EPY - 550
Protective	BLH Barrier	BLH Barrier
Covering	C	C

Figure 3.2.3 plots apparent strain versus temperature ($^{\circ}F$) for the single element and rosette strain gages respectively. This graph was experimentally derived by "baking" the test plate in an oven and recording the apparent strains and temperature. The graph will be used for an apparent thermal correction to the experimental strains because the gages were calibrated for a different type of aluminum base plate (2024). [23, 24]

2. Temperature sensors.

All temperature sensors used were chromel/alumel thermocouples made from Leads and Northrup No. 28 wires. Each thermocouple was spot welded onto the test specimen

Temperature in °F

50   100   150   200   250   300   350

SINGLE GAGE

ROSETTE GAGE

50 μ
100 μ
150 μ
200 μ
250 μ
300 μ
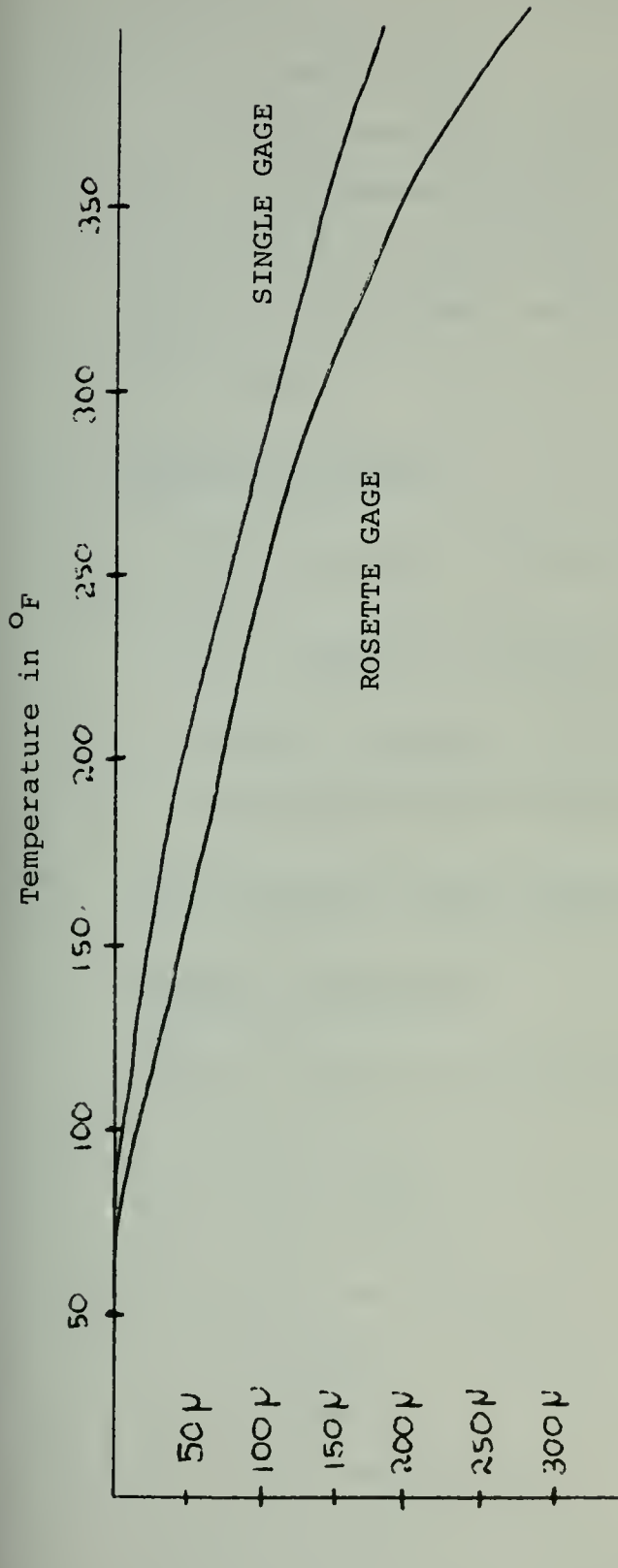
MICROSTRAIN (in./ in.)

BLH SR-4 Strain Gage

Apparent Strain Specimen   5052-H32

Cage Family   FAB FAE

Lot Number   277,284-1

Serial Number   4, ML

FIGURE 3.2.3   STRAIN GAGE APPARENT TEMPERATURE CHARACTERISTICS

and protected by No. 33 Sauereisen Sealing Cement.

3. Instrumentation.

Strain gages and thermocouples were connected to give a continuous read-out, as indicated schematically in Figure 3.2.4 and Figure 3.2.5. All circuits were fed into a Honeywell continuous-recording, 12 channel visicorder.

Welding Equipment

1. Power supply - An Airco 500 amp model 5DCR-224-A.

2. Wire feeder - Aircomatic head model AMH-D.

3. Welding process - GMA (MIG) process using an Airco model AMC-C, DCRP with Argon as a shielding gas.

3.3 - Conduct of the Experiment

Welding Conditions

Initial selected weld conditions are detailed below.

weld length	12 in.
nozzle speed	.3 in./sec.
wire feed speed	433 in./ min.
voltage	23 volts
current	290 amps
room temperature	78° F
arc length	0.50 in.
wire consumption rate	16 in./min.
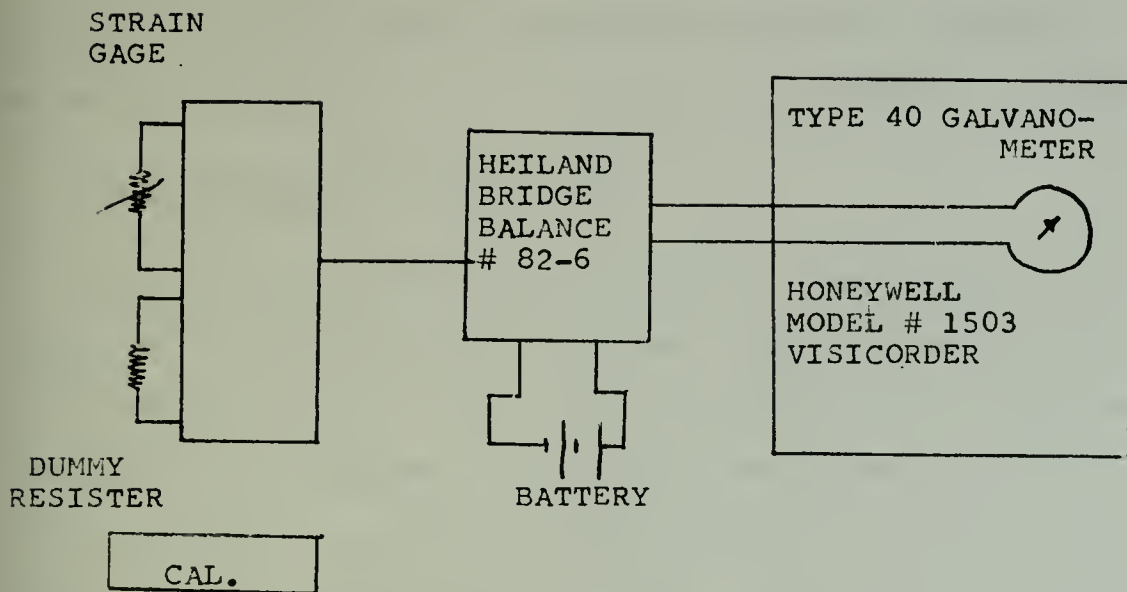
FIGURE 3.2.4   STRAIN GAGE INSTRUMENT CIRCUIT
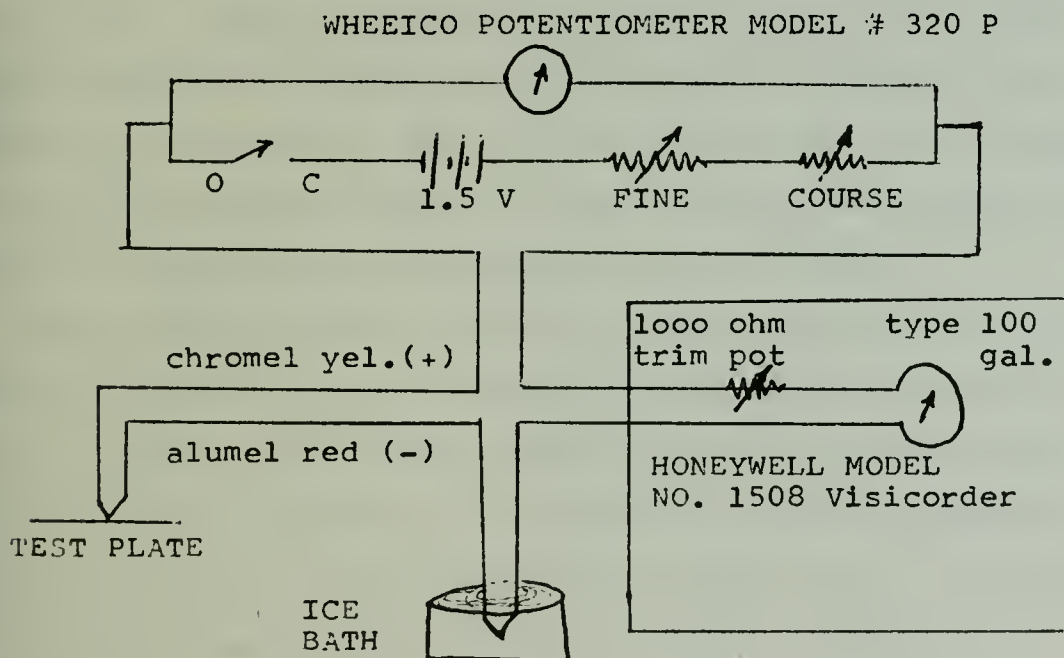
FIGURE 3.2.5   THERMOCOUPLE INSTRUMENT CIRCUIT

Wire feed speed was selected to insure a smooth, contin-
uous weld with as little "noise" and spatter as possible
because of its pick-up by the recorder as electronic distortion.

Experimental test procedure

The welding configuration is shown schematically in
Figure 3.2.1. The test specimen was jigged up and tilted
to approximately 45°. The instrumentation on the plate was
connected and calibrated to the instrument package. The
welding machine was lined up and positioned over the run-on
tab at the left end of the test jig. Welding speed and wire
feed speed (i.e., current and voltage) were set on the welding
machine. The recorder was activated and the arc struck in
the fillet. Marks were made on the recording paper as the
nozzle reached the plate, passed the plate centerline and
reached the plate end. The arc was extinguished as it passed
on to the run-off tab and while the recorder was running, the
plate was rotated 180 degrees and allowed to cool.

The welding machine was then realigned to weld the second
fillet. When the first series of thermocouples nearest the
weld registered below 150°F (approximately 10 minutes) the
second arc was initiated and allowed to run to the opposite
run-off tab in the same manner as the first pass. The plate
was again allowed to cool with the recorder periodically
running until asymtotic readings were reached. The plate
was then disconnected from the instrument package and con-
straining jig. During the exercise, readings were taken of
time, temperature, strain, weld length, travel speed, current,

voltage and appearance of the weld. Once the plate was
removed from the test stand it was measured for distortion.

3.4 - Results

Data Reduction

Since the results obtained from this experiment are to
be used in comparison with a computer simulated model producing
ϵ_y, ϵ_z, and γ_{yz}, it was not found necessary to resolve
the strain components into principle strains. After making
the appropriate "apparent thermal strain" corrections using
Figure 3.2.3, the actual strains from the rectangular rosette
(ϵ_a, ϵ_b, ϵ_c) were converted into ϵ_x, ϵ_y and γ_{xy},
using the matix equation below.

$$
\begin{bmatrix} \epsilon_x \\ \epsilon_y \\ \gamma_{xy} \end{bmatrix}
=
\begin{bmatrix} 1 & -1 & 1 \\ 0 & 1 & 0 \\ 1 & 0 & -1 \end{bmatrix}
\cdot
\begin{bmatrix} \epsilon_a \\ \epsilon_b \\ \epsilon_c \end{bmatrix}
$$

Plate temperature profile, timewise corrected for a
centerline reading, was plotted on Figure 3.4.1. The
resulting strains were plotted on Figure 3.4.2, Figure 3.4.3,
Figure 3.4.4, and Figure 3.4.5. Figure 3.4.6 represents
a two-dimensional centerline profile of resulting out-of-plane
distortion.

General Comments

1. There is some doubt as to the reliability of the

FIGURE 3.4.1 TIME-TEMPERATURE HISTORY OF

DOUBLE PASS WELD ON I/2" 5052

1.5 " from centerline

4. " from centerline

RUN A   RUN B

TEMPERATURE °F.
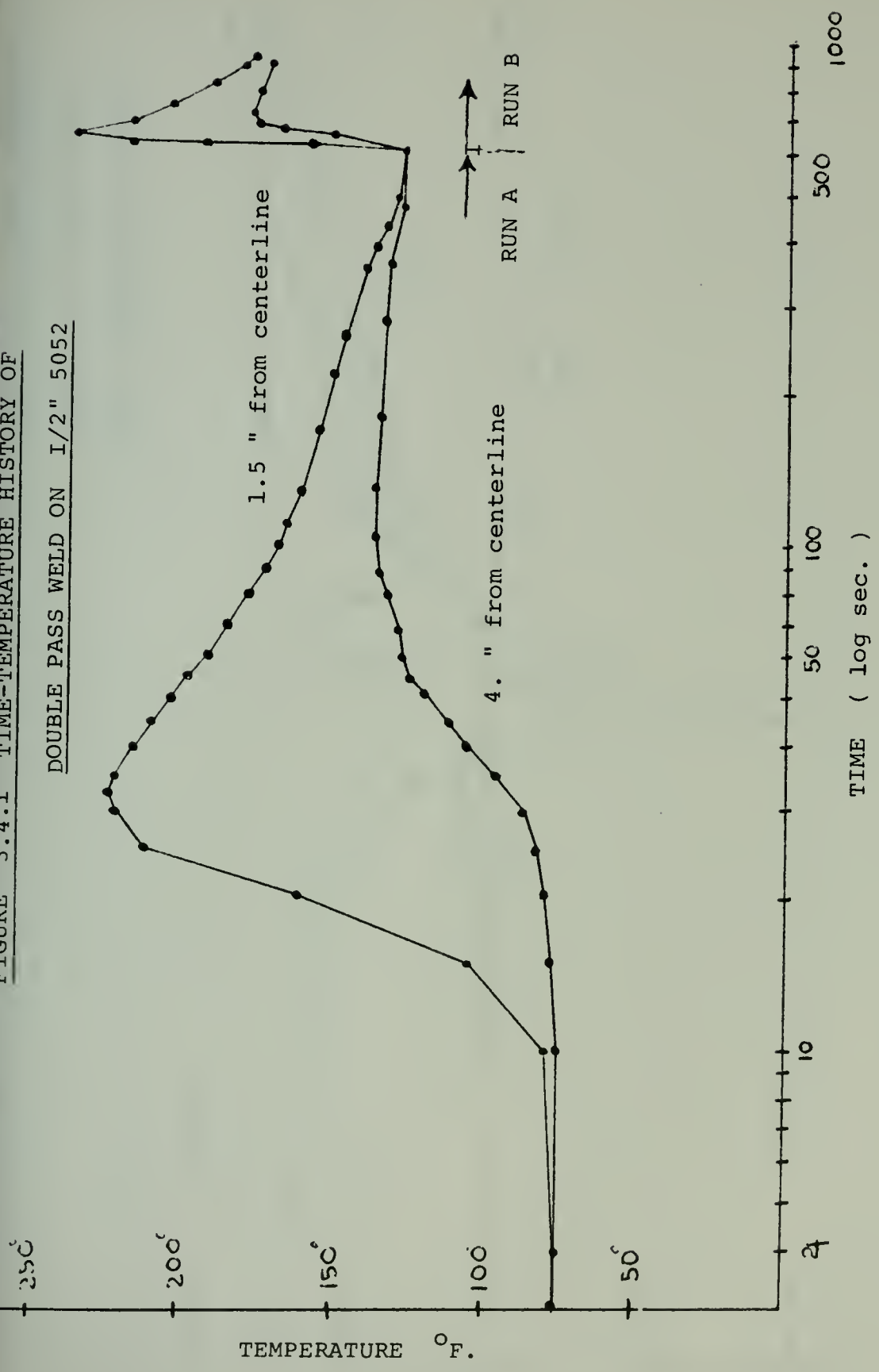
TIME (log sec.)

FIGURE 3.4.2   TRANSVERSE STRAIN VERSUS
TIME AT 1.5" FROM CENTER-
LINE   5052-H32 Al. ALLOY
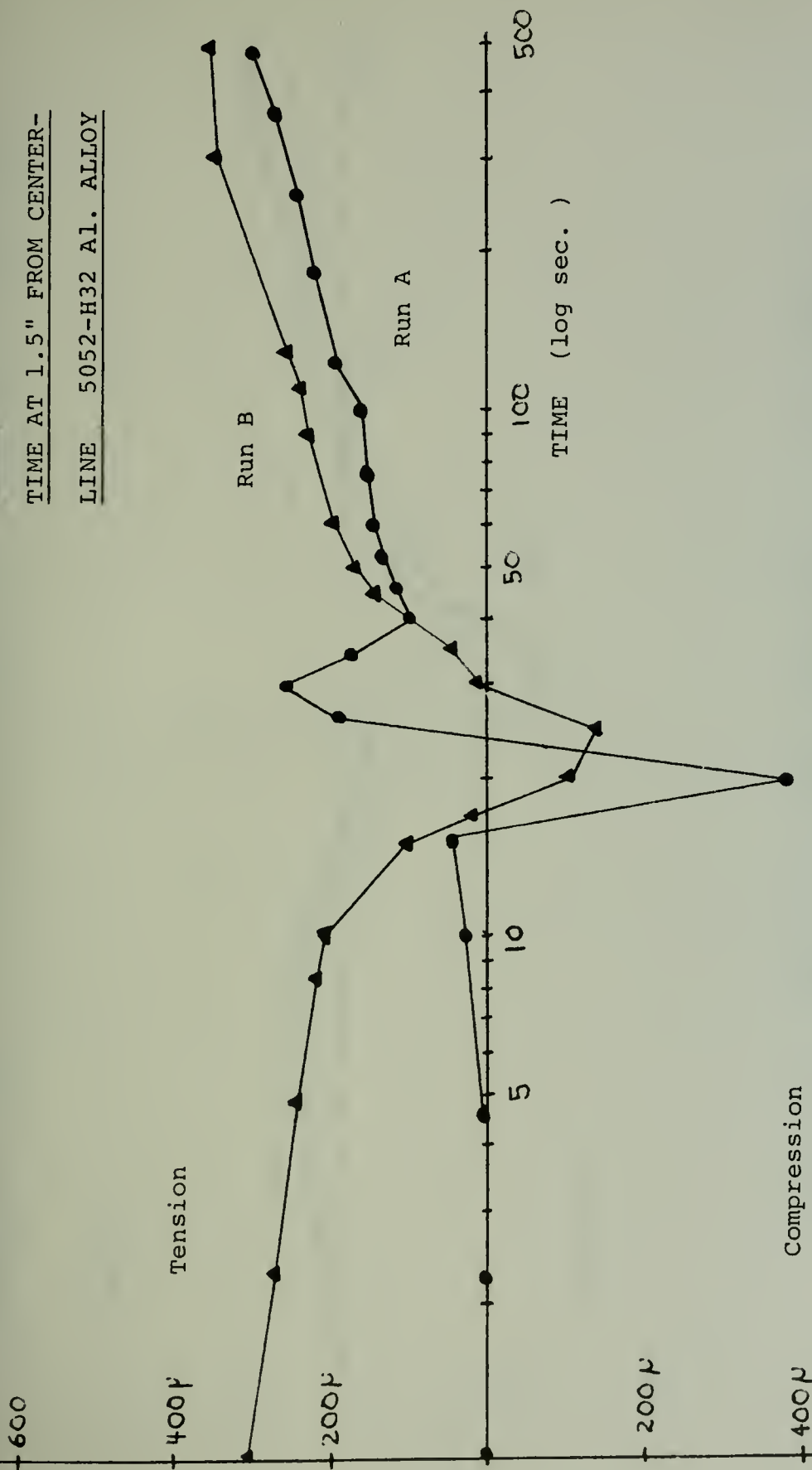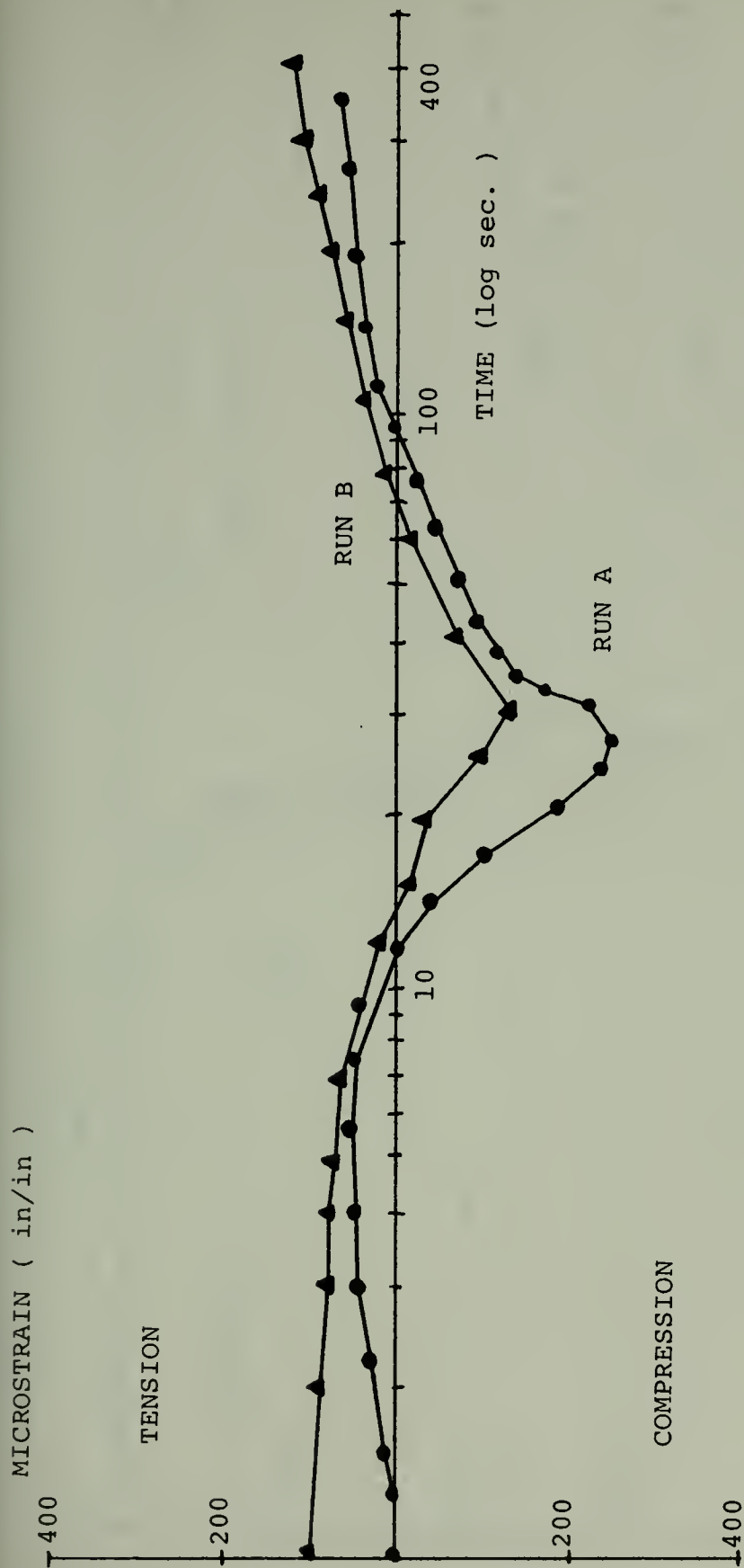
FIGURE 3.4.3 TRANSVERSE STRAIN VERSUS TIME AT 4" FROM CENTERLINE

FOR 5052-H32 Al. ALLOY
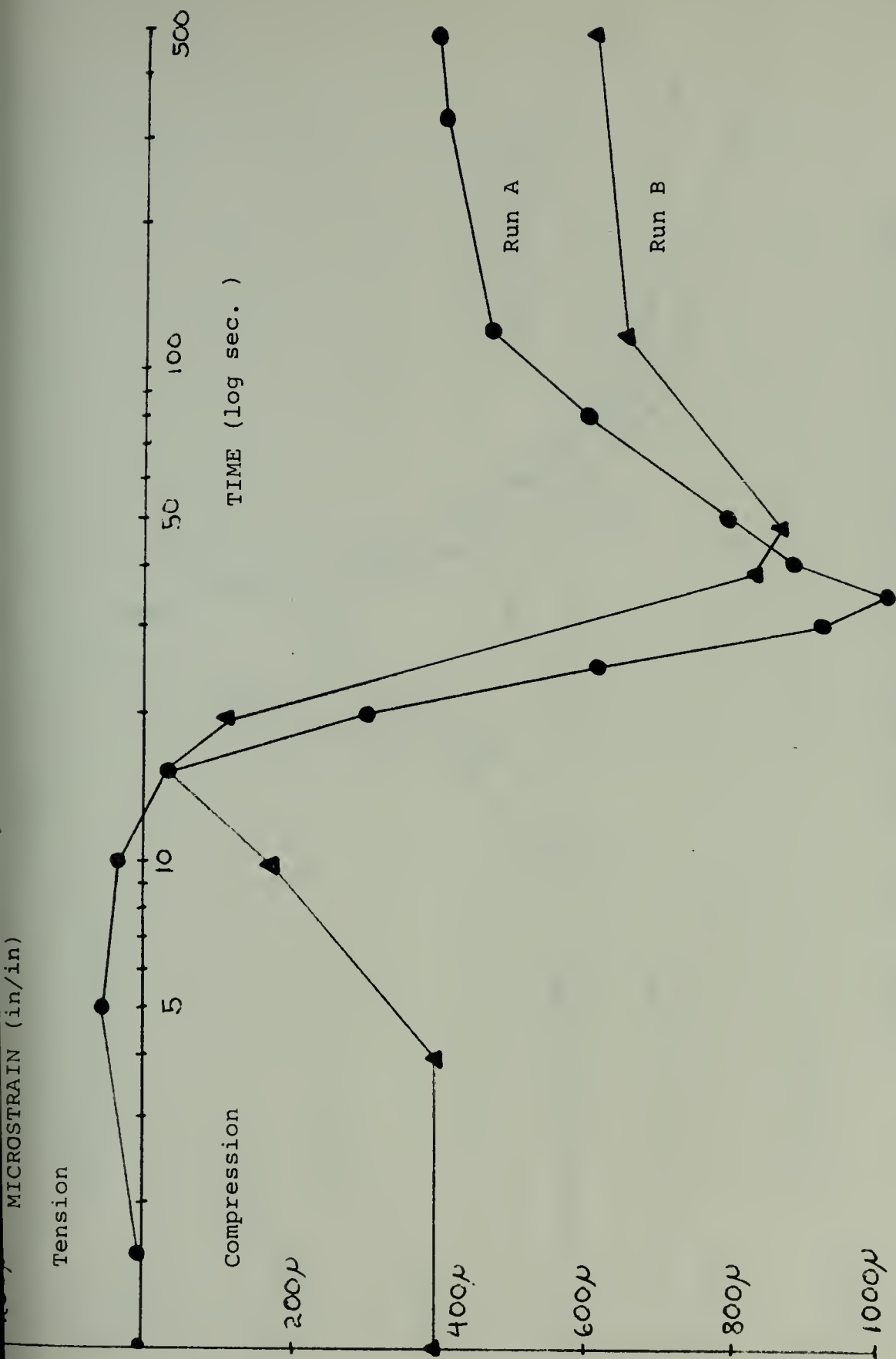
FIGURE 3.4.4   LONGITUDINAL STRAIN VERSUS TIME AT 1.5" FROM CENTERLINE
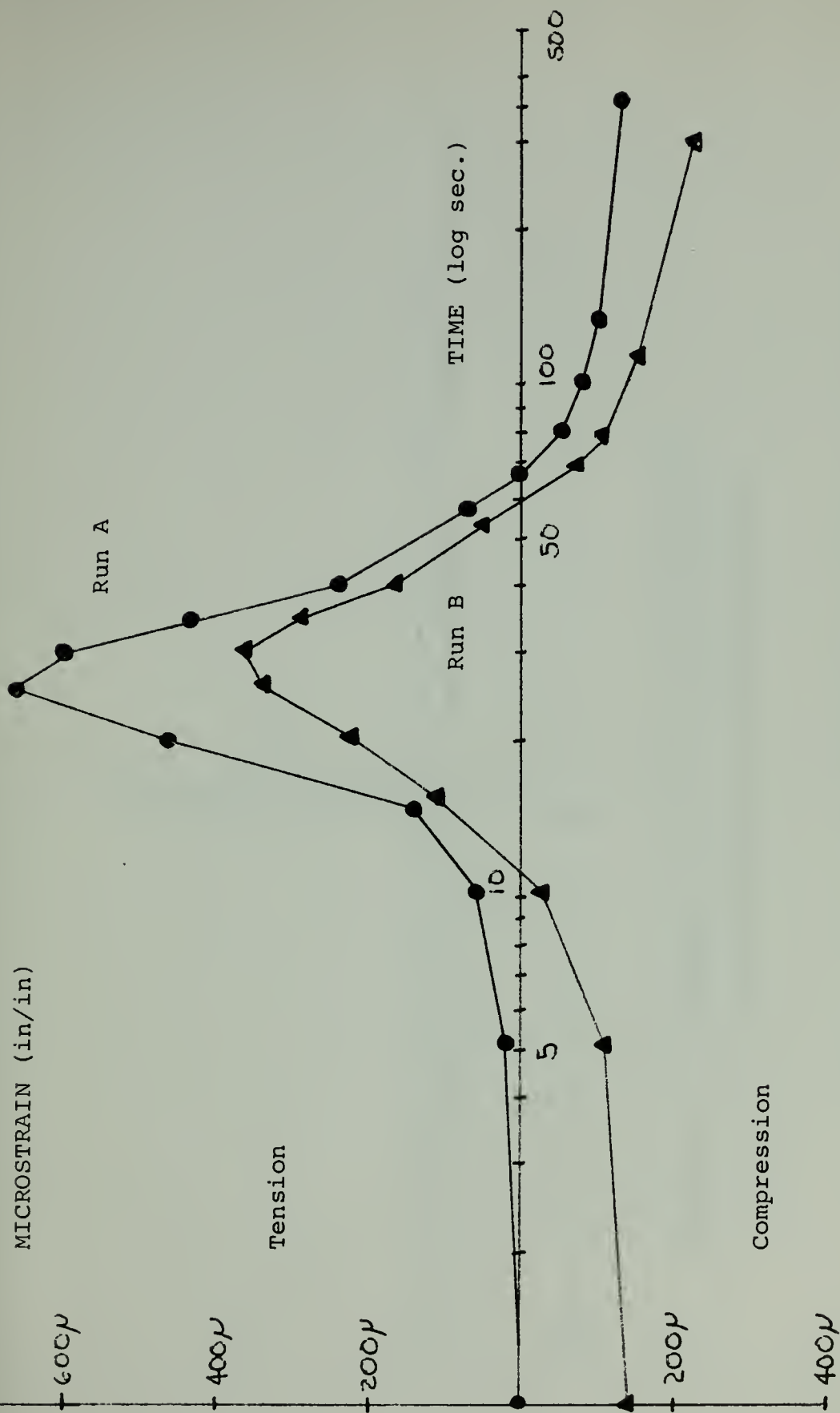
FIGURE 3.4.5 LONGITUDINAL STRAIN VERSUS TIME AT 4." FROM
CENTERLINE FOR 5052-H32 Al.ALLOY

-71-
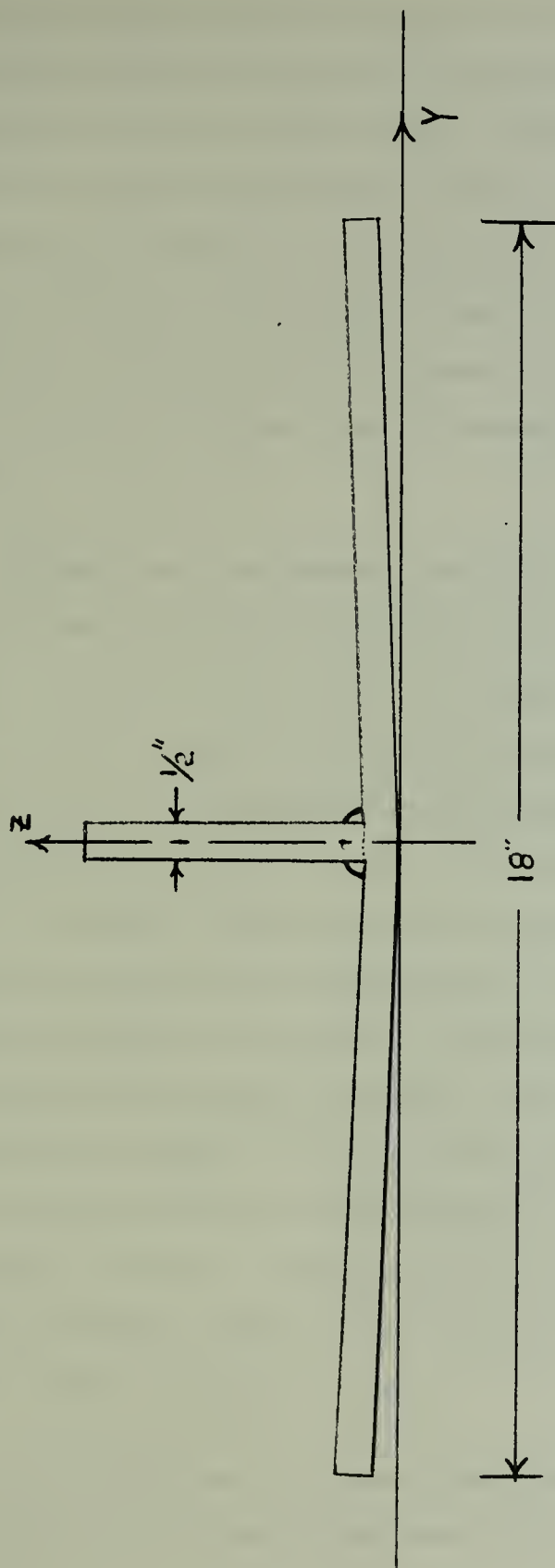
FIGURE 3.4.6 RESIDUAL ANGULAR OUT-OF-PLANE DISTORTION

OF TEST SPECIMEN 5052-H32 Al.ALLOY

welding machine used with respect to weld quality.
Although weld parameters such as speed, voltage, current,
and wire feed rate were closely monitored, the machine
could not duplicate the same weld, using the same
parameters. Although an efficiency of .75 for the
welding process was assumed, that efficiency shall be
adjusted in Chapter 4 to conform to actual heat input
as a function of experimental temperature profiles
(Figure 3.4.1).

2. Although the recommended welding procedures were
used during this experiment[18] (volts, amps, welding
speed, wire feed rate), the heat input did not generate
a very large temperature rise in the base plate (see
Figure 3.4.1). Subsequently, the strains developed on
the recorder were found to be of the same magnitude
as the apparent strains needed to correct the strain
gages for temperature compensation. Although the true
strains graphed on Figures 3.4.2 through 3.4.5 look
reasonable and compare favorably with trends observed
in previous works[6,22,25] it is the author's suggestion
that future experimentation diverge from recommended
parameters and use inputs geared to produce higher heat
inputs and temperatures. One method would be to use
slower nozzle traveling speed.

3. There should be increased development of experimen-
tal techniques in analyzing temperature and strains in

the region annexing the heat affected zone when welding
fillet welds. Most of the distortions and large gradiants
occur at this point, while the baseplate is little
affected except for transient thermal influences.

4. It was assumed that temperatures and strains were
uniform in the vertical plane and for that reason gages
were attached only to the top of the plate.

5. Longitudinal strain (ε_x) was recorded and plotted
(Figures 3.4.4 and 3.4.5) for comparative purposes; so
it might be justified, at this point, to note that
longitudinal strains dominated transverse strains at
both locations monitored (1.5" and 4.0" from centerline).
This factor will strongly influence the success of relying
only on two dimensions (y and z) in the computer model
tested in Chapter 4.

4.0 - COMPUTER ANALYSIS OF FILLET
WELDED ALUMINUM ALLOY

4.1 - General

In Chapter 3 the experimental model generated time-temperature and time-strain histories for fillet welded 5052-H32 aluminum alloy. In this chapter, using a simulated model of the experiment performed in Chapter 3, an elasto-plastic finite-element computer program will be used to examine thermal stresses and metal movement during welding.

It is not the objective of this work to describe details of the MIT program. This has already been done in several references. [25, 26, 27, 28] It is the objective of this chapter to test the state-of-art of computer technology at MIT with respect to accuracy and ability of current software to simulate fillet type welding.

This program has been evaluated against bead-on-plate, butt joints, and flame heating with good agreement between analytical predictions and experimental data. The program, at present, is being evaluated against not only fillet welds (in this work) but girth welding of a cylindrical shell, and thermal stresses and longitudinal distortion of a built-up tee-beam.

In this chapter the comparative analysis shall be based on temperature, strain (ϵ_y) history and residual

angular distortion (out-of-plane). The steps in analysis
shall be as follows:

a. Temperature analysis using approximate flat plate
    theory and inputs from the experimental test
    done in Chapter 3.

b. Temperature analysis using the MIT finite element,
    two-dimensional, program with

    1. constant property inputs as a function of
        temperature, and

    2. variable property inputs as a function of
        temperature.

c. Thermal stress and metal movement evaluation using
    MIT finite element, two-dimensional, program.

4.2 - Temperature Analysis by Analytical Solution

For relatively simple "flat plate" problems such as
bead-on-plate and butt welding, investigators have found
good agreement between observed and calculated results
using the Rosenthal equation for a quick and easy analy-
tical solution of temperature history. The basic equation
is laid out below.

$$T = T_o + \frac{q}{2\pi} e^{-\left(\frac{V_e w}{2k}\right)} K_o \left(\frac{V_e}{2k} r\right) \quad ,$$

where

$$q = \frac{1}{t} \eta \; 0.24 \; V \; I \quad ,$$

$$r = \sqrt{w^2 + y^2} \quad ,$$

$$w = x - V_e \cdot T_i \quad , \text{ and}$$

K_o is a modified Bessel function of

second kind and zero order,

T is temperature (°F),

T_o is initial temperature (°F),

V is voltage,

I is current (amps),

η is welding efficiency,

q is intensity of heat source,

k is thermal conductivity,

t is plate thickness (inches),

y is the welding coordinate perpen-

dicular to weld path (x),

T_i is time (seconds), and

V_e is welding speed (inch/second).

This form of analysis was chosen as a first approxima-
tion to the actual experiment. For entering arguments
the values below were brought forward from Chapter 3.

$$t = .50 \text{ in.}$$

$$V = 23 \text{ Volts}$$

$$I = 270 \text{ amps}$$

-77-

$$T_o = 78^\circ \text{ F}$$

$$\eta = 75\% \quad \text{(reference 3, page 4-4)}$$

$$k = .185 \times 10^{-2} \frac{\text{BTU}}{\text{in sec } ^\circ\text{F}}$$

$$V_e = .3 \text{ in/sec}$$

Other input values required by the one-dimensional program were also brought forward from Chapter 3. They are shown below.

$$c_p = .23 \frac{\text{BTU}}{\text{lb } ^\circ\text{F}} \quad ,$$

$$\rho = .097 \text{ lb/in}^3 \quad .$$

Also needed were

$$\text{Thermal power} = 4.97 \text{ BTU/sec} ,$$

$$\text{Heat intensity} = 9.94 \text{ BTU/sec} ,$$

$$\text{Melting temperature} = 1120^\circ \text{ F} \quad .$$

Figure 4.2.1 compares experimental results with the approximate flat plate temperature solution. Possible reasons for the large disparity are listed below.

a. Material properties and yield criterion are not constant throughout the range of observed temperatures.

b. A flat plate is too simplified for use as a model in approximating the temperature distribution around the fillet during welding.

FIGURE 4.2.1. PLATE THICKNESS VERSUS TIME
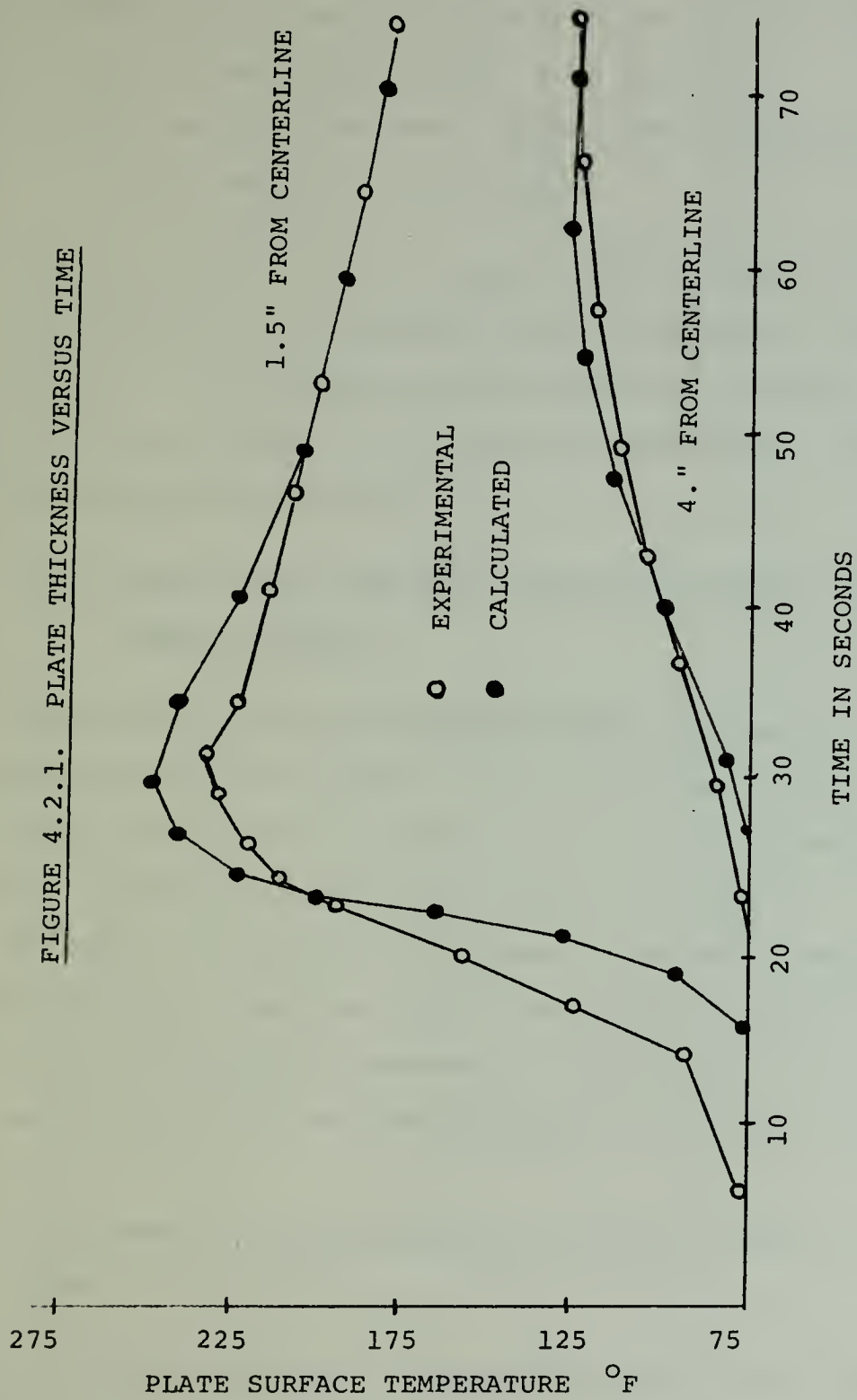
c. The analytical solution assumes a concentrated
   heat source when in actuality the heat is applied
   over a large area (about ¼ to ½ inch).

d. The specimen has some finite size not accounted for
   by the analytical solution.

At this point, the analytical, one-dimensional, solu-
tion was dropped as a realistic tool in describing fillet
welding. It is believed that one-dimensional programs,
while useful as a guide for simplified geometrics, cannot
handle complex arrangements.

4.3 - Temperature Analysis by Two-Dimensional, Finite
   Element Program

The MIT heat flow and thermal stress programs are
formulated based on the generalized variational principle,
and include temperature dependence of material properties,
as well as, yield criterion and effects of bending.

A simple mesh pattern was chosen in order to reserve
computer storage space for short time steps (1 second) and
long time intervals (1200 seconds). Figure 4.3.1 shows
the mesh pattern used for the analysis of the fillet weld
area.

The boundary conditions used in the mesh model are
as follows:

a. Elements located in the fillet area do not exist
   before the heat source (filler wire) pass.

- 80-

FIGURE 4.3.1 FINITE ELEMENT MESH PATTERN

SCALE 1" = 1"

SCALE 1" = 2"
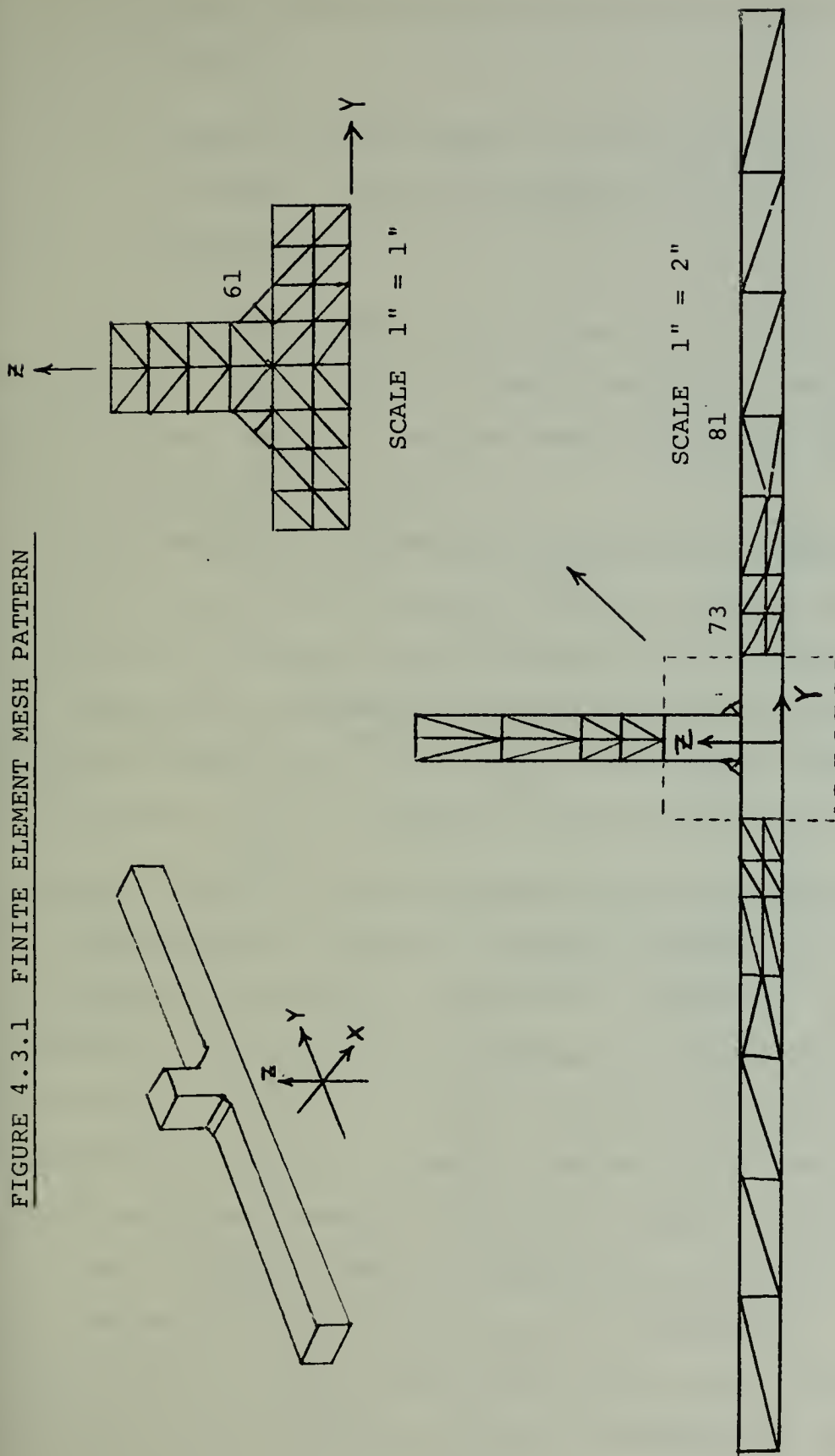
REFERANCE APPENDIX D FOR NODE AND ELEMENT NUMBERING AND LOCATION

b. Molten fillet elements have zero rigidity and
    stress.

c. Elements in the upper tee are considered fixed
    in space. All other elements are free of external
    constraints.

A further assumption made is that for a first approx-
imation heat input shall be a point source located at node
61. The heat input is constant over a .9 second time
(the x coordinate) interval.

The temperature dependent properties of thermal con-
ductivity, density and specific heat are plotted versus
temperature on Figures 4.3.2 through 4.3.4, respectively.
For simplicity, straight line approximations were made
from the given data. [29,30,31,32] Since thermal diffusivity
(λ) equals $\dfrac{k}{c_p}$, Figure 4.3.5 was plotted with the
calulated values of thermal diffusivity versus temperature.

Reviewing the variance of thermal diffusivity over
the expected temperature range (80° F - 1200° F), it is
noted that λ varies by only a maximum of 3% from λ at room
temperature. Since the change in thermal diffusivity can
be equated to material property variance with temperature,
it can be assumed that, for 5052-H32, material properties
are nearly constant over the temperature range expected.
This assumption is only applicable for temperature calcu-
lations and was tested successfully with a small test
program. It was therefore assumed unnecessary to include

-82-

FIGURE 4.3.2 THERMAL CONDUCTIVITY VERSUS

TEMPERATURE FOR 5052-H32 Al. ALLOY [30]
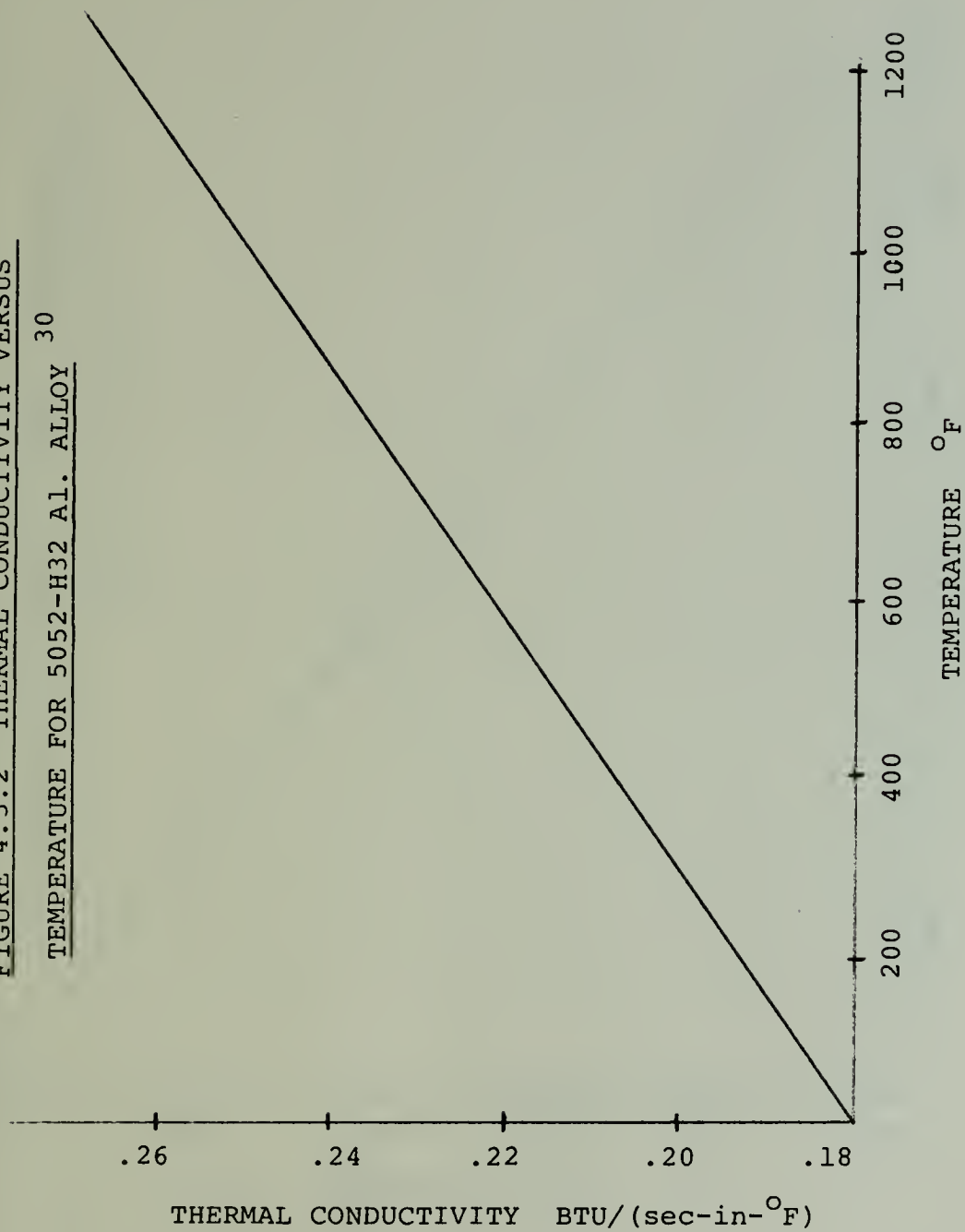
FIGURE 4.3.3 DENSITY VERSUS TEMPERATURE FOR 5052-H32 Al. ALLOY 29,30,31
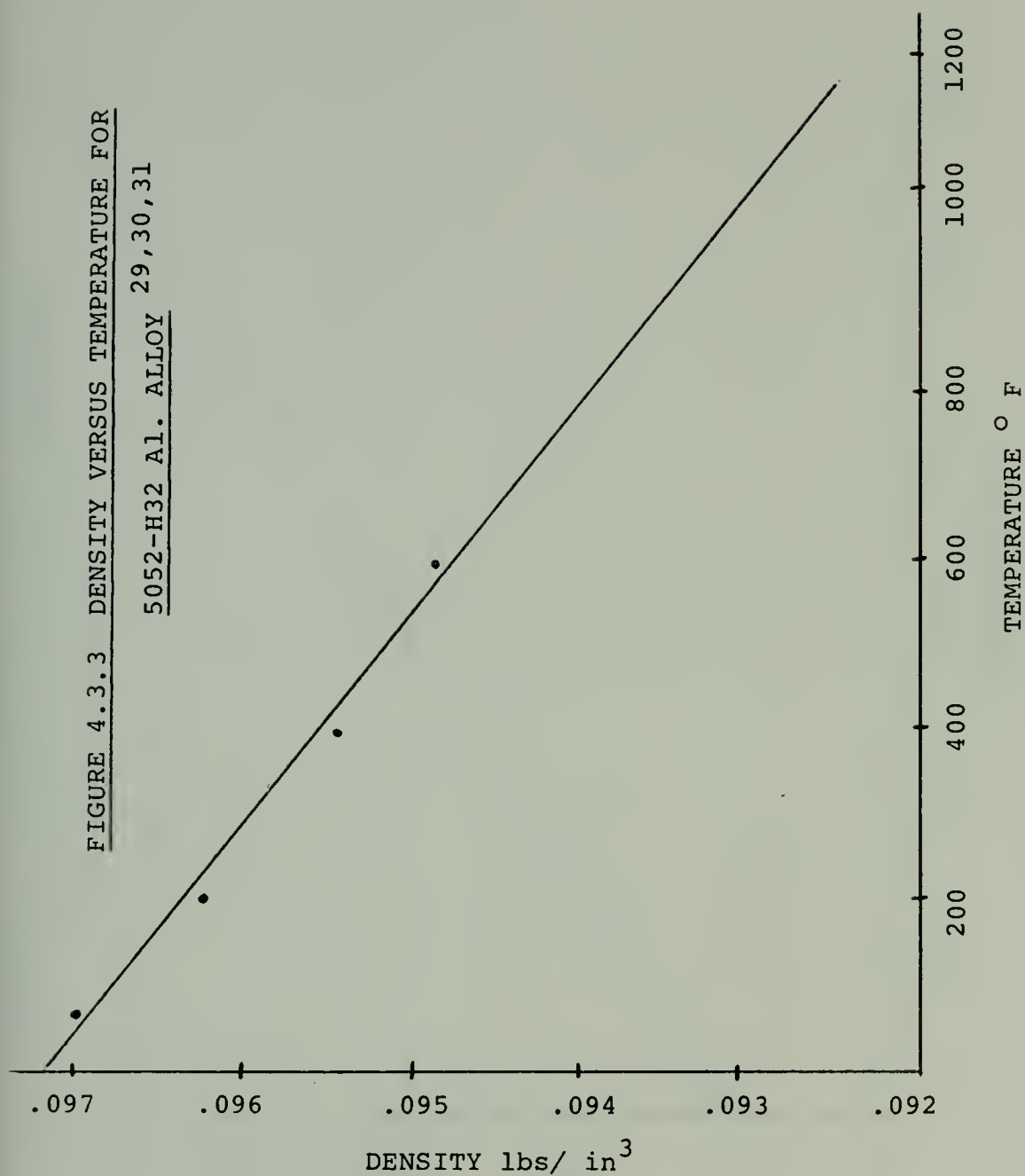
FIGURE 4.3.4 SPECIFIC HEAT VERSUS TEMPERATURE

FOR 5052-H32 Al. ALLOY 29,31
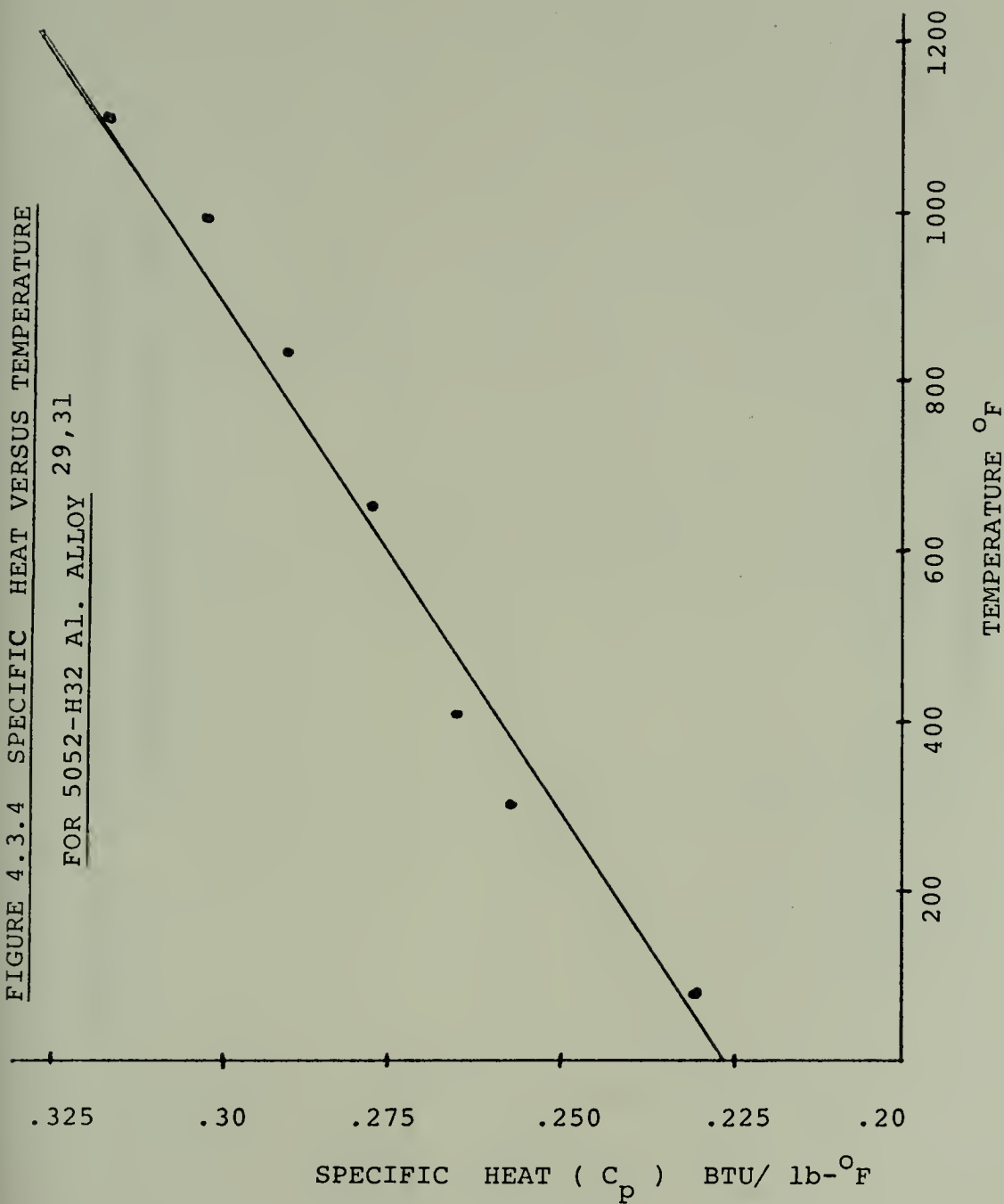
FIGURE 4.3.5   COMPUTED THERMAL DIFFUSIVITY VERSUS

TEMPERATURE FOR 5052-H32 Al. ALLOY
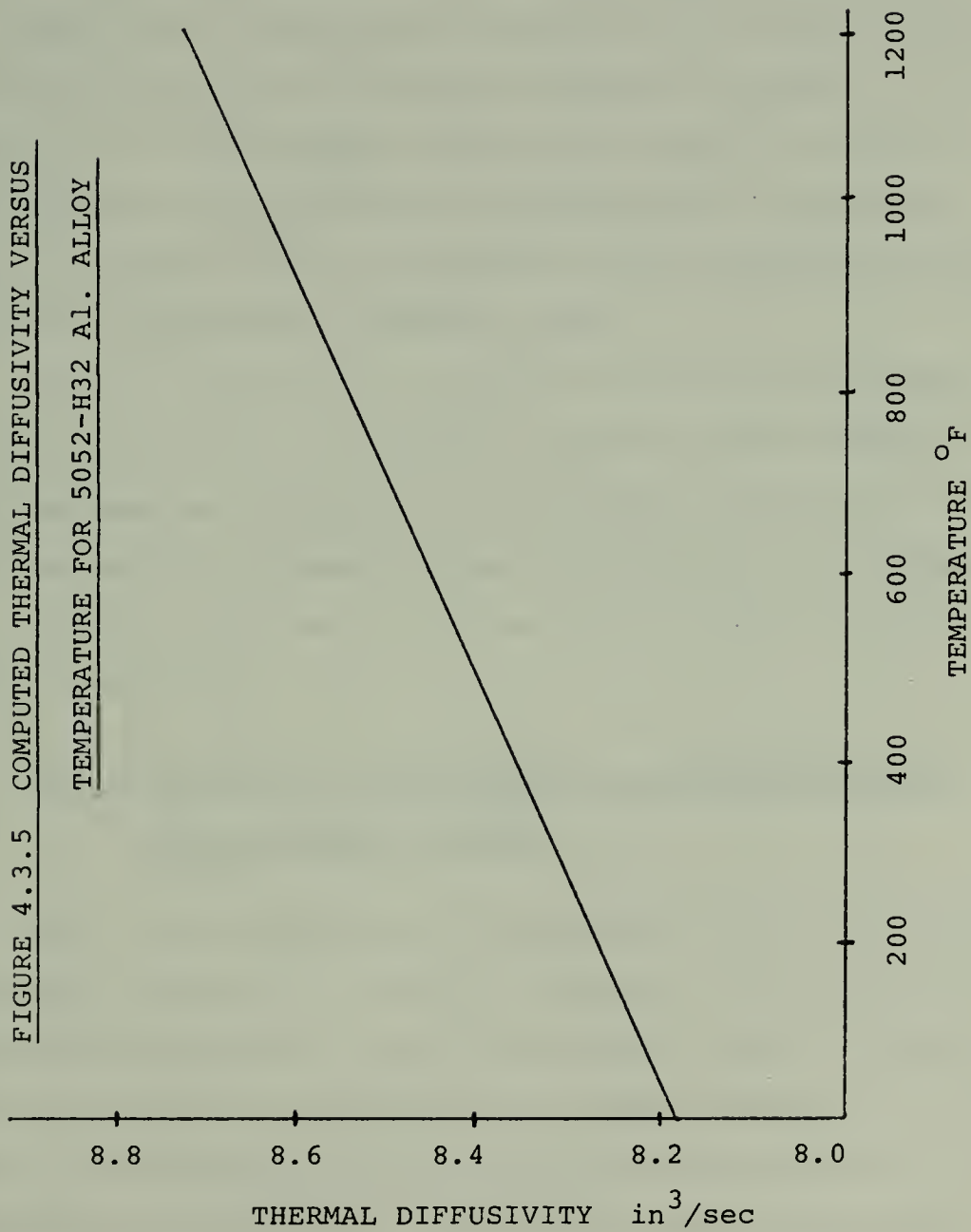
temperature functionals in the time-temperature finite element program.

Since the one-dimensional program was unable to approximate a satisfactory analytic solution in Section 4.2, a trial and error method must now be adopted to "guess" the proper heat input history needed for the basic driving function in the finite element temperature program. With Figure 3.4.1 for guidance, and knowing that only one heat input profile will satisfy the experimental temperature results, Figure 4.3.6 was generated (after spending several weeks and over $700 in computer time).

With all inputs now available for the finite element temperature program, a computer run can be made producing time-temperature histories of all nodes in the mesh. Figure 4.3.7 shows the agreement between experimental and theoretical results at 1.5 and 4.0 inches from the plate centerline (the y direction).

4.4 – Strain and Displacement by a Two-Dimensional Finite Element Program

With good agreement for temperature at the two specific locations observed (1.5 and 4.0 inches), it is a relatively straight-forward step to run the thermal strain and metal movement program. The same mesh pattern (Figure 4.3.1) is used in conjunction with the time-temperature history computed in Section 4.3. For a first approximation, the following inputs were assumed to be constant with all

FIGURE 4.3.6 HEAT INPUT VERSUS TIME FOR 100% EFFICIENCY
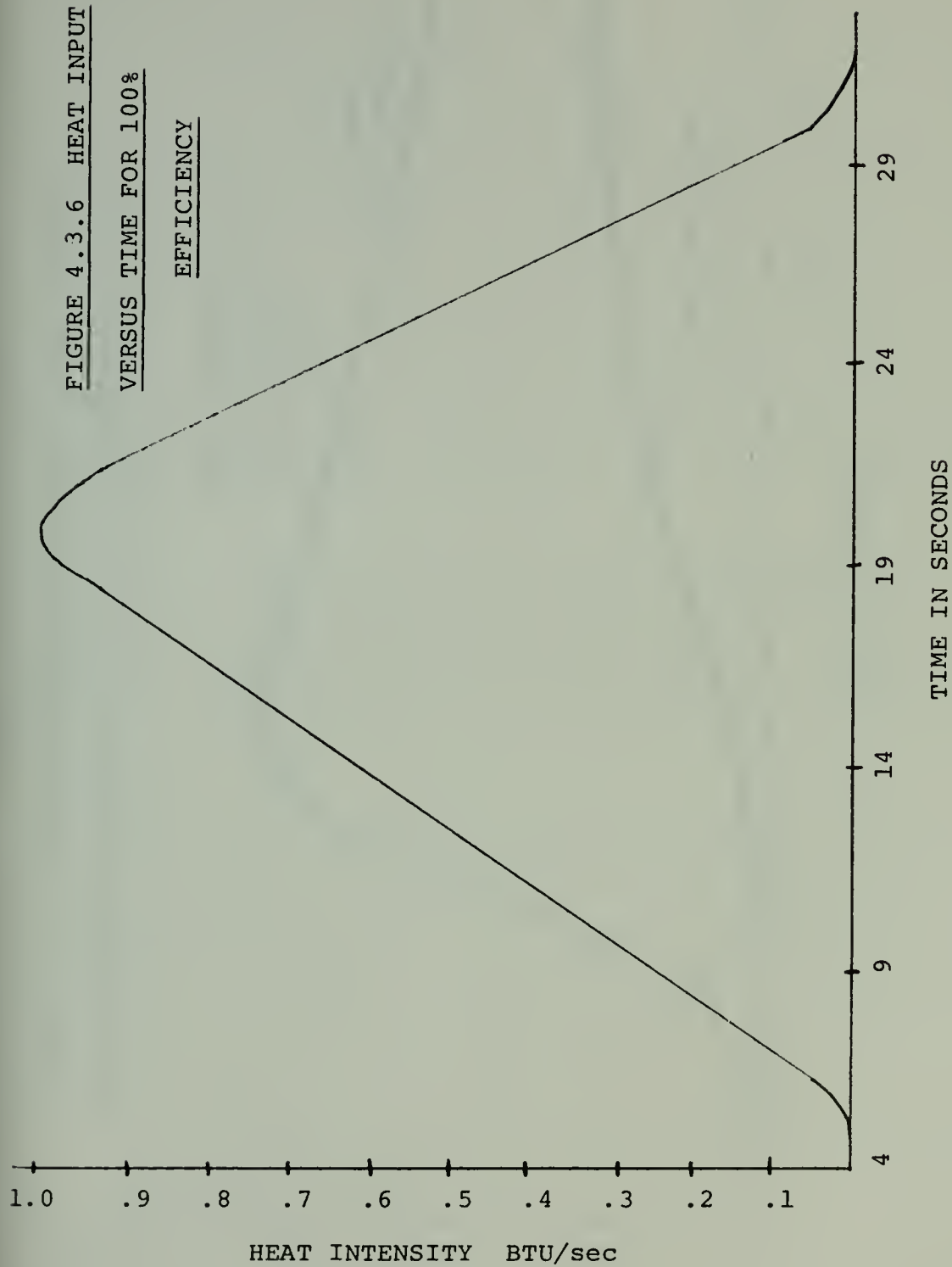
FIGURE 4.3.7 TIME-TEMPERATURE HISTORY FROM TWO DIMENSIONAL

FINITE ELEMENT PROGRAM AT 1.5 AND 4.0 INCHES FROM WELDLINE
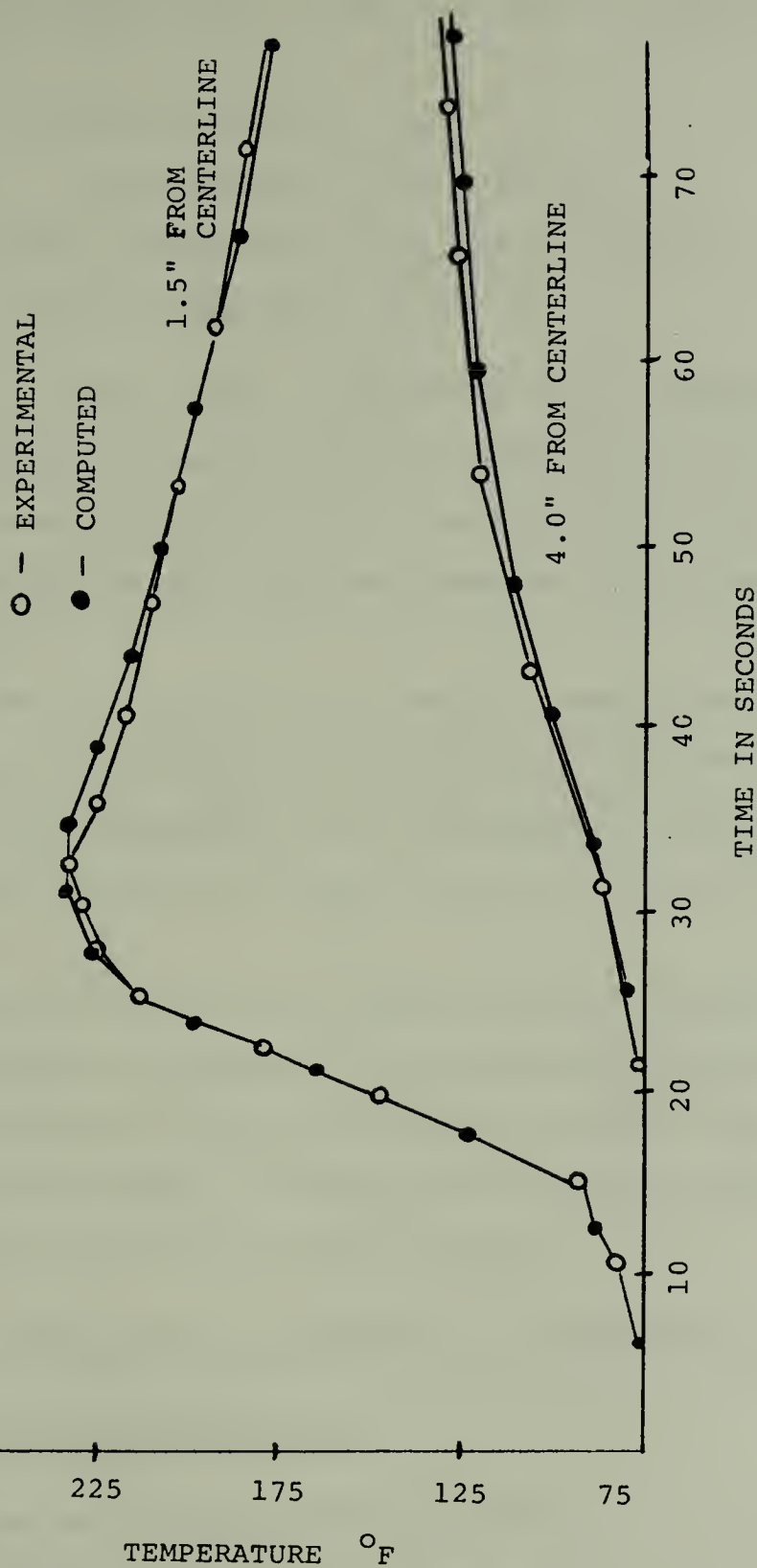
temperatures (the author notes that this is hardly the
case):

$$\text{poisson's ratio} = .3$$
$$\text{yield stress} = 30 \times 10^3 \text{ psi}$$
$$\text{thermal expansion} = 12.8 \times 10^{-6} \text{ in/}^\circ \text{F}$$
$$\text{strain hardening} = 0.0$$

Only a single pass on side "A" of the "simulated" plate
was calculated for an approximate comparison with the
observed results in Chapter 3. The simulation only ran for
120 seconds but enough data was computed for a good general
comparison.

Appendix D shows initial computer constraints and a
sample time step output of this program. Recorded for
each node are temperature and displacement, and for each
element are incremental strain (ε_y, ε_z, γ_{yz}) and plastic
indicator.

Figures 4.4.1 and 4.4.2 show a graphic comparison
between observed (Chapter 3) and calculated transverse
mechanical strains (ε_y) at 1.5 and 4.0 inches from the
transverse centerline. Figure 4.4.3 shows the time-displace-
ment history of the plate end (node 87).

4.5 - Comparison of Computed and Experimental Results

Temperature Distribution

The temperature distribution needed for the analysis
of thermal stresses and distortions was calculated in

-91-

MICROSTRAIN (in/in)

FIGURE 4.4.1 MECHANICAL STRAIN (ϵ_Y) HISTORY COMPARISON

AT 1.5" FROM THE WELDLINE

TENSION

COMPRESSION

TIME (log sec.)

● – EXPERIMENTAL

▲ – COMPUTED
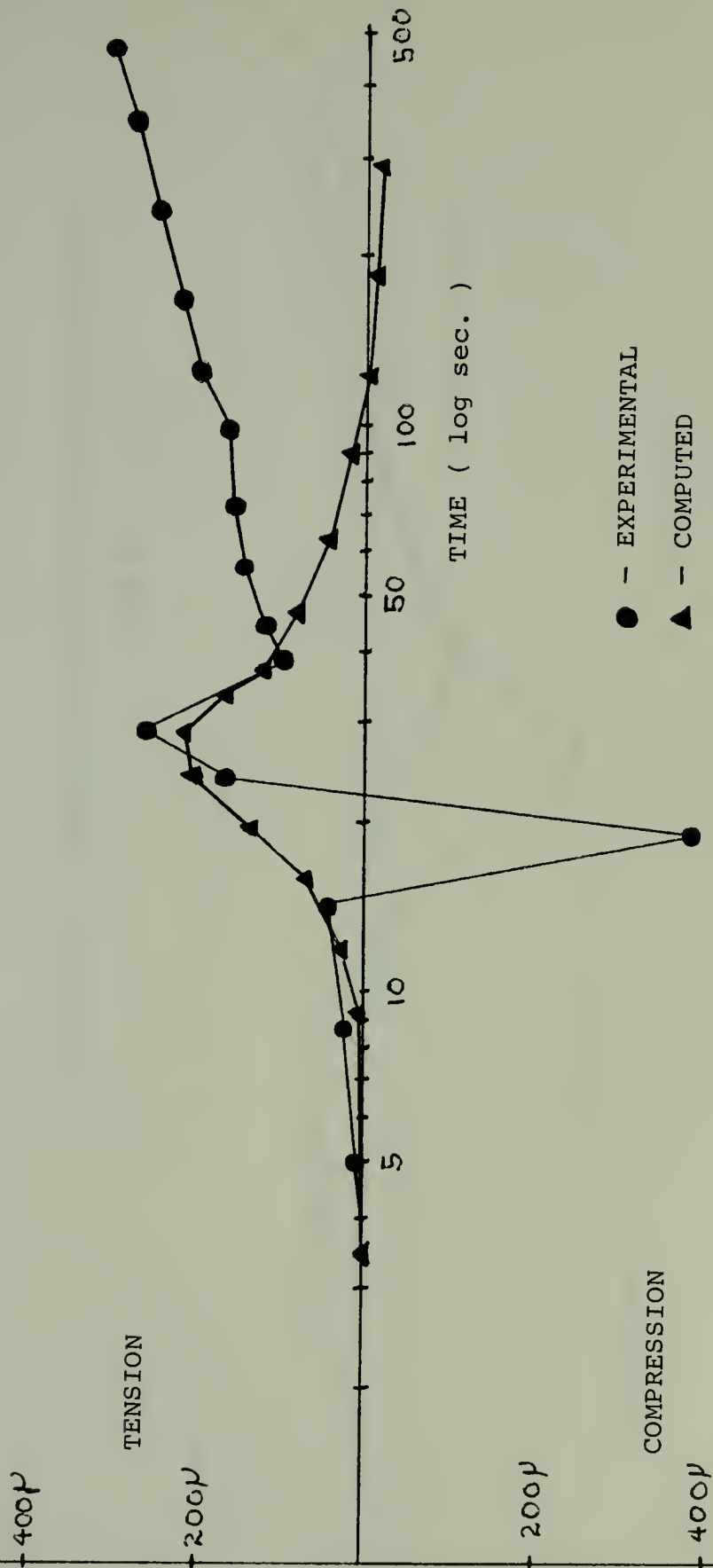
MICROSTRAIN (in/in)
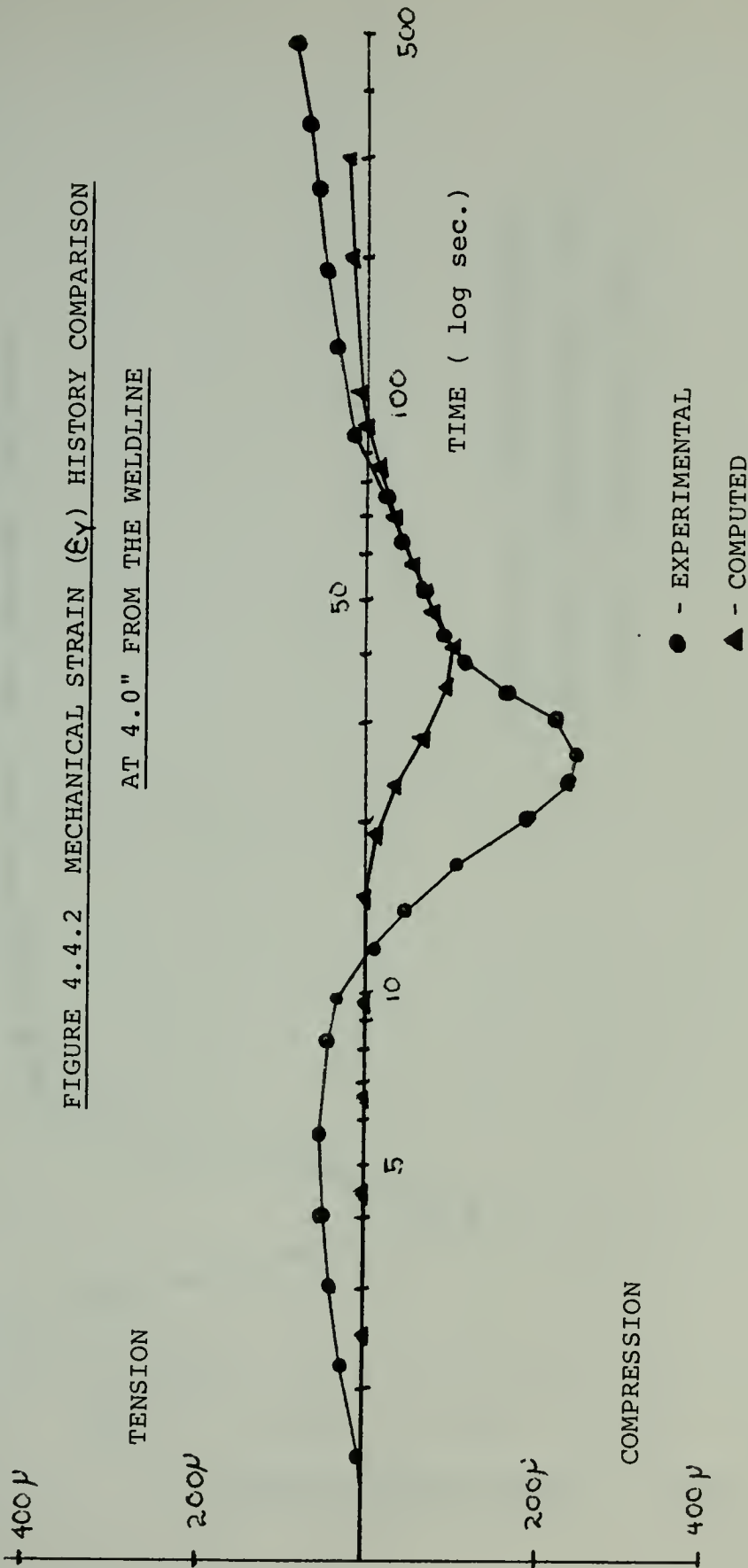
FIGURE 4.4.2 MECHANICAL STRAIN (ϵ_Y) HISTORY COMPARISON

AT 4.0" FROM THE WELDLINE

TIME (log sec.)

TENSION

COMPRESSION

400 μ

200 μ

200 μ

400 μ

5

10

50

100

500

● - EXPERIMENTAL
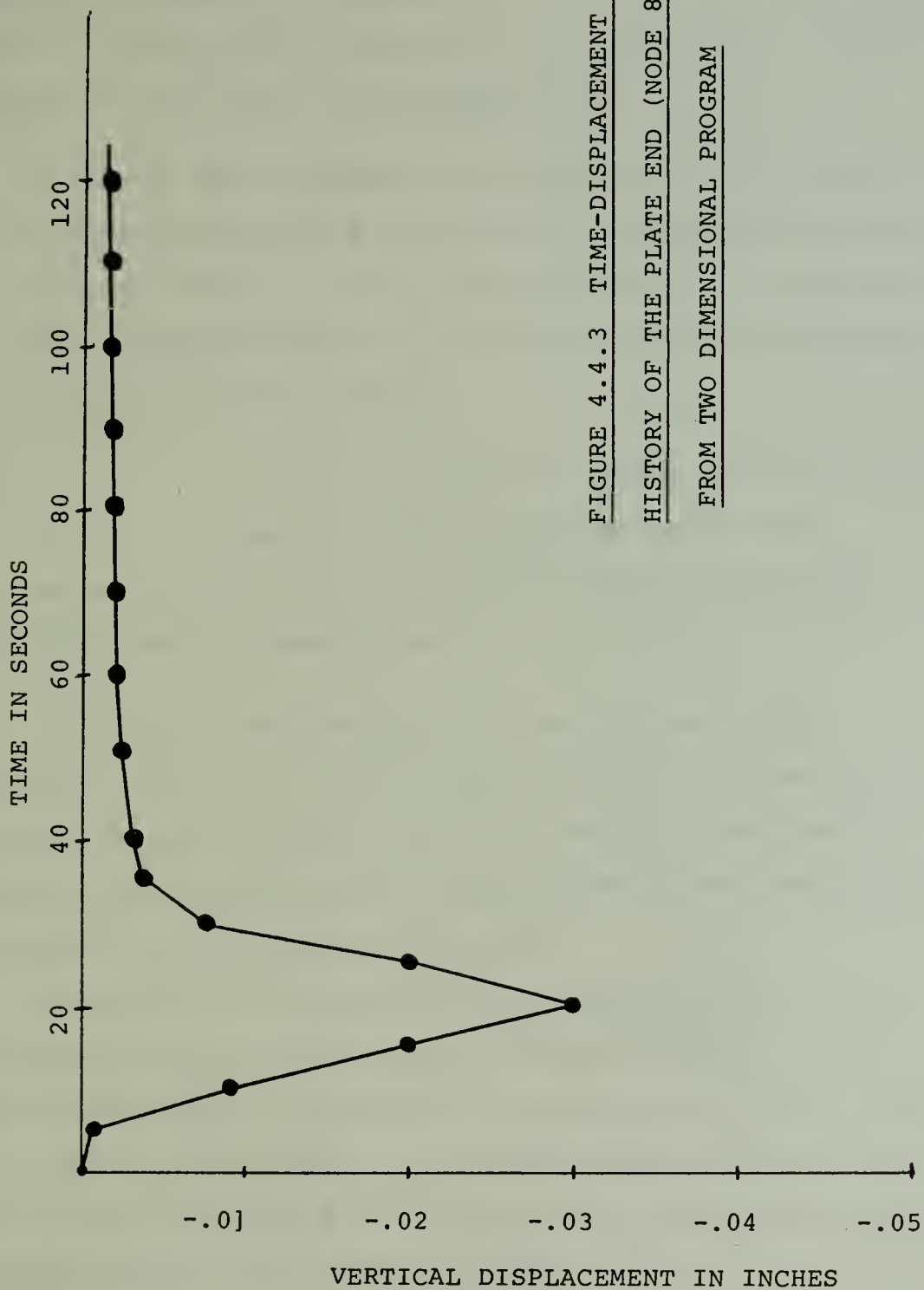
▲ - COMPUTED

FIGURE 4.4.3 TIME-DISPLACEMENT

HISTORY OF THE PLATE END (NODE 87)

FROM TWO DIMENSIONAL PROGRAM

Section 4.3. Figure 4.3.7 shows good agreement between experimental and computed temperature histories at two specific locations. To examine the two-dimensional computer output a little closer, Figure 4.5.1 is provided. In this figure two significant errors are noticed -

a. The maximum temperature at any point in the plate never exceeds 740° F and yet the liquidus temperature is about 1200° F. This means that there is no molten heat affected zone and not even enough heat generated to melt the filler wire.

b. At all locations beyond five inches from the weld-line the temperature never increases above room temperature (78° F). This is not consistent with experimental observations.

An immediate explanation to this problem is not available. There is serious doubt that the "derived" heat intensity history (Figure 4.3.6) is realistic and yet it gives good approximations of temperature at the two points observed, 1.5 inches and 4.0 inches.

The author is confident that the experimental data is realistic because several data runs were made, and temperature and strain readings were averaged over several gages. It is also believed that the assumed welding efficiency of .75 was high but when a lower value was tried, temperatures were even lower than in Figure 4.5.1.

-94-

FIGURE 4.5.1 TEMPERATURE VERSUS
UPPER SURFACE PLATE LOCATION FROM
TRANSVERSE CENTERLINE FOR 1/2 " Al.

$T_{max.}$ = 740°F

TEMPERATURE ^{O}F

STEP TIME

R.T.

TRANSVERSE LOCATION FROM PLATE CENTERLINE IN INCHES
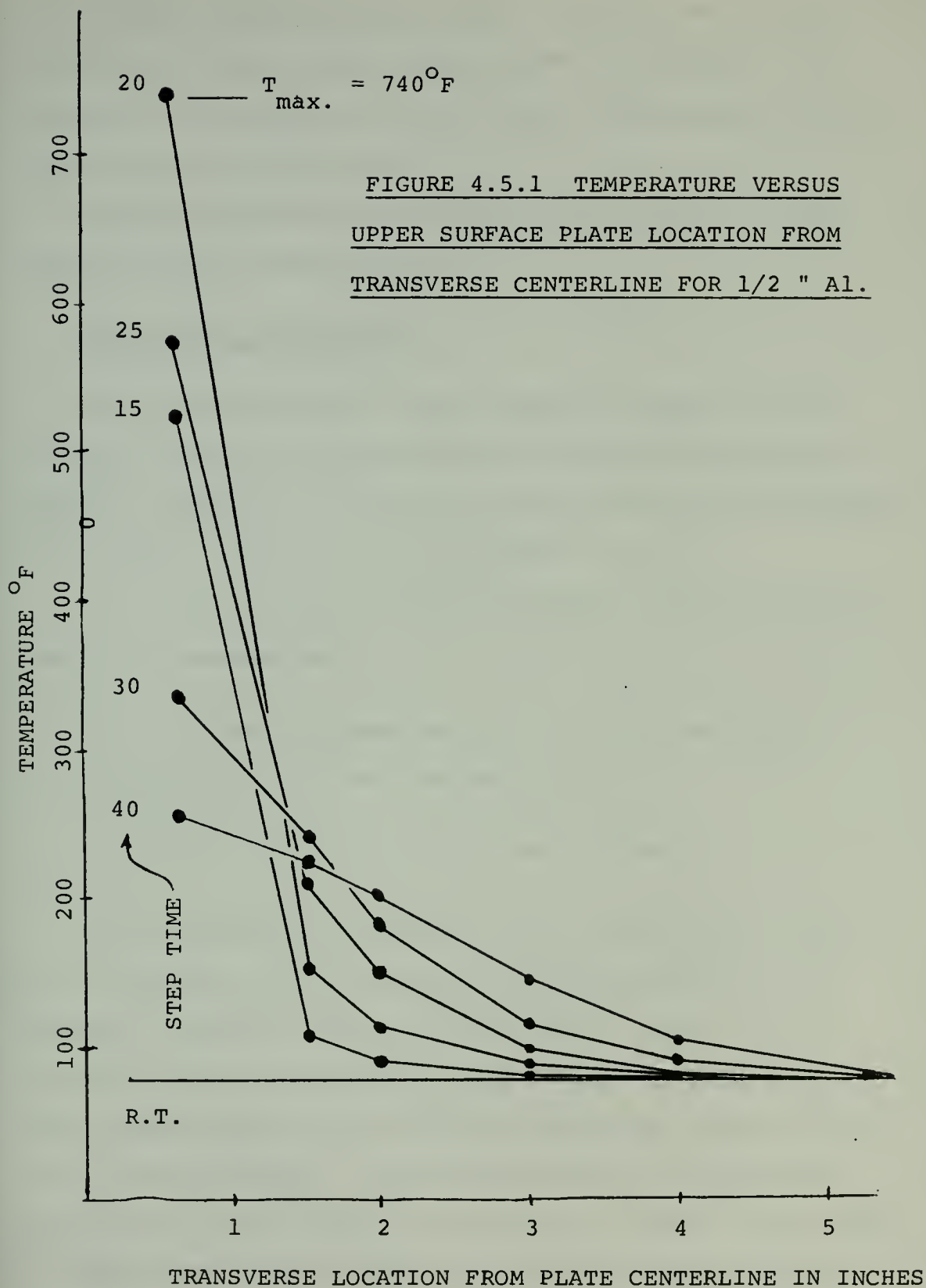
A point source was used and in reality the heat is applied over a significant area around the nozzle. But when this was modeled into the system, temperatures again turned out to be very low.

Further research is necessary in the model of this complex shape in two-dimensions.

Strain and Displacement

The two-dimensional finite element thermal stress and metal movement program did not produce satisfactory results. Figures 4.4.1 and 4.4.2 show significant disagreement between computed and experimental results.

It is the author's belief that this resulted from two inaccurate assumptions -

a. That longitudinal strain, ε_x, did not play a significant role for the model, and

b. That the plate was in plane stress.

If the figures in Chapter 3 for longitudinal strain, ε_x, (Figures 3.4.4 and 3.4.5) are superimposed on the computed transverse strains from Section 4.4, it can be seen that where experimental longitudinal strains are small, experimental and computed transverse strains (ε_y) are in good agreement. Where experimental longitudinal strains are large, Figures 4.4.1 and 4.4.2 show that there is a wide divergence between experimental and computed transverse strains. This would indicate a strong coupling

-96-

relationship between longitudinal and transverse strains.

Displacements were not analyzed because of the poor results for temperature and strain found around the fillet area. Actual displacement histories are very sensitive to fillet conditions since most of the actual plate movement occurs in that area.

The author has two follow-up suggestions for the continuation of this analysis. Based on the observations discussed above, a model assuming plane strain should be attempted. If theory can substantiate experimental results, it will be shown that transverse and longitudinal strains will be related by poisson's ratio.

If this model fails, it will probably be due to the fact that the model is too simplified and three-dimensions will be necessary to correctly couple all the interacting influences. Due to the amount of time and resources left to the author, this study shall be postponed.

Analytical Extrapolation of Experimental
Data Found in Chapter 2

From previous thesis work [8] on out-of-plane angular distortion of aluminum alloy, Figure A.1 has been generated from single pass GMA welding. The experiment performed in Chapter 2 has been modeled as shown below, where

P is the line load (lbs.),

X is the coordinate direction of the weld,

t is the plate thickness (inches), and

a is the longitudinal plate span (inches).
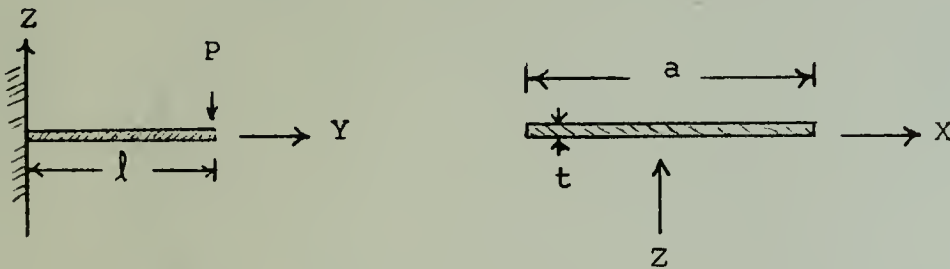
Examining reference 21, we find for $Y = \ell$

$$\theta = \frac{2 \, P \, \ell^2}{E \, I_z} \, , \tag{1}$$

$$I_z = \frac{t^3 \, a}{4} \, , \tag{2}$$

FIGURE A.1 VARIATION OF FREE ANGULAR CHANGE IN DISTORTION

VERSUS PLATE THICKNESS

$$\delta = \frac{P \ell^3}{3 E I_z} \quad , \tag{3}$$
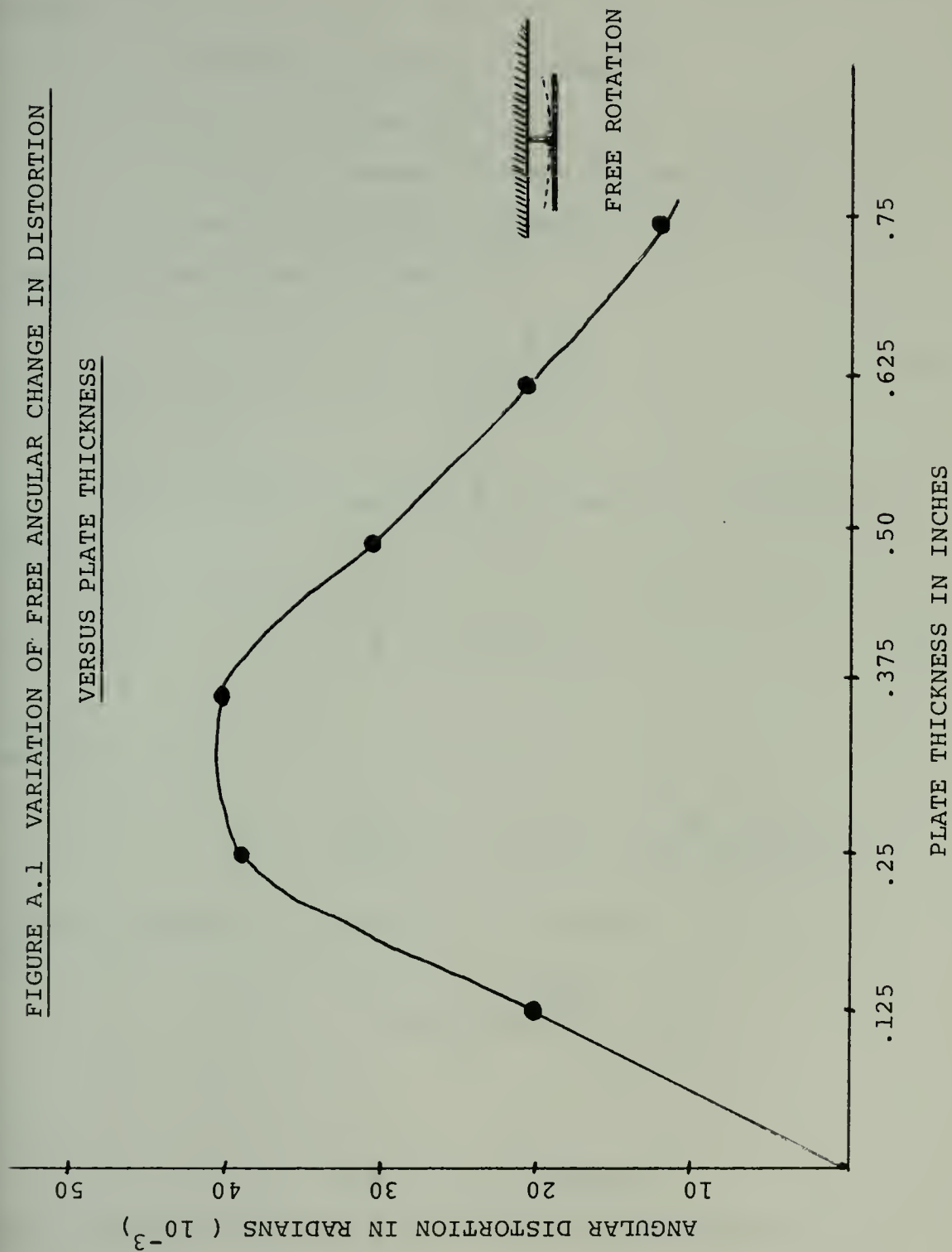
where

θ is the angular rotation (radians),

E is Young's modulus (psi),

I is the second moment of area (inches^4), and

δ is the displacement (inches).

Combining equations (1) and (2),

$$\theta = \frac{2 P \ell^2}{E t^3 a} \quad . \tag{4}$$

For all plates examined ℓ, E, and a are constant. Thus,

$$\theta = (K) \frac{P}{t^3} \quad , \tag{5}$$

where

$$K = \frac{\ell^2}{2 E a} = 1.2 \times 10^{-6} \text{ in}^3/\text{lb} .$$

Solving equation (5) for $\theta = 1 \times 10^{-3}$,

$$P\theta = \frac{t^3 (1 \times 10^{-3})}{K} = \frac{t^3}{K'} \quad ,$$

where

$$K' = 1.2 \times 10^{-3} \text{ in}^3/\text{lb.}$$

We can immediately see that the line load necessary to

produce a radian change is a single function of plate thickness cubed. By correlating with plate thickness, we can find the line loads necessary to produce or remove the curves found in Figure A.1.

t	P^θ	θ_{FREE}	P_{FREE}
inches	lbs/rad	rad	lbs
.125	1.3	21	27
.25	13	38	495
.375	44	40	1760
.50	104	30	3120
.625	203	20.5	4162
.75	352	12	4224

Figure A.2 plots line load necessary to remove angular distortion against plate thickness.

From Chapter 2 the values of deflection necessary to ideally remove the free angular distortion are known for 3/8" and 1/2". For the 3" flanged tee, the values can be taken from Figure 2.4.3. The values are

$$t = .375" \qquad \delta = .085"$$
$$t = .50" \qquad \delta = .19" \quad .$$

Using equation (3), line load P can be found for the above values;

FIGURE A.2 LINE LOAD VERSUS PLATE THICKNESS
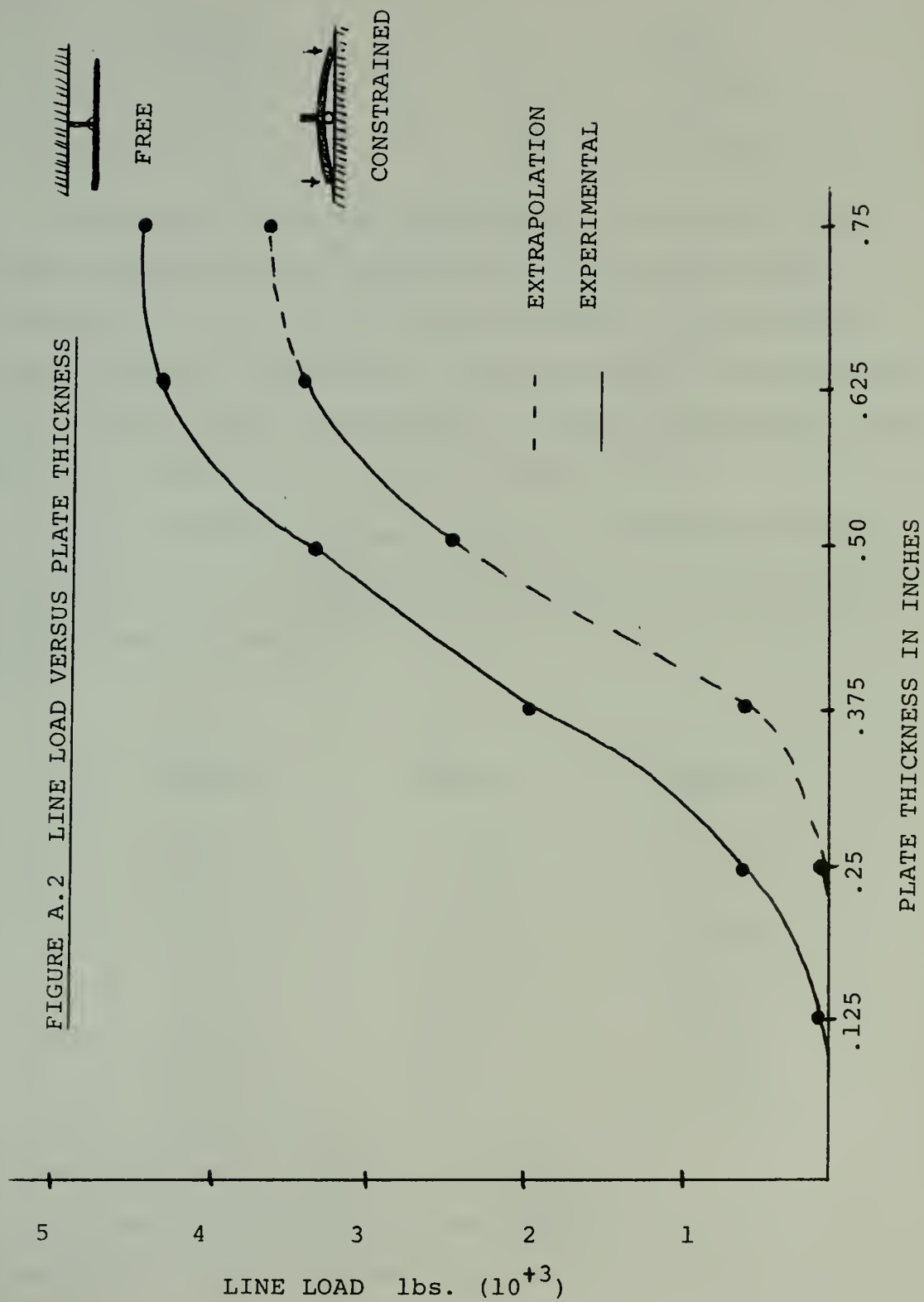
$$P = \frac{3 \, \delta \, E \, I_z}{\ell^3} \quad ,$$

t	P
.375"	480 lbs
.50 "	2525 lbs .

These points are now superimposed on Figure A.2 and, if the assumption can be made that for the same plate properties (a, ℓ , t, E) the curves will only be offset by the degree of constraint, we can contour a line through the two data points from Chapter 2 and in conjunction with the line generated from data in reference 8.

Using equation (3) again and the extrapolated line in Figure A.2, the deflections necessary for distortion removal can be found.

t	P	
inches	lbs	inches
.125	0	0
.25	50	.03
.375	480	.085
.50	2526	.19
.625	3300	.128
.75	3600	.081

Figure A.3 reflects this table graphically.

Figure A.3 reflects the two primary influences on prestraining aluminum plate to remove distortion. At

FIGURE A.3 IDEAL LINER HEIGHT VERSUS PLATE THICKNESS

● — EXPERIMENTAL

◉ — EXTRAPOLATED

PLATE THICKNESS IN INCHES

IDEAL LINER HEIGHT IN INCHES x10^{-2}
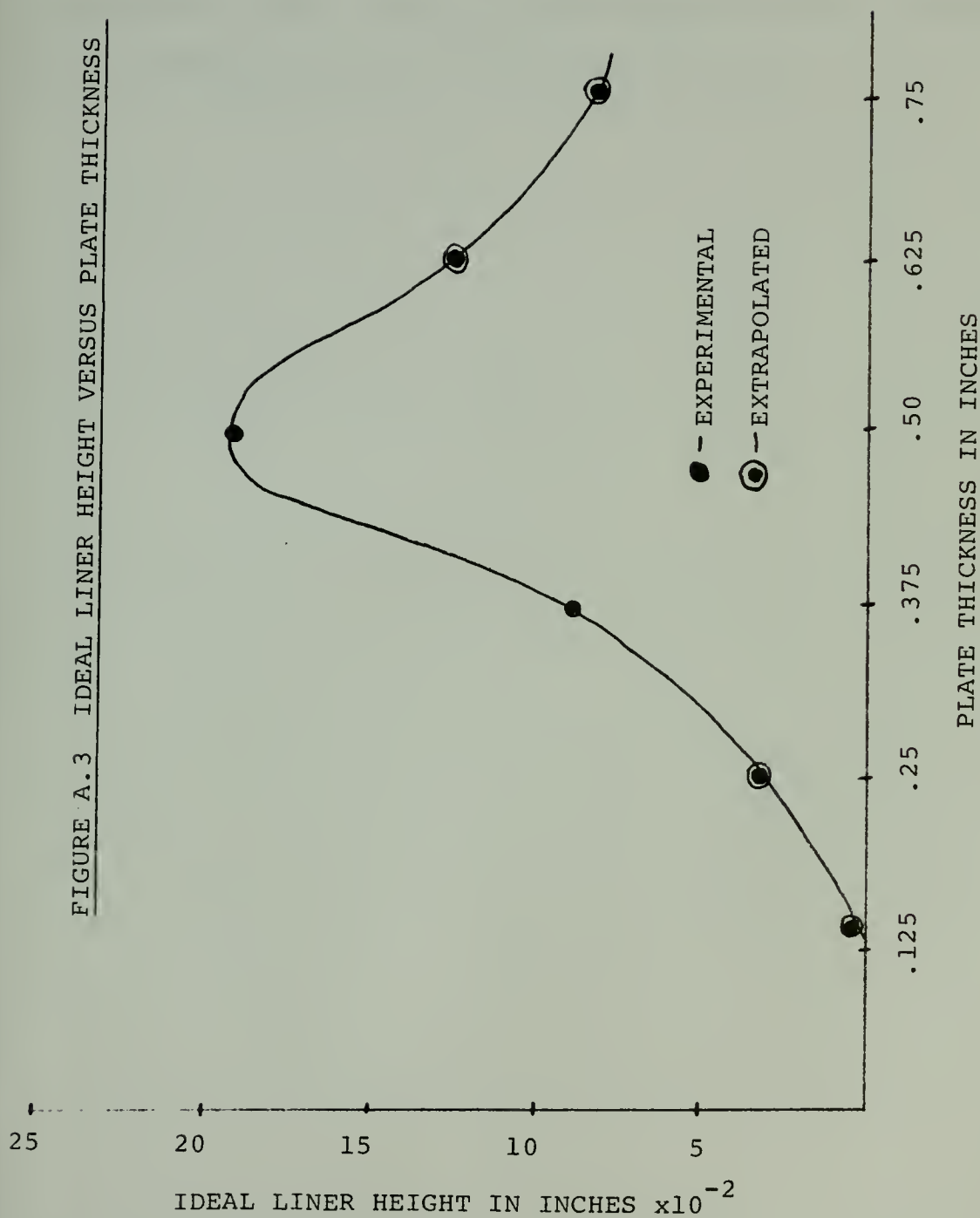
low thicknesses (1/4", 3/8") there is high angular distortion,
and as thickness increases, the line load necessary to
make a change of one radian goes up cubically. At large
thicknesses (5/8", 3/4", and above) plate rigidity produces
small distortions and the liner size decreases.

APPENDIX B

Surface Strain Model

The data generated in Chapter 2 can only be useful if it is evaluated in terms of a common function that is applicable to many situations where the prestraining technique would be useful. Of the several possibilities (stress, strain, degree of constraint, loading) strain appeared to be the most useful. Experimentally, strain measurements are now well within the "state of the art". Theoretical strain models for many configurations can be found in numerous textbooks.[21, 33]

Therefore, under this assumption the prestraining technique of Chapter 2 was correlated by strain as a function of plate span and degree of prestrining (i.e., liner height). Several plates of various thicknesses and of the same description as the ½" plate used in Chapter 3 were equipped with strain gages and prestrained. As in Chapter 3, each plate had an 18" span and a 12" length. Mechanical strain was recorded at several locations on the transverse centerline of the plate and a curve fitted to predict the induced surface strain at the longitudinal center of the plate.

Figure B.1 is the result of this study. By entering on the proper plate description line (plate size and

FIGURE B.1 CENTERLINE MAX. STRAIN VERSUS

LINER SIZE FOR SEVERAL PLATE THICKNESSES

FROM A STATIC TEST OF 5052-H32 Al-ALLOY
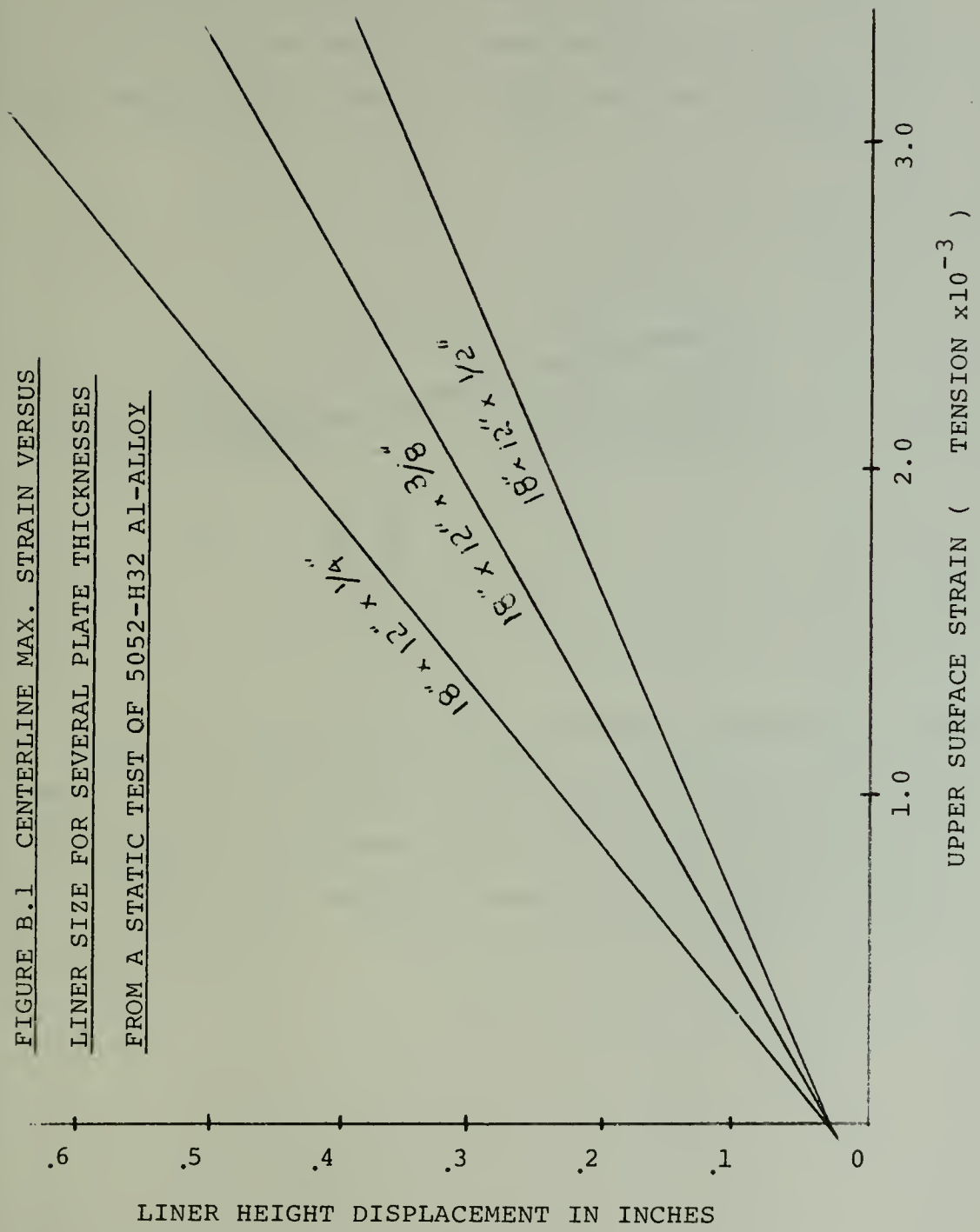
thickness) with the intended liner height, the maximum
centerline (transverse) strain can be estimated.

In Chapter 2 the plates used experimentally were
24" by 24". By assuming a linear approximation of liner
height versus plate length, Figure B.2 was developed.

$$\delta_{12} = \frac{12}{9} \delta_9$$
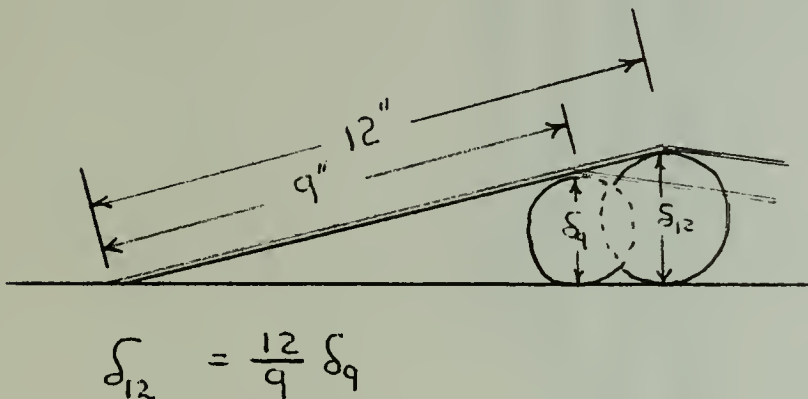
It can be assumed that the maximum longitudinal strain
along the fillet weldline for 24" plate (length) will not
be significantly different from the strains measured for
the 12" plate when using the same roller diameter. Refer
to Figure 1.3.1.
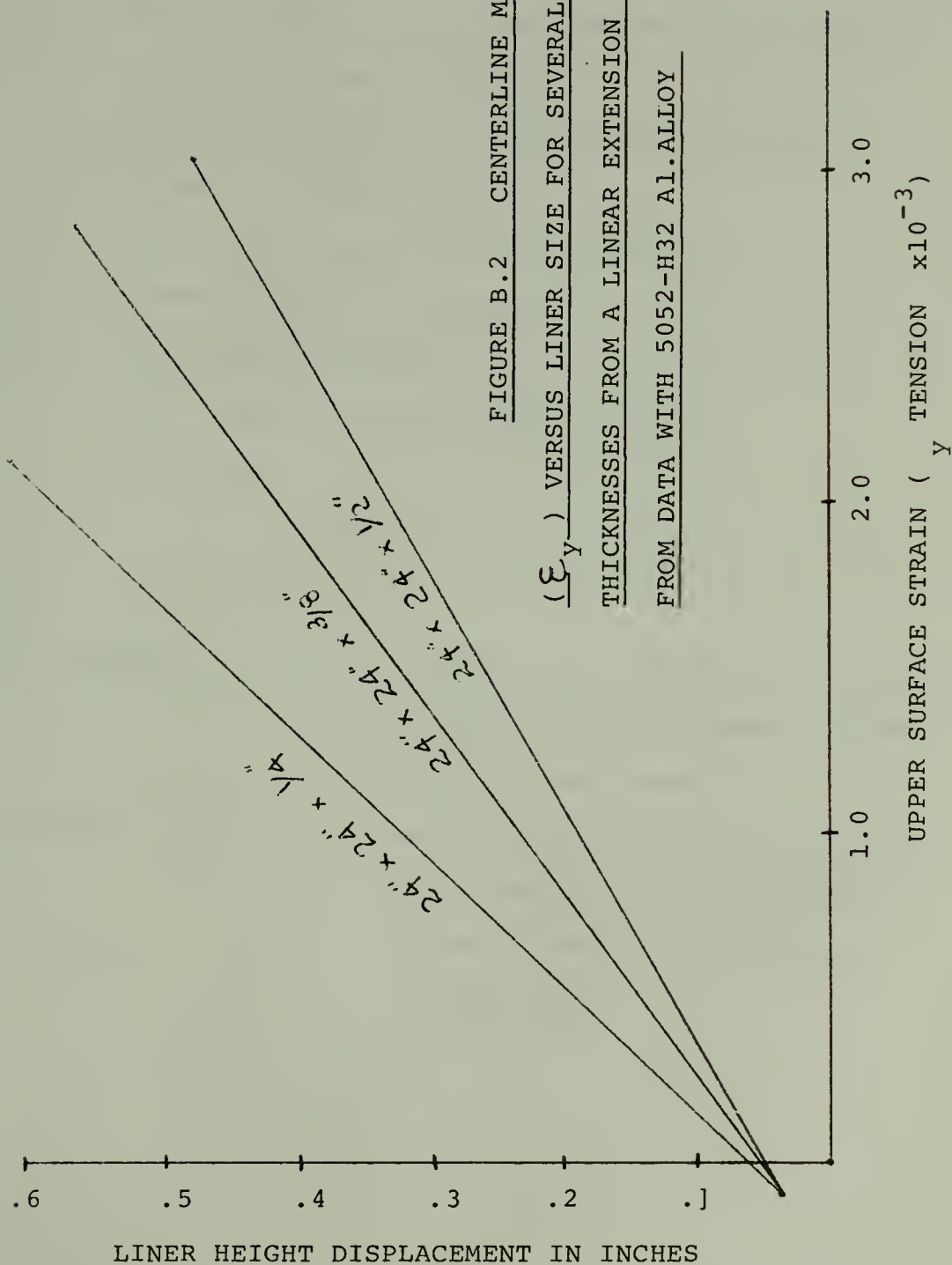
FIGURE B.2   CENTERLINE MAX. STRAIN
(ε_y) VERSUS LINER SIZE FOR SEVERAL PLATE
THICKNESSES FROM A LINEAR EXTENSION DONE
FROM DATA WITH 5052-H32 Al.ALLOY

APPENDIX C

Symbols and Definitions

δ – Displacement, distortion, deflection (inches)

t – Plate thickness (inches)

θ – Angular distortion – out-of-plane (radians)

E – Young's modulus (psi)

P – Line Load along plate ends (lbs/in)

I – Second moment of area (in^4)

a – Plate span (inches)

ℓ – One – half of plate width (inches)

η – Efficiency

Liner (roller) – A round bar placed under the plate before welding to cause induced reverse curvature.

Transverse – Perpendicular to weld direction– for experiments, Y coordinate.

Longitudinal – In the direction of welding, X coordinate.

***** INPUT DATA *****

ELEMENT= 110   NODE= 87   NTIME= 90

NODE NAMES IN EACH ELEMENTS

1(	1	3	4	2(	1	4	2	31(	3	5	6	4(	3	6	4
5(	5	7	8	6(	5	8	6	71(	7	9	10	8(	7	10	8
9(	9	11	14	10(	9	12	13	111(	9	13	16	12(	12	16	13
13(	13	14	17	14(	12	15	19	151(	13	16	19	16(	15	19	16
17(	16	17	20	18(	15	18	22	191(	16	18	22	20(	18	22	19
21(	19	20	23	22(	18	21	25	231(	19	21	25	24(	21	25	22
25(	22	23	26	26(	21	24	28	271(	22	24	29	28(	24	29	25
29(	25	26	30	30(	24	28	30	311(	25	30	39	32(	28	31	27
33(	28	30	40	34(	30	40	27	351(	29	41	31	36(	40	41	32
37(	29	31	32	38(	40	42	32	391(	32	42	34	40(	42	43	34
41(	31	42	36	42(	31	44	32	431(	32	44	36	44(	44	46	36
45(	43	44	36	46(	33	44	34	471(	34	46	38	48(	46	47	38
49(	45	46	37	50(	35	46	36	511(	37	48	39	52(	48	49	40
53(	47	48	40	54(	37	48	38	551(	39	42	53	56(	51	52	41
57(	50	51	41	58(	40	51	39	591(	41	54	55	60(	53	54	43
61(	41	42	43	62(	54	56	44	631(	43	56	45	64(	56	58	45
65(	43	44	45	66(	55	57	46	671(	45	58	47	68(	58	60	47
69(	45	46	47	70(	57	59	48	711(	47	60	49	72(	59	62	50
73(	47	48	50	74(	59	63	52	751(	63	64	52	76(	62	64	52
77(	62	51	53	78(	62	65	63	791(	65	66	63	80(	64	66	54
81(	52	53	61	82(	65	68	66	831(	66	69	63	84(	66	69	56
85(	52	64	67	86(	68	71	69	871(	69	72	66	88(	69	72	58
89(	69	67	70	90(	71	74	72	911(	72	75	69	92(	72	75	62
93(	72	70	73	94(	76	77	75	951(	75	78	72	96(	75	78	64
97(	75	73	76	98(	76	80	78	991(	77	78	75	100(	78	85	66
101(	78	76	79	102(	80	83	81	1031(	80	82	78	104(	81	85	69
105(	80	82	81	106(	83	87	85	1071(	82	84	78	108(	84	85	70
109(	84	86	85	110(	86	87	85								

COORDINATES (X,Y)

Node	X	Y	Node	X	Y	Node	X	Y	Node	X	Y
1	0.0	-9.000	2	0.500	-9.000	3	0.500	-7.000	4	0.0	-7.000
5	0.0	-5.500	6	0.500	-5.500	7	0.500	-4.000	8	0.0	-4.000
9	0.0	-3.000	13	0.250	-3.000	11	0.250	-3.000	12	0.500	-2.000
13	0.250	-2.000	14	0.500	-2.300	15	0.500	-1.500	16	0.3	-1.500
17	0.500	-1.000	22	0.0	-1.000	19	0.250	-1.000	20	0.250	-1.000
21	0.0	-0.750	25	0.250	-0.500	23	0.500	-0.750	24	0.500	-0.500
25	0.250	-0.500	30	0.530	-0.500	27	0.500	-0.375	28	0.625	-0.250
29	0.250	-0.250	34	0.250	-0.250	31	0.250	-0.250	32	0.750	-0.250
33	1.250	-0.250	38	1.530	-0.250	35	1.500	-0.250	36	2.300	-0.250
37	3.500	-0.250	42	4.500	-0.250	39	4.500	0.0	43	0.3	0.0
41	0.0	0.0	46	0.0	0.0	47	0.0	0.0	44	1.000	0.0
45	0.0	0.0	52	1.500	0.0	51	0.250	0.0	48	2.500	0.0
49	0.0	0.0	54	4.500	0.0	55	0.250	0.0	52	1.250	0.250
53	0.250	0.750	59	2.500	0.250	59	0.500	0.0	56	3.500	0.250
57	0.250	0.250	62	0.625	0.500	63	0.500	0.0	60	0.250	0.500
61	0.375	0.0	66	0.0	0.150	67	0.750	0.0	64	0.500	0.0
65	0.750	0.0	73	0.250	1.000	71	1.500	0.0	68	1.000	0.0
69	1.000	0.250	74	0.500	2.000	75	2.000	0.0	72	1.500	0.250
73	1.500	0.500	78	0.0	3.030	79	3.000	0.0	76	2.000	0.500
77	3.000	0.0	82	0.500	5.500	83	5.500	0.0	80	0.500	0.500
81	4.000	0.0	86	0.500	9.000	87	9.000	0.0	84	0.500	0.500
85	7.000	0.0									

** IBCON AND IPHTG **

Node	IBCON	IPHTG	Node			Node			Node		
1	1	-2	4	0	-2	5	0	-2	8	0	-1
11	0	-2	14	0	-2	15	0	-1	18	0	-1
21	0	-1	24	0	-1	25	0	-1	28	0	0
31	0	0	34	0	0	35	0	0	38	0	0
41	0	0	44	0	0	45	0	0	48	0	0
51	0	0	54	0	0	55	0	0	58	0	0
61	0	0	64	0	0	65	0	0	68	0	0
71	0	0	74	0	0	75	0	0	78	0	0
81	0	0	84	0	0	85	0	0	88	0	0

TIME LIMIT =   121.000

SCF =   1.000

INITIAL TEMPERATURE =   78.000

TOTAL DISPLACEMENT

NODE	U	V	NODE	U	V	NODE	U	V	NODE	U	V
1	-0.3079E-02	0.4433E-02	2	-0.2626E-02	0.4249E-02	3	-0.3080E-02	0.2595E-02	4	-0.2621E-02	0.2595E-02
5	-0.3380E-02	0.1219E-02	6	-0.2622E-02	0.1219E-02	7	-0.3081E-02	0.1575E-03	8	-0.2622E-02	-0.1567E-03
9	-0.3079E-02	-0.1084E-02	10	-0.2846E-02	-0.1075E-02	11	-0.2623E-02	-0.1066E-02	12	-0.3000E-02	-0.2037E-02
13	-0.2755E-02	-0.1543E-02	14	-0.2535E-02	-0.1553E-02	15	-0.2842E-02	-0.2581E-02	16	-0.2610E-02	-0.2574E-02
17	-0.2390E-02	-0.2365E-02	18	-0.2483E-02	-0.3149E-02	19	-0.2249E-02	-0.2970E-02	20	-0.2097E-02	-0.2760E-02
21	-0.1340E-02	-0.3553E-02	22	-0.2012E-02	-0.3233E-02	23	-0.1801E-02	-0.2906E-02	24	-0.1987E-02	-0.3341E-02
25	-0.1024E-02	-0.3519E-02	26	-0.1401E-02	-0.3051E-02	27	0.0	0.0	28	-0.1502E-02	-0.4417E-02
29	-0.1103E-02	-0.3836E-02	30	-0.1440E-01	-0.3201E-02	31	-0.6757E-03	-0.7442E-02	32	-0.5124E-03	-0.1750E-02
31	-0.3627E-03	-0.1225E-02	34	-0.2282E-03	-0.3469E-03	35	-0.1141E-03	-0.3711E-03	36	-0.3253E-04	-0.1601E-03
37	-0.7740E-03	-0.1332E-02	38	0.0	0.0	39	-0.8563E-03	-0.4520E-02	40	-0.4232E-03	-0.4208E-02
41	-0.1294E-03	-0.3415E-03	42	0.2651E-04	-0.2550E-02	43	0.8942E-04	-0.1832E-02	44	0.9241E-04	-0.1785E-02
45	-0.1309E-04	-0.6790E-03	46	0.5234E-04	-0.3913E-03	47	0.3211E-03	-0.1610E-03	48	0.7945E-05	-0.1146E-04
49	0.0	0.0	50	-0.5031E-04	-0.5411E-02	51	0.4212E-03	-0.3463E-02	52	0.8573E-03	-0.3634E-02
53	0.1915E-03	-0.2345E-02	54	0.1641E-03	-0.1742E-02	55	0.5682E-03	-0.1193E-02	56	0.3936E-03	-0.8144E-03
57	0.2205E-03	-0.3402E-03	58	0.5693E-04	-0.1441E-03	59	0.2359E-04	-0.5289E-05	60	0.0	0.0
61	0.0	0.0	62	0.8175E-03	-0.5927E-02	63	0.1351E-02	-0.5149E-02	64	0.1970E-02	-0.4174E-02
65	0.1571E-02	-0.6398E-02	66	0.2149E-02	-0.5737E-02	67	0.2999E-02	-0.5004E-02	68	0.2116E-02	-0.6965E-02
69	0.2740E-02	-0.6365E-02	70	0.3513E-02	-0.5271E-02	71	0.2915E-02	-0.8071E-02	72	0.3486E-02	-0.7813E-02
73	0.4252E-02	-0.7554E-02	74	0.3112E-02	-0.5375E-02	75	0.3842E-02	-0.9272E-02	76	0.4605E-02	-0.9168E-02
77	0.3146E-02	-0.1227E-01	78	0.4284E-02	-0.1224E-02	79	0.4837E-02	-0.1222E-01	80	0.3363E-02	-0.1521E-01
81	0.4947E-02	-0.1521E-01	82	0.3356E-02	-0.1966E-01	83	0.4940E-02	-0.1966E-01	84	0.3349E-02	-0.2411E-01
85	0.4833E-02	-0.2411E-01	86	0.3341E-02	-0.3005E-01	87	0.4925E-02	-0.3005E-01			

THERMOPHYSICAL PROPERTIES

SPECIFIC HEAT = 0.23300

THERMAL CONDUCTIVITIES
(X DIRECTION) = 0.00185
(Y DIRECTION) = 0.00185

DENSITY= 0.05700

THICKNESS OF EACH ELEMENT

1	0.90000	2	0.90000	3	0.90000	4	0.90000	5	0.90000
6	0.90000	7	0.90000	8	0.90000	9	0.90000	10	0.90000
11	0.90000	12	0.90000	13	0.90000	14	0.90000	15	0.90000
16	0.90000	17	0.90000	18	0.90000	19	0.90000	20	0.90000
21	0.90000	22	0.90000	23	0.90000	24	0.90000	25	0.90000
26	0.90000	27	0.90000	28	0.90000	29	0.90000	30	0.90000
31	0.90000	32	0.90000	33	0.90000	34	0.90000	35	0.90000
36	0.90000	37	0.90000	38	0.90000	39	0.90000	40	0.90000
41	0.90000	42	0.90000	43	0.90000	44	0.90000	45	0.90000
46	0.90000	47	0.90000	48	0.90000	49	0.90000	50	0.90000
51	0.90000	52	0.90000	53	0.90000	54	0.90000	55	0.90000
56	0.90000	57	0.90000	58	0.90000	59	0.90000	60	0.90000
61	0.90000	62	0.90000	63	0.90000	64	0.90000	65	0.90000
66	0.90000	67	0.90000	68	0.90000	69	0.90000	70	0.90000
71	0.90000	72	0.90000	73	0.90000	74	0.90000	75	0.90000
76	0.90000	77	0.90000	78	0.90000	79	0.90000	80	0.90000
81	0.90000	82	0.90000	83	0.90000	84	0.90000	85	0.90000
86	0.90000	87	0.90000	88	0.90000	89	0.90000	90	0.90000
91	0.90000	92	0.90000	93	0.90000	94	0.90000	95	0.90000
96	0.90000	97	0.90000	98	0.90000	99	0.90000	100	0.90000
101	0.90000	102	0.90000	103	0.90000	104	0.90000	105	0.90000
106	0.90000	107	0.90000	108	0.90000	109	0.90000	110	0.90000

TIME STEP **********

1	1.0000	2	1.0000	3	1.0000	4	1.0000	5	1.0000

****

| 6 | 1.0000 | 7 | 1.0000 | 8 | 1.0000 | 9 | 1.0000 | 10 | 1.0000 |

****

| 11 | 1.0000 | 12 | 1.0000 | 13 | 1.0000 | 14 | 1.0000 | 15 | 1.0000 |

****

| 16 | 1.0000 | 17 | 1.0000 | 18 | 1.0000 | 19 | 1.0000 | 20 | 1.0000 |

****

| 21 | 1.0000 | 22 | 1.0000 | 23 | 1.0000 | 24 | 1.0000 | 25 | 1.0000 |

****

| 26 | 1.0000 | 27 | 1.0000 | 28 | 1.0000 | 29 | 1.0000 | 30 | 1.0000 |

****

| 31 | 1.0000 | 32 | 1.0000 | 33 | 1.0000 | 34 | 1.0000 | 35 | 1.0000 |

****

| 36 | 1.0000 | 37 | 1.0000 | 38 | 1.0000 | 39 | 1.0000 | 40 | 1.0000 |

****

| 41 | 1.0000 | 42 | 1.0000 | 43 | 1.0000 | 44 | 1.0000 | 45 | 1.0000 |

****

| 46 | 1.0000 | 47 | 1.0000 | 48 | 1.0000 | 49 | 1.0000 | 50 | 1.0000 |

****

| 51 | 1.0000 | 52 | 1.0000 | 53 | 1.0000 | 54 | 1.0000 | 55 | 1.0000 |

****

| 56 | 1.0000 | 57 | 1.0000 | 58 | 1.0000 | 59 | 1.0000 | 60 | 1.0000 |

| 61 | 2.0000 | 62 | 2.0000 | 63 | 2.0000 | 64 | 2.0000 | 65 | 2.0000 |

****

| 66 | 2.0000 | 67 | 2.0000 | 68 | 2.0000 | 69 | 2.0000 | 70 | 2.0000 |

****

| 71 | 2.0000 | 72 | 2.0000 | 73 | 2.0000 | 74 | 2.0000 | 75 | 2.0000 |

****

| 76 | 2.0000 | 77 | 2.0000 | 78 | 2.0000 | 79 | 2.0000 | 80 | 2.0000 |

****

| 81 | 2.0000 | 82 | 2.0000 | 83 | 2.0000 | 84 | 2.0000 | 85 | 2.0000 |

****

| 86 | 2.0000 | 87 | 2.0000 | 88 | 2.0000 | 89 | 2.0000 | 90 | 2.0000 |

ISTEP= 17   (TIME= 17.0)

TEMPERATURE

1		2		3		4		5		6		7		8	
1	78.00	2	74.00	3	74.00	4	78.00	5	78.00	6	78.00	7	78.00	8	78.00
9	79.10	10	70.20	11	75.30	12	75.30	13	90.50	14	90.50	15	90.60	16	109.80
17	139.10	18	146.00	19	146.00	20	146.30	21	174.90	22	174.90	23	176.50	24	211.90
25	216.10	26	224.50	27	228.50	28	267.60	29	261.20	30	254.30	31	278.70	32	259.00
33	341.30	34	178.60	35	178.60	36	126.00	37	83.40	38	83.40	39	78.00	40	311.10
41	78.10	42	322.50	43	178.50	44	272.90	45	179.40	46	179.40	47	126.40	48	80.50
49	126.30	50	332.70	51	360.00	52	360.00	53	429.80	54	296.90	55	296.90	56	180.80
57	276.90	58	98.80	59	78.30	60	78.30	61	740.40	62	321.50	63	321.50	64	439.40
65	154.00	66	287.10	67	309.40	68	309.40	69	230.90	70	230.90	71	234.90	72	153.30
73	111.70	74	111.70	75	111.80	76	111.80	77	82.30	78	82.40	79	82.40	80	78.10
81	77.90	82	78.10	83	78.00	84	78.00	85	78.00	86	78.00	87	78.00	88	78.00

TIME=   17.000

INCREMENTAL STRAIN COMPONENTS (EPSX,EPSY,GAM)

node	value	node	value	node	value	node	value
1	-0.1720E-09	2	-0.1313E-07	3	-0.2699E-07		
4	-0.1672E-08	5	0.3313E-07	6	-0.6985E-08		
7	-0.1977E-05	8	0.7794E-05	9	-0.7455E-08		
10	-0.5759E-05	11	-0.1794E-05	12	0.5745E-05		
13	0.4555E-05	14	-0.1681E-04	15	-0.4763E-05		
16	-0.1575E-05	17	0.1635E-04	18	0.7355E-04		
19	-0.1221E-04	20	-0.1457E-04	21	-0.1118E-04		
22	-0.1414E-04	23	-0.1740E-04	24	-0.5091E-05		
25	-0.1163E-04	26	-0.1760E-04	27	0.9565E-05		
28	-0.2112E-04	29	-0.1442E-04	30	-0.7961E-05		
31	-0.1512E-04	32	-0.1722E-04	33	0.1422E-04		
34	-0.2895E-02	35	0.1597E-04	36	0.1707E-05		
37	-0.1355E-04	38	0.2453E-05	39	0.5534E-05		
40	-0.4141E-05	41	-0.5132E-05	42	0.6083E-05		
43	-0.1310E-04	44	0.1119E-04	45	-0.1558E-04		
46	-0.6165E-05	47	-0.2327E-04	48	-0.1684E-04		
49	-0.1748E-04	50	-0.1565E-04	51	-0.1917E-04		
52	-0.2087E-04	53	-0.5123E-05	54	0.7946E-05		
55	-0.4236E-05	56	0.1562E-04	57	0.8717E-06		
58	-0.1316E-04	59	-0.6637E-04	60	0.8284E-05		
61	-0.7657E-05	62	0.2713E-05	63	-0.1329E-04		
64	-0.1535E-04	65	-0.1795E-05	66	0.1453E-04		
67	-0.2279E-04	68	-0.1236E-04	69	-0.2077E-04		
70	-0.2245E-04	71	-0.1913E-04	72	0.1114E-04		
73	-0.7653E-05	74	-0.2473E-05	75	-0.4267E-05		
76	-0.3655E-05	77	-0.1266E-04	78	-0.6617E-06		
79	-0.1093E-04	80	-0.2474E-07	81	-0.8097E-02		
82	-0.1713E-05	83	-0.1034E-04	84	-0.2549E-05		
85	0.1356E-04	86	-0.9326E-05	87	0.4326E-05		
88	-0.5449E-03	89	0.1803E-04	90	-0.2937E-04		
91	0.1696E-04	92	-0.1413E-04	93	0.1971E-04		
94	-0.1341E-04	95	-0.1773E-04	96	-0.8915E-05		
97	-0.1504E-04	98	-0.1713E-04	99	0.1078E-04		
100	-0.1304E-04	101	0.1317E-04	102	-0.4484E-05		
103	-0.1556E-04	104	-0.4615E-05	105	0.6658E-06		
106	0.6054E-07	107	-0.1383E-06	108	-0.2016E-06		
109	-0.2442E-08	110	0.1765E-07		0.9023E-09		

LIST OF REFERENCES

1. Aroca, S. B., "Aluminum as a Shipbuilding Material", M. S. Thesis, MIT, May, 1969.

2. Current Welding Processes, ed. by Arthur L. Phillips, American Welding Society, 1968.

3. Masubuchi, K., "Lecture Notes and Text on Welding Engineering", Subject 13.17j, MIT, 1973.

4. Masubuchi, K., "Lecture Notes and Text on Ocean Engineering Material", Subject 13.15j, MIT, 1973.

5. Walsh, R. A., "Investigation of Distortion Removal in Welded Structures", Thesis xIII-A, MIT, May, 1969.

6. Masubuchi, K., "Residual Stresses and Distortion in Welded Aluminum Structures and Their Effects on Service Performance", Welding Research Council Bulletin, No. 174, July, 1972.

7. Masabuchi, K., "Control of Distortion and Shrinkage in Welding", Welding Research Council Bulletin, No. 149, April, 1970.

8. Taniguchi, C., "Out-of-Plane Distortion Caused by Fillet Welds in Aluminum", M. S. Thesis, MIT, 1972.

9. Masubuchi, K., "Integration of NASA Sponsored Studies on Aluminum Welding", under Contract No. NAS 8-24364 to George C. Marshall Space Flight Center, NASA, June, 1972.

10. Kihara, H., Watanbe, M., Masubuchi, K., and Satoh, K., "Researches on Welding Stress and Shrinkage Distortion in Japan", Vol. 4, 60th Anniversary Series of the Society of Naval Architects of Japan, Tokyo, 1959.

11. Holt, Richard E., "Flame Straightening Basics", Welding Engineer, Vol. 50, 1965, pp. 49 - 52.

12. Duffy, D. K., "Distortion Removal in Structural Weldments", M. S. Thesis, MIT, May, 1970.

13. "Stress Relieve Big Weldments in Minutes with Vibration", Machinery, 74, May, 1968, pp. 100 - 103.

14. Wozney, G. P. and Crawmer, G. R., "An Investigation of Vibrational Stress Relief in Steel", <u>Welding Journal</u>, 47(9), Res. Suppl., 411s -419s, 1968.

15. Cole, D. Q., "Development of Techniques for Controlling Warpage and Residual Stresses in Welded Structures", NASA CR - 61235, Final Report prepared under Contract No. NAS8-21174 Harvey Engineering Laboratories to G. C. Marshall Space Flight Center, NASA, July, 1968.

16. Kumose, T., Yoshida, T., Abbe, T., and Onoue, H., "Prediction of Angular Distortion Caused by One-pass Fillet Welding", <u>The Welding Journal</u>, October, 1954.

17. <u>Engineering Materials Handbook</u>, ed. by C. L. Mantell, Mc Graw - Hill, New York, 1958.

18. <u>Alcoa Aluminum Handbook</u>, Aluminum Company of America.

19. "Aluminum Alloys", Vol. I, <u>Materials Properties Handbook</u>, The Royal Aeronautical Society, London, 1966.

20. <u>Aluminum Standards and Data</u>, The Aluminum Association, New York, 1969.

21. Timoshenko, S., <u>Strength of Materials</u>, D. Van Nostrand Co., Third Ed., 1955.

22. Bryon, Jon Jasper, "Analysis of Two Dimensional Thermal Strains and Metal Movement During Welding", M. S. Thesis, MIT, 1973.

23. Murray, W. M., Lecture series on strain analysis, MIT, 1970.

24. Masubuchi, K., "Nondestructive Measurement of Residual Stresses in Metals and Metal Structures", RSIC - 410, Redstone Scientific Information Center, U. S. Army Missile Command, Redstone Arsenal, Alabama, April, 1965.

25. Masubuchi, K., Simmons, F. B., and Monroe, R. E., "Analysis of Thermal Stresses and Metal Movement During Welding", RSIC - 820, Redstone Scientific Information Center, Redstone Arsenal, Alabama, July, 1969.

26. Masubuchi, K. and Iwaki, T., "Welding Stress Analysis by Numerical Experiments by Finite Element Method", Additional paper to the report "Residual Stress Analysis Techniques for Weldment Study" by K. Masubuchi, presented at 1972 SESA Spring Meeting, Cleveland, Ohio, May, 1972.
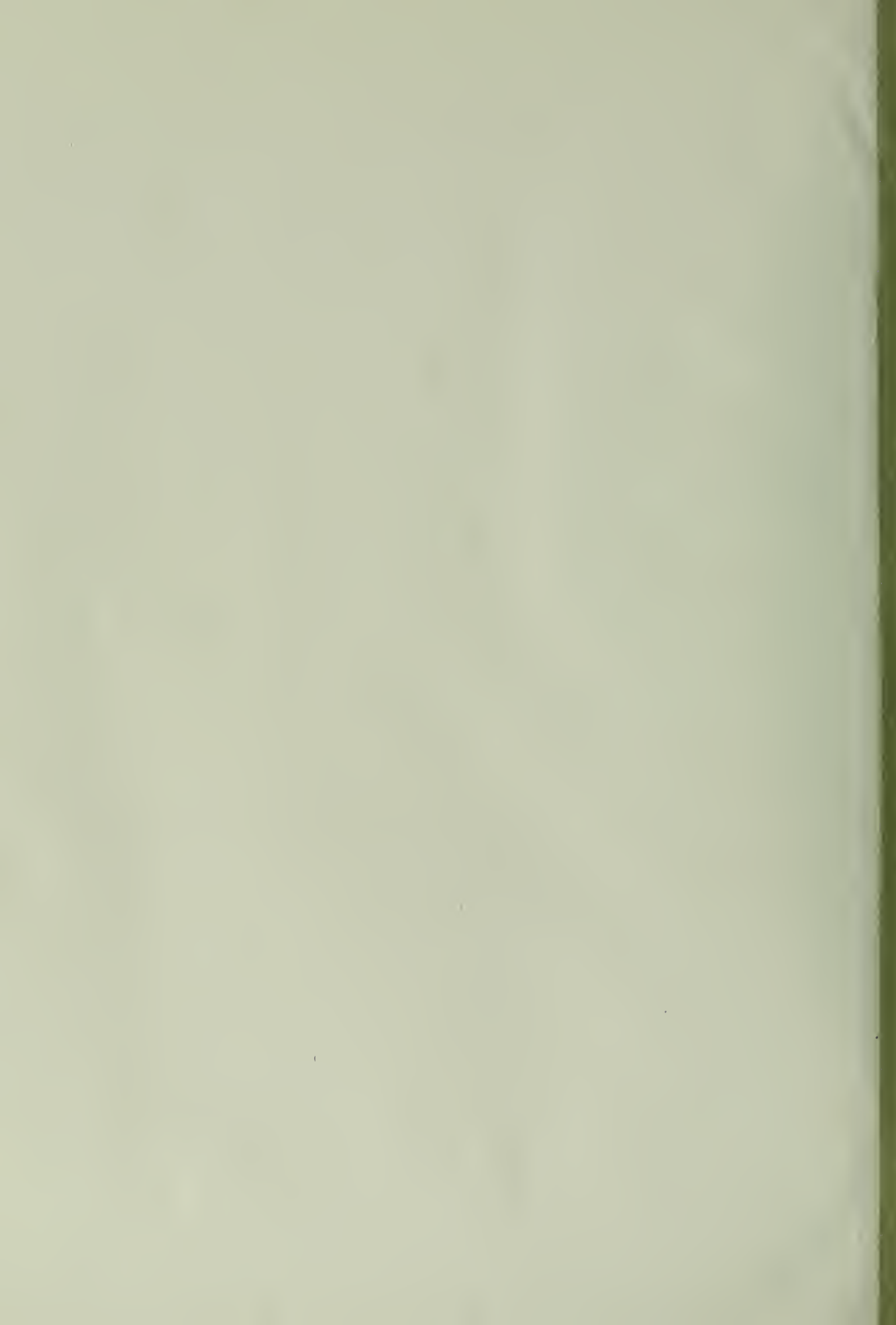
27. Muraki, T., and Masabuchi, K., "First Interim Report on Phase B of Thermal Analysis of M551 Experiment for Materials Processing in Space", under Contract NAS 8-28732, to G. C. Marshall Space Flight Center, January, 1973.

28. Muraki, T., Bryan, J., and Masubuchi, K., "Analysis of Thermal Stresses and Metal Movement During Welding", MIT, March, 1974.

29. "Nonferrous Multiple Alloys", Part II, "Nonferrous Alloys", Vol. 2, Thermophysical Properties of High Temperature Solid Material, 1967.

30. "Thermal Conductivity, Metallic Elements and Alloys", Vol. 1, Thermophysical Properties of Matter, The TPRC Data Series, 1970.

31. "Elements", Vol. 1, Thermophysical Properties of High Temperature Solid Materials, ed. by Y. S. Touloukian, 1967.

32. "Thermal Diffusivity", Vol. 10, Thermophysical Properties Of Matter, ed. by Y. S. Touloukian, 1967.

.